UNIVERSITÉ DU QUÉBEC À CHICOUTIMI

MÉMOIRE PRÉSENTÉ À
L'UNIVERSITÉ DU QUÉBEC À CHICOUTIMI
COMME EXIGENCE PARTIELLE
DE LA MAÎTRISE EN INGÉNIERIE

Par

Fanglin Cai

Conception et analyse mécaniques des pièces en aluminium
pour application automobile

Janvier 2007

UNIVERSITÉ DU QUÉBEC À CHICOUTIMI

MÉMOIRE PRÉSENTÉ À
L'UNIVERSITÉ DU QUÉBEC À CHICOUTIMI
COMME EXIGENCE PARTIELLE
DE LA MAÎTRISE EN INGÉNIERIE

By

Fanglin Cai

Design and mechanical analysis of aluminum parts
for automobile application

January 2007

Le progrès utilise des fois des virgules, mais jamais des points
Progress sometimes uses a comma, but never a full stop
学无止境

RESUME

Les alliages en aluminium sont en voie de devenir un matériau important dans la fabrication des pièces d'automobiles. Cette recherche a pour but d'étudier la capacité de l'alliage en aluminium de remplacer l'acier dans la fabrication des bras de contrôle de suspension des automobiles. La pièce en aluminium est conçue par des logiciels de modélisation et simulation utilisant la méthode ESO (Evalutionary Structural Optimization) qui permettent d'optimiser la forme et le poids de la pièce sous différents paramètres de contrainte. La résistance mécanique et les vibrations subis par les bras de suspension seront aussi analysées. Finalement, les résultats seront comparés avec les performances de l'acier.

ABSTRACT

Aluminum alloy is an emerging material in the manufacturing of automobile parts. This research is aimed at studying whether an aluminum alloy can effectively replace steel in the manufacturing of automobile control suspension arms. The design of the aluminum part is done through the use of modelization and simulation software and the ESO (Evolutionary Structural Optimization) method that allow to develop the shape and weight of the part under given stress conditions. Mechanical strength and vibration movements of the control suspension arms will also be studied. Finally, the results will be compared with the performance of steel parts.

ACKNOWLEDGEMENTS

I am deeply indebted to my advisor, Professor Mohamed Bouazara, for his invaluable guidance and constant support. Without his help, it isn't possible to successfully complete my work.

I am grateful to Mr. Marcel Paquet, Mr. Marc J. Richard and Mr. Zhan Zhang for their helpful advice and recommendations.

I would like to thank the members of the UQAC for their support and their service; especially to Mr. Etienne Lafrenière.

I would to acknowledge several colleagues, particularly Hatem Mrad, Abdelhamid Saoudi, Changqing Zheng and Samuel Gosselin-Brisson, for their help and for creating a kindly study atmosphere.

Finally, I would like to express my deepest gratitude to my family and my parents, understanding and love that I received from my husband. Without their encouragement and support, I would not have been able to fulfill my goal of completing my Master's degree successfully.

TABLE OF CONTENTS

LIST OF TABLES

LIST OF FIGURES

CHAPTER 1

CHAPTER 1   Introduction

Today, the application of light alloys designed to reduce weight is becoming a stringent need in the transport industry due to environmental and social pressure. Fuel consumption and emission of polluting gases are strongly dependent on car weight and for this reason the automotive industry is looking at innovative process technologies which make use of light alloys and new design methodologies [1, 2]. Aluminum helps build a better car because it delivers environmental, safety and driving performance advantages. 1) Environmental performance: Aluminum saves weight, which leads to fewer emissions and greater fuel economy. 2) Safety performance: Aluminum can absorb more crash energy. 3) Driving performance: Cutting weight by using aluminum parts can help cars and trucks brake quicker, handle better and accelerate faster [3]. That is why aluminum is the fastest growing material in the automobile industry today. Figure 1.1 illustrates current aluminum applications on vehicles produced in North America.

1.1   Problematic

The suspension control arms are important parts in a vehicle (see the Figure 1.2) [4]. Conventionally, these parts were made of steel, which is a heavy metal. Their geometry designs were done by means of traditional engineering methods. Today we try to use

Figure 1.1 showing cutaway car diagram with labels: Cylinder Head, Cylinder Head Cover, Intake Manifold, Hood, Radiator, Bumper Reinforce, Cylinder Block, Suspension Arm, Transmission Case, Disk Wheel
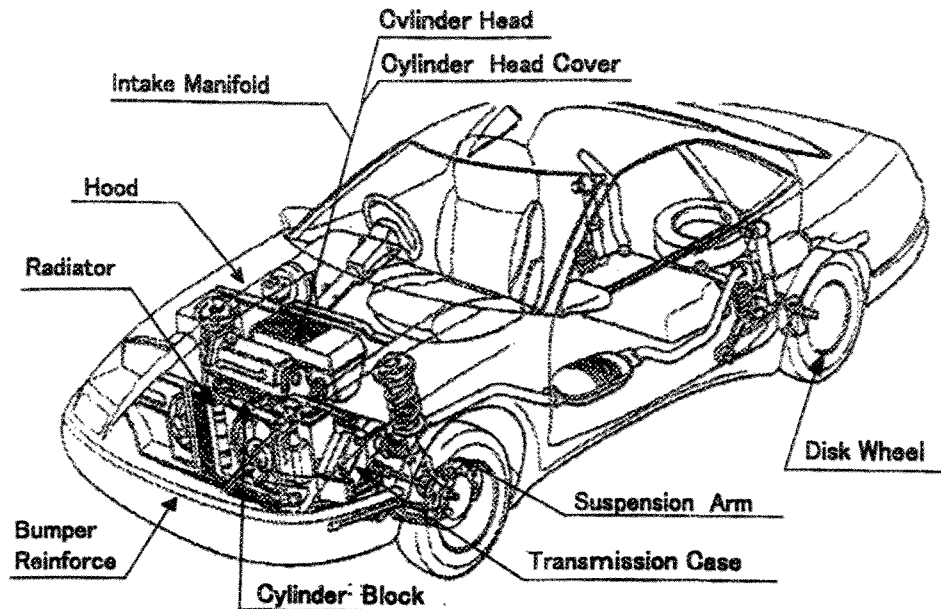
Figure 1.1   Current aluminum applications on vehicles produced in North America.

aluminum, which is a lighter metal, to fabricate these parts instead of steel. We also use modern engineering methods to design and optimize the geometry design of these parts to continue to reduce weight, for instance, numerical modelization and simulation methods. Why do we need to do this work? Because aluminum and steel are two different metals, therefore they have different mechanical properties. In order to determine if aluminum can be used instead of steel in automobile parts, the engineer must go through many steps, such as: design, manufacture part, testing, change design and repeat the steps again and again. It is a consuming process in terms of time, material and cost. The static and dynamic simulation analysis methods are used to cut weight, optimize shape, measure strength and displacement of dynamic behaviour and vibration. It saves time and helps the engineer to

design the system more easily and efficiently. Simulation analysis enables the engineer to calculate dynamic and static strengths in order to reduce weight. The validity of this method is demonstrated through two applications of aluminum alloys that replace steel alloys for suspension control arms. There are two examples of control arms in steel and in aluminum (see Figure 1.3) and two examples of different designs of control arm (see Figure 1.4). We can see by these examples that the design of aluminum suspension arm is not easy. The problematic is that the aluminum part must satisfy the same performance as the steel part.
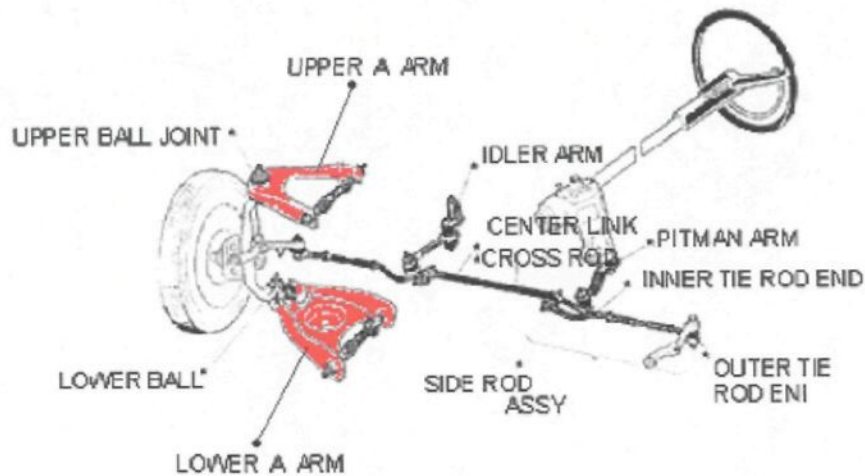
Figure 1.2   Suspension arm system.
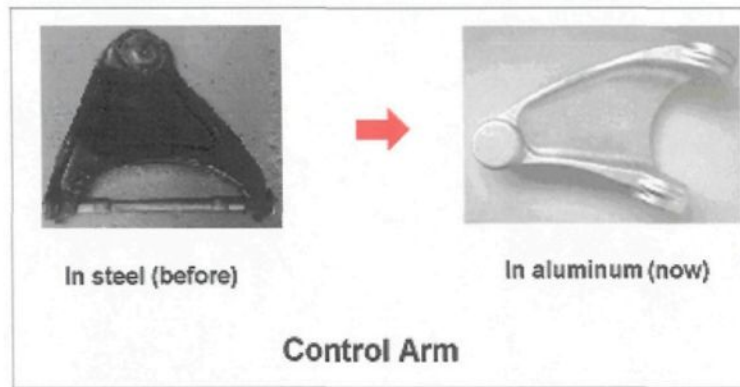
Figure 1.3   Examples of two control arms in different material.
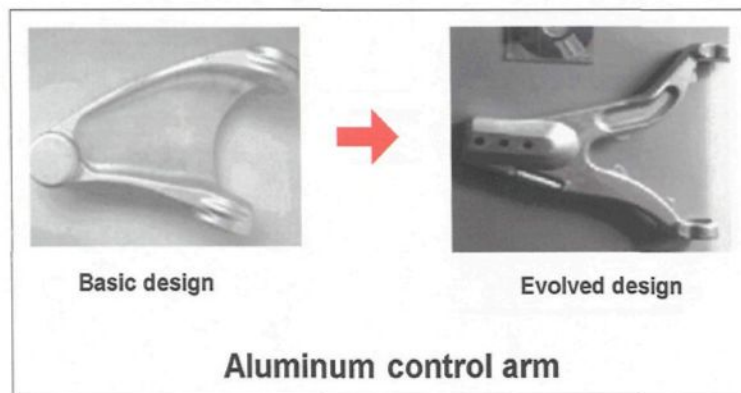
Figure 1.4   Examples of two different designs of control arm.

1.2   Objectives

The present work was undertaken to develop aluminum parts of automobile by finite element simulation method. The main objectives of the study were as follow:

1) Static and dynamic study of automobile behaviour for aluminum mechanical parts (control arms).

2) The design of suspension control upper and lower arms.

3) Simulate and analyse suspension arms by FEM.

4) Evaluate stress analysis for two aluminum automobile parts with ESO (Evolutionary Structural Optimization) advanced methods:

   - Weight cutting and shape optimization for aluminum upper control arms;

   - Dynamic analysis of vibrations for aluminum lower control arms;

5) Performance and weight comparison between steel and aluminum parts.

In this chapter, we generally introduce the application of aluminum in the automotive industry, which is the objective of this study. Also we submit the problematic of this study and highlight the works that we will perform.

CHAPTER 2

CHAPTER 2   Literature review

2.1   ALUMINUM ALLOYS FOR AUTOMOBILE APPLICATIONS AND WEIGHT SAVINGS

Today, the aluminum content of average passenger car is 267 pounds per vehicle; the average light truck aluminum content is 279 pounds per vehicle. Figure 2.1 shows examples of current aluminum applications in vehicles produced in North America. Figure 2.2 is some of aluminum alloy parts application in automobile [5, 6].
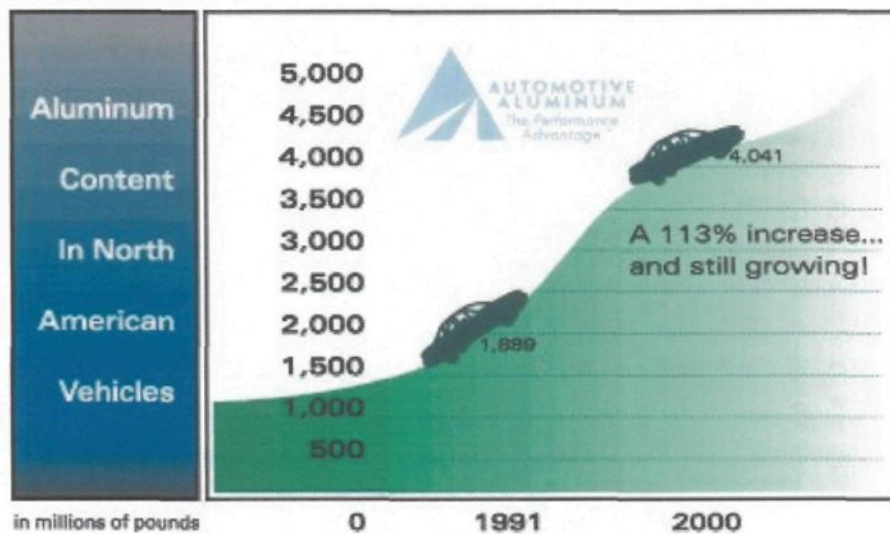
Figure 2.1   Aluminum content in North American vehicles.

Multi-link, Rear suspension support assembled 19.6kg, A357 welded with 6061 struts, T5 and T6

Engine suspension mounts A357, T5 50% Weight reduction

STEERING KNUCKLE A357, T5 Substitution of cast iron part

Multi-link, Rear suspension support 8.5kg, A357, T5
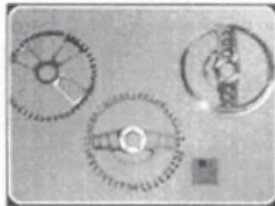
Aluminium forged steering whee
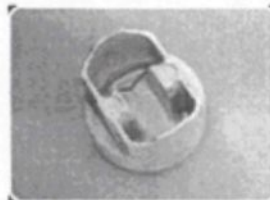
Aluminium forged piston

Aluminium forged wheel rim

DSCN6952

aluminium forged disk
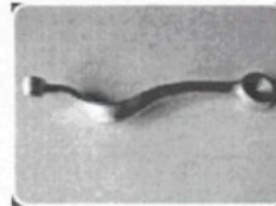
BMW suspension arms (1)

AL 7075 forged drive flange (4)
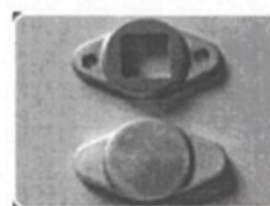
AL 6082 Bracket

Audi aluminium forged suspension

Figure 2.2   Aluminum parts of car.

Aluminum can offer a weight saving of up to 55 percent compared to an equivalent steel structure, while matching or exceeding crashworthiness standards of same-sized steel structures. The lifetime fuel savings of these vehicles can amount to 500 - 700 gallons of gasoline, or about $600 in the U.S. today, and more than three times that amount in Europe and Japan. Many companies in the world now have aluminum-intensive test vehicles on the road, providing a weight reduction of 46 percent in the structure, with no loss in crash protection. Table 2.1 below for the Ford Taurus/Sable-based aluminum-intensive vehicle (AIV) illustrates what can be achieved in such a vehicle where the unibody structure is weld bonded for efficient joining. The structure has not been redesigned yet, a weight saving of 46% was achieved.

	Steel	Aluminum	Weight Saved	% Chg
Body structure (lbs.)	596	320	276	-46
Hood, deck & fenders (lbs.)	90	38	52	-58
Front and rear doors (lbs.)	132	79	53	-40
Total body-in-white (lbs.)	818	437	381	-47
Torsional rigidity (ft. lb./deg)*	7.4	11.0	—	+49
Total vehicle (lbs.)	3245	2894	381	-11.6

Table 2.1 The Ford Taurus/Sable-based aluminum-intensive vehicle weight savings

Primary weight saving also enables many of the other vehicle systems to be downsized, such as the engine, transmission, brakes, suspension, wheels, etc. Figure 2.3 shows how hypothetical secondary weight saving in a mid-sized Sedan could lead to a total weight reduction of over 700 lbs. The steadily growing usage of aluminum is largely

related to its success in applications that ensure or optimize mobility whether in automotive, aviation or shipbuilding. At the same time, the light metal faces some challenging trends: greater transportation needs in an increasingly global business world; innovations in competing materials; and increasing price pressure. This urges and enforces the aluminum industry to strengthen efficiency, focus portfolios, continue research & development and inform about their material's competitive advantages.

Primary and secondary weight savings breakdown for an aluminum vehicle based on regression analysis of 1972-1993 passenger cars
Baseline (3100 lb)← Saving 727 lb →NY (2373lb)

Aluminum Structure --275

Aluminum Chassis --105

Powertrain --137

Suspension --28

Brakes --27

Steeling --13

Fuel Tank --23

Wheels --29

Exhaust System --10

Drivetrain --36

Other --44

Figure 2.3   Weight savings breakdown for aluminum.

2.1.1 Aluminum alloy advantage

Aluminum can compete successfully with less costly materials because of the advantages it brings in primary and secondary weight saving, structural performance and design flexibility. It is an important material in fabricating industries; especially in the aeronautics and automobile manufacturing area, where lightweight and high-strength components with complex configurations are required. This natural combination of high strength with lightweight, outstanding properties of aluminum alloy, has led to a rapidly expanding range of applications [7].

Strength with lightweight

Strength is the ability to resist loads. Aluminum has a density one third that of steel and coupled with its high strength, the strength/weight ratio of the strongest aluminum alloy is among the highest available in commercial materials.

Hardness

Hardness is resistance to indentation. Pure aluminum has a low hardness. However, some aluminum alloy can get higher hardness after solution artificial ageing. For example, the hardness of 7079-T6 can be as high as 135 BHN.

Low elastic modulus

Elastic modulus is stress per unit strain. The elastic modulus of aluminum is one third that of steel. Therefore, aluminum stresses due to impact and imposed deformations are low.

Toughness at low temperature

Toughness is the ability to absorb energy without fracturing. Aluminum alloys may be used at temperatures of up to 500F, but for applications above 200F the design stresses require

some modification, at low temperatures, aluminum alloys become stronger and they are not subject to brittle fractures.

Good ductility

Ductility is a material that has the ability to stretch out or deform elastically under load. Aluminum alloy has an excellent ductility. It can be manufacture into almost any form; the resulting surfaces are clean and smooth.

2.2 Suspension system

The primary job of the suspension on any vehicle is to isolate the chassis from shock loading and vibration. The suspension does all this by allowing the wheels to move vertically, with respect to the chassis. Secondly, it prevents the car from shaking itself to pieces. The suspension must help and not impair the stability and handling of the entire car. This is accomplished with a damping system that also helps in the load distribution onto the wheels. Suspension consists of two basic components [8]:

Springs: These come in three types. They are coil springs, torsion bars and leaf springs.

Shock absorber: They dampen the vertical motion induced by driving the car along a rough surface. If the car only had springs, it would boat and wallow along the road until the passengers get physically sick. Shock absorbers perform two functions. First, they absorb any larger-than-average bumps in the road so that the shock isn't transmitted to the car chassis. Second, they keep the suspension at as full a travel as possible for the given road conditions. Shock absorbers keep the wheels planted on the road. Technically, they are actually dampers. Even more technically, they are velocity-sensitive hydraulic damping

devices, in other words, the faster they move, the more resistance there is to that movement. They work in conjunction with the springs. The spring allows movement of the wheel to allow the energy in the road shock to be transformed into kinetic energy of the unsprung mass, where upon it is dissipated by the damper.

2.2.1 Suspension model

In the past, the main materials for suspension arms were steel. We have here steel tubular A-arm, and steel sub-frame (see Figure 2.4 [8]). Most suspensions in use today are of the independent type (see Figure 2.5). As indicated by the name, an independent suspension works on its own and does not affect the suspension of the other wheels. With careful design, several advantages of the independent suspension come to light. The following four types of system [9] are all essentially a variation on the same theme. (a) and (b) is Coil Spring type 1 and 2 for double-A arm suspension; (c) Double Wishbone and (d) Multi-link suspension.

QSA1738S
HONDA

HONDA Civic
(Upper control arm)

A-ARMS & D-ARMS

BAW
LCAR4404966
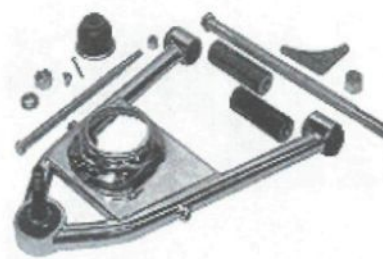
TUBULAR LOWER A-ARMS

LOWER A-ARMS

LOWER A-ARMS

Figure 2.4   Conventional suspension arms

(a)

(b)

(c)

(d)
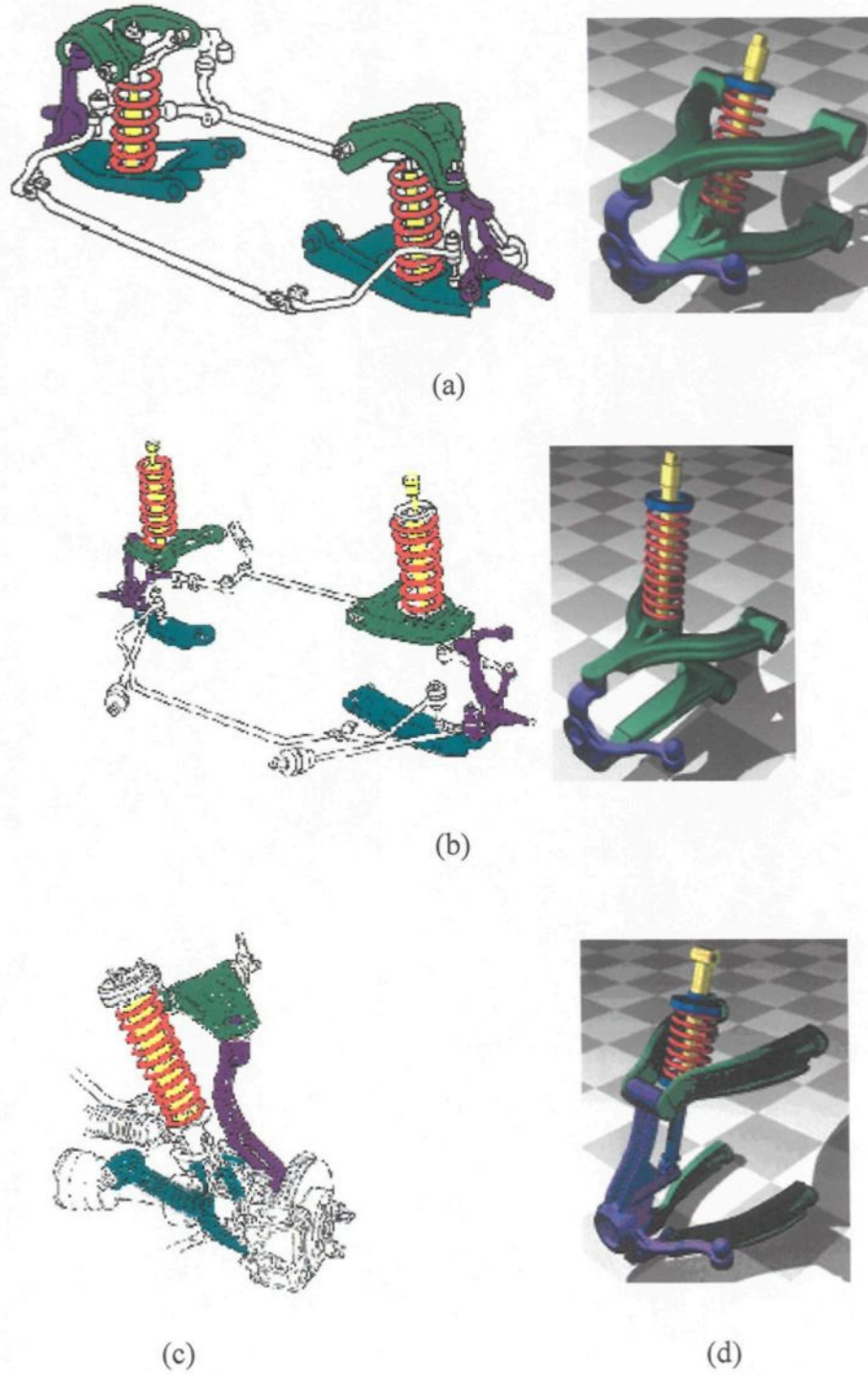
Figure 2.5   (a) Coil Spring type 1, (b) Coil Spring type 2,
(c) Double Wishbone and (d) Multi-link suspension.

2.3 Mechanical vibration

Automotive suspension is a vibration system. When designing suspension parts, the vibration must be studied. Mechanical vibration is always associated with the fluctuation of mechanical loads; therefore, with fluctuation of mechanical stresses, there is fatigue failure of mechanical components such as the loosening of threaded connections, friction and wear, and damage of electronics and other delicate components. Finally, vibration can affect comfort, performance and the health of people subjected to it, as in sickness due to ship (or high-rise building) oscillation. These facts make it imperative that engineers understand the vibration behaviour of every mechanical component, machine, structure, and system.

2.3.1 Acceptable vibration levels

Figure 2.6 shows their proposed recommendations for acceptable levels of vertical vibration on standing and sitting human beings, expressed in terms of acceleration.
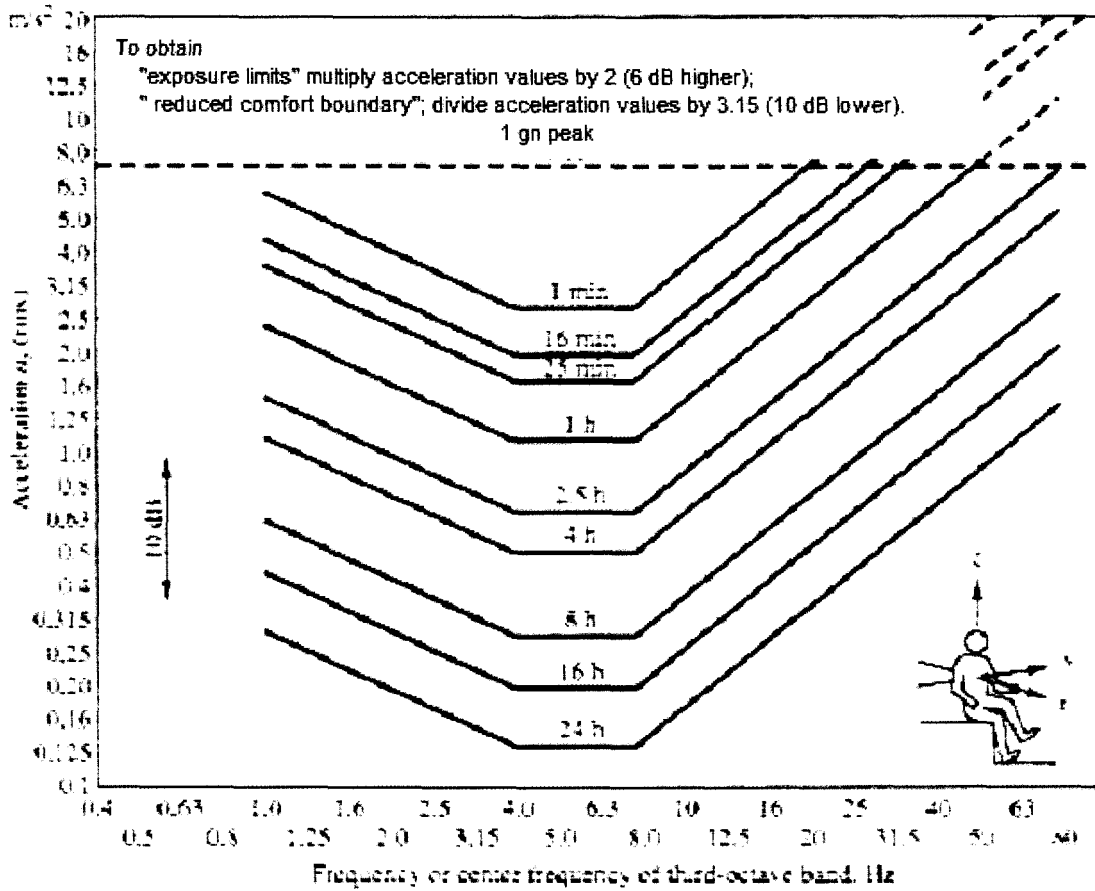
Figure 2.6   ISO—suggested acceptable vertical vibration levels.

In other case, Figure 2.7 is a conversion nomogram, relating harmonic vibration frequency, acceleration, velocity and displacement. The range of operating conditions for a variety of systems is indicated on the same figure [9].
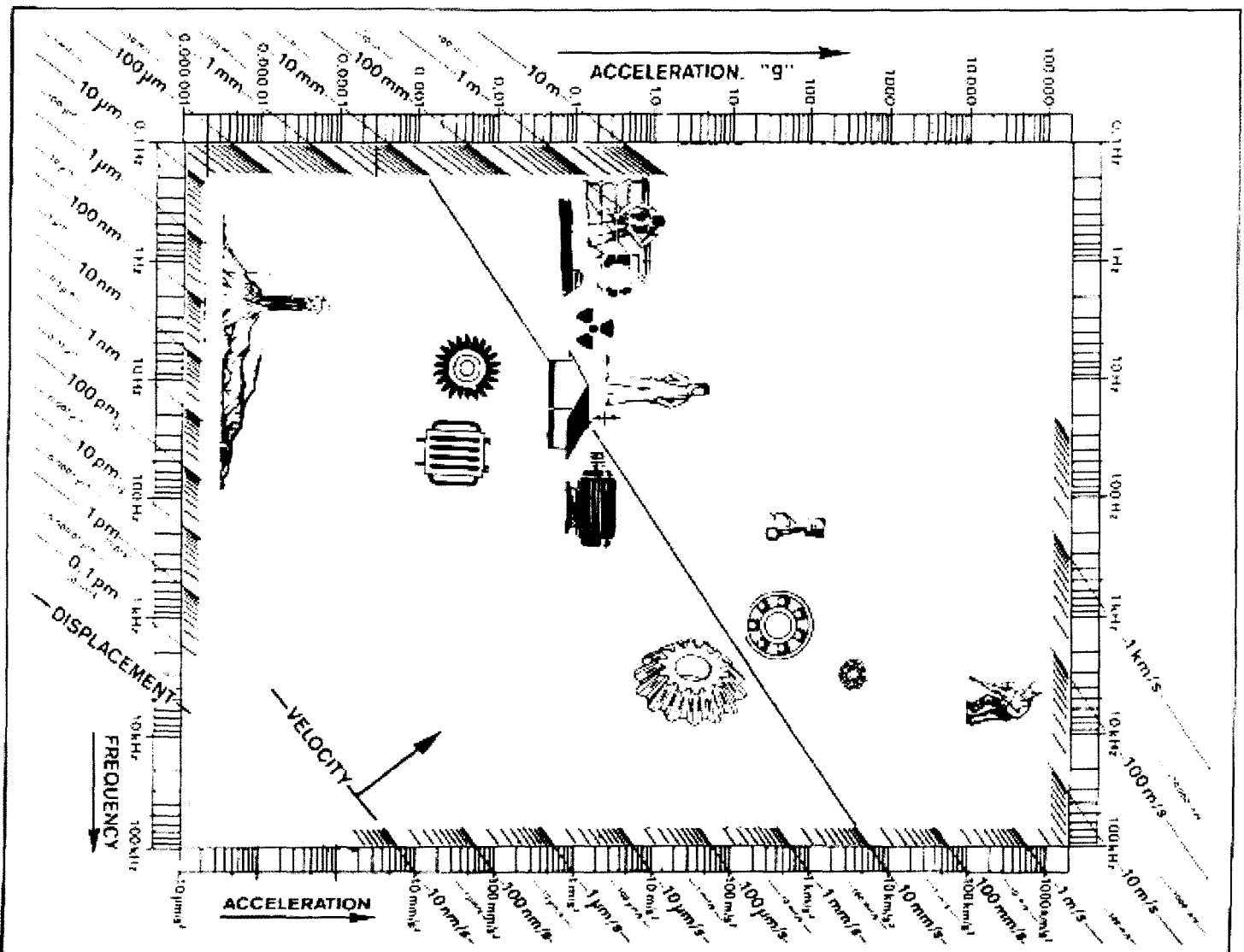
Figure 2.7 Vibration range levels nomogram.

2.3.2 Vibratory system and motion

To modelize a vibratory automotive system, there are many models in literature, for instance Figure 2.8, it is one kind of vibrating automotive systems [9].
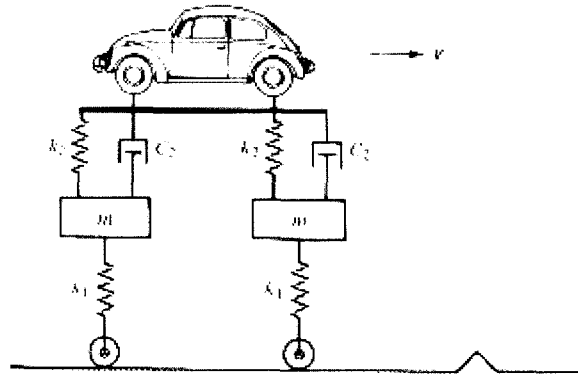
Figure 2.8   Modeling of Vibrating Automotive Systems.

The study of vibration is concerned with the oscillatory motions of bodies and the forces associated with them. All bodies possessing mass and elasticity are capable of vibration. Thus, most engineering machines and structures experience vibration to some degree, and their design generally requires consideration of their oscillatory behaviour.

Oscillatory systems can be broadly characterized as linear (Figure 2.9) or nonlinear (Figure 2.10) [9, 10 and 11]. For linear systems, the principle of superposition holds, and the mathematical techniques available for their treatment are well developed. In contrast, techniques for the analysis of nonlinear systems are less well known, and difficult to apply. However, some knowledge of nonlinear systems is desirable, because all systems tend to become nonlinear with increasing amplitude of oscillation.
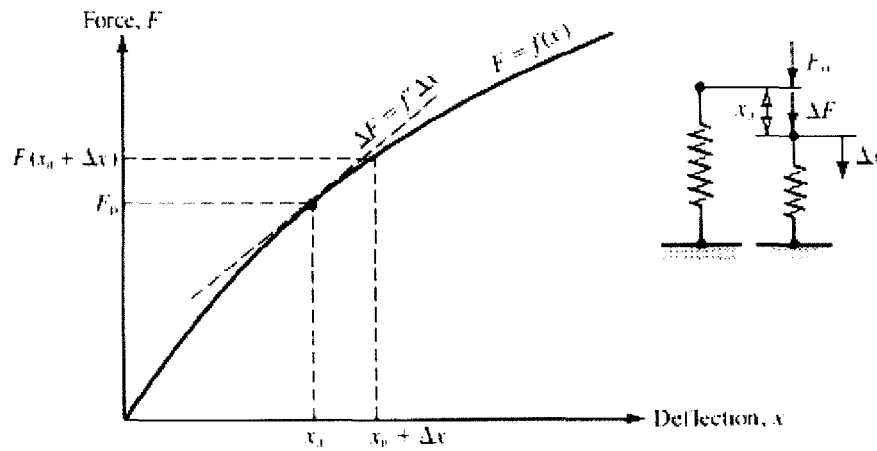
Figure 2.9   Spring linearization.
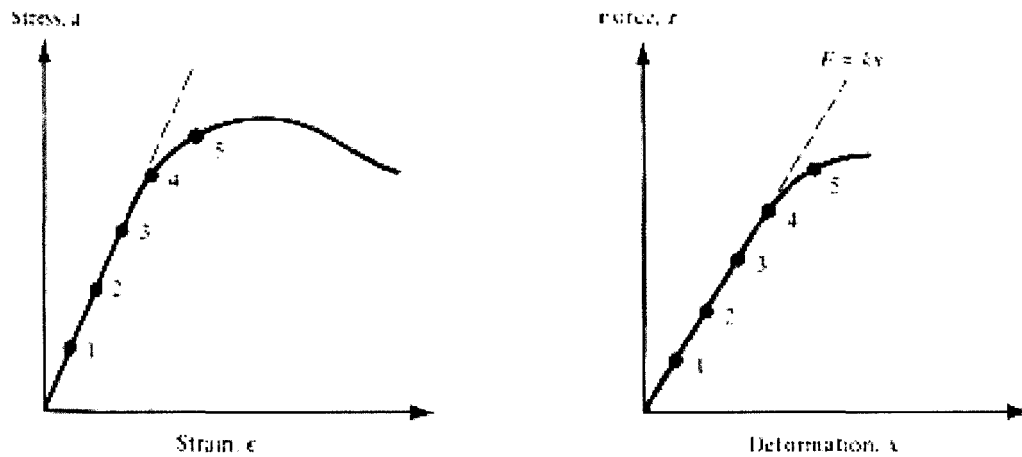
Figure 2.10   Spring nonlinearity.

There are two general classes of vibrations—free and forced. Free vibration takes

place when a system oscillates under the action of forces inherent in the system itself, and

when externally impressed forces are absent. The system under free vibration will vibrate at

one or more of its natural frequencies, which are properties of the dynamical system established by its mass and stiffness distribution.

2.3.3 Newton's second law of motion

The generalized model representing this class of problems is shown in Figure 2.11. The displacement $x(t)$ of the mass is measured from the static equilibrium position. Displacement is positive in the downward direction, and so are the velocity $\dot{x}(t)$ and the acceleration $\ddot{x}(t)$. A positive force on the mass m will produce a positive acceleration of the mass and vice versa. Referring to the free-body sketch, the forces acting on the mass are (1) the gravitational force mg, which is constant, (2) the spring force kx, which always opposes the displacement, (3) the damping force $c\dot{x}$, which always opposes the velocity, and (4) the excitation force, which is assumed to equal to $F_0 \sin \omega t$.
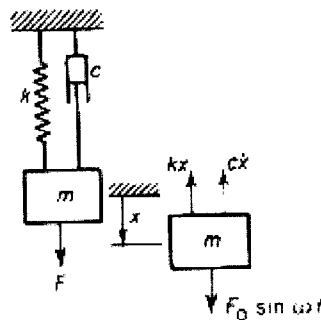
Figure 2.11 Viscously damped system with harmonic excitation.

Newton's second law of motion states that the rate of change of momentum is proportional to the impressed force and takes place in the direction of the straight line in which the force acts. If the mass is constant, the rate of change of momentum is equal to the

mass times its acceleration. From the free-body sketch in Figure 2.11, the equation of motion of the system is [12]:

$$m\ddot{x} + c\dot{x} + kx = F_0 \sin \omega t \qquad (2.1)$$

2.3.4 Motion for suspension system of automobile

Automotive suspension is a two-degree of freedom systems. We use a quarter car suspension model as illustrated in Figure 2.12 [13] and suspension system as shown by Figure 2.13 [14, 15].
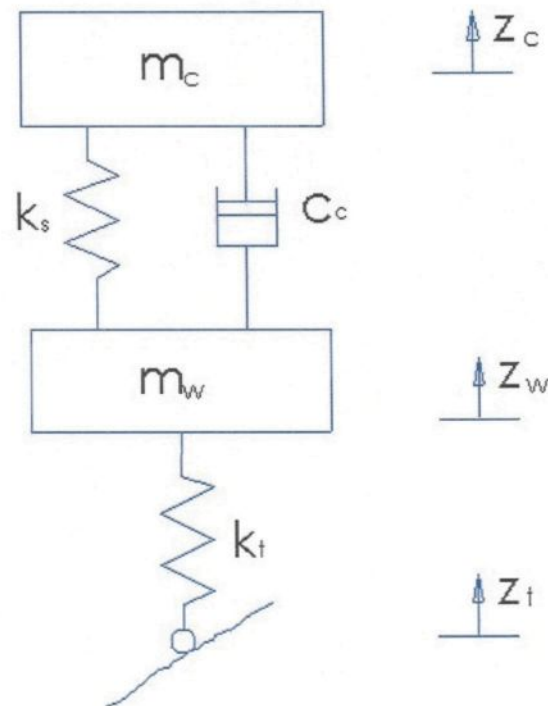
Figure 2.12   Quarter car passive suspension model.
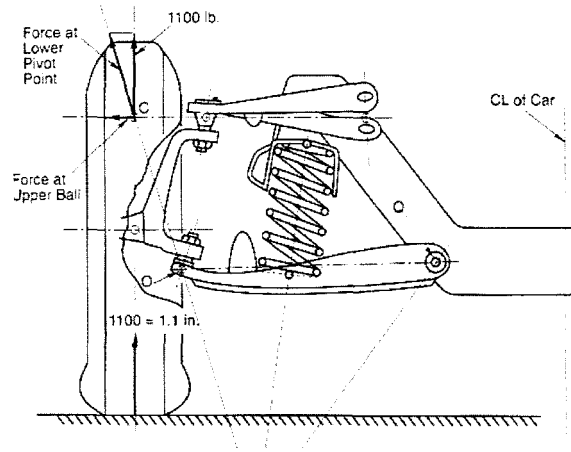
Figure 2.13   Suspension system.

Natural frequency is the rate of energy interchange between the kinetic and the potential energies of a system during its cyclic motion. As the mass passes through the static equilibrium position, the potential energy is zero [9].

$$\omega_n = \sqrt{k/m} \qquad (2.2)$$

where: ω_n is natural frequency

k is coefficient of spring

m is mass

In the case of the chassis natural frequency, we use the suspension rate and the chassis mass in the equation above. Thus,

$$\omega_c = \sqrt{k_s/m_c} \qquad (2.3)$$

For the wheel natural frequency ω_w, it is necessary to take into account K_s and K_t because the wheel oscillates between the suspension and tire springs. Although these

two springs are on opposite sides of the wheel/hub/knuckle mass, the mass would feel the same force if the two springs were in parallel on one side of the mass. In other words, the two springs, K_s and K_t, are in parallel and their composite rate is their sum.

$$\omega_w = \sqrt{(k_s + k_t)/m_w} \qquad (2.4)$$

2.4   Optimization methods

Today, new and faster computer technology is increasing the use of software iteratively to apply finite element analysis to design, while varying dimensional characteristics of the design. This is called size and shape optimization. Most commonly, shape optimization is the process of changing the physical dimensions of a structural part to reduce weight while staying within design constraints, usually maximum stress or deflection.

There are many optimization methods in the literature. Here present two shape optimization methods: the Simplex optimization method and Fuzzy sets for multicriteria optimization [16].

2.4.1   The Simplex optimization method

The simplex methods are based on an initial design of k+1 trials, where k is the number of variables. A k+1 geometric figure in a k-dimensional space is called a simplex. The corners of this figure are called vertices. With two variables, the first simplex design is base on three trials (see Figure 2.14), for three variables, it is base on four trials, etc. This

number of trials is also the minimum for defining a direction of improvement. After the

initial trials, the simplex process is sequential, with the addition and evaluation of one new

trial at a time. The simplex searches systematically for the best levels of the control

variables. The optimization process ends when the optimization objective is reached or

when the responses cannot be improved further.
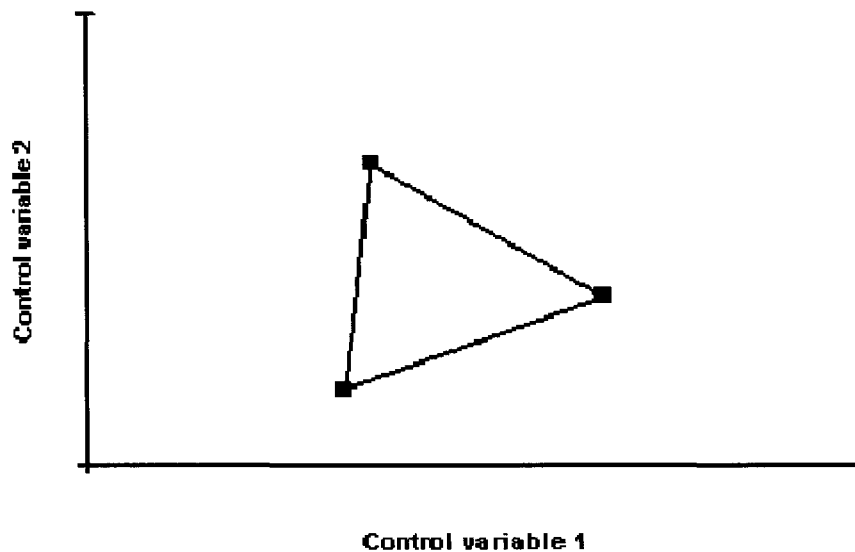
Figure 2.14   A simplex defined by three different trial conditions for two control
variables.

2.4.2 Fuzzy sets for multicriteria optimization

1) Membership function

In fuzzy set theory, the term "target" can be represented with a characteristic

function varying with the response variable. This function, varying between 0 and 1, is the

membership function of the variable in question. "Close to the target" can for example be represented by all values above 0.7 [16]. It is shown in Figure 2.15. The membership functions will of course vary significantly in shape depending on the characteristic described. The basic idea is however the same: To translate, or transform, different response variables into a measure that can be adequately compared and combined with others. Example: In the MultiSimplex software, it is possible to define three types of optimization objectives, with accompanying membership functions. Derringer and Such first suggested these functions in 1980. The relative importance of individual response variables can also vary. One may be very important, while another may be only moderately important.
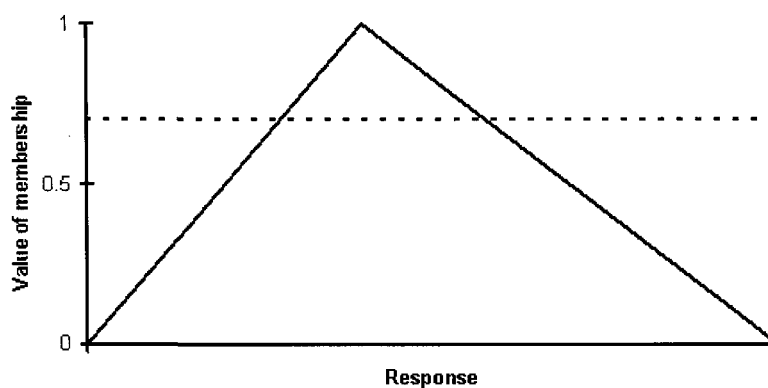
Figure 2.15 Example of membership function for the fuzzy set "target".

2) The maximization and minimization of membership function

The transformations used in the MultiSimplex software to create membership functions for maximization problems (minimization of Y_i is equivalent to maximization of $-Y_i$) are expressed as:

$$m(y_i) = \begin{cases} 0, Y_i \leq Y_{min} \\ \left[\dfrac{Y_i - Y_{min}}{Y_{max} - Y_{min}} \right]^R, Y_{min} < Y_i < Y_{max} \\ 1, Y_i \geq Y_{max} \end{cases} \qquad (2.5)$$

Where

Y_{min} is the low limit for acceptable values of Y_i.

Y_{max} is the value above, which a further increase is without significance.

R is a constant that can take different values.

All responses where the objective is maximization or minimization can be transformed compared and combined using these membership functions. By changing the constant R, it is possible to specify many different membership functions (Figure 2.16). Values of R above 1.0 will result in a slow increase from the unacceptable limit and fast near the high limit. If the constant R has the value 1.0, the function will be strictly proportional between the limits. Values of R below 1.0 will result in a fast increase from the unacceptable limit and slow near the high limit.
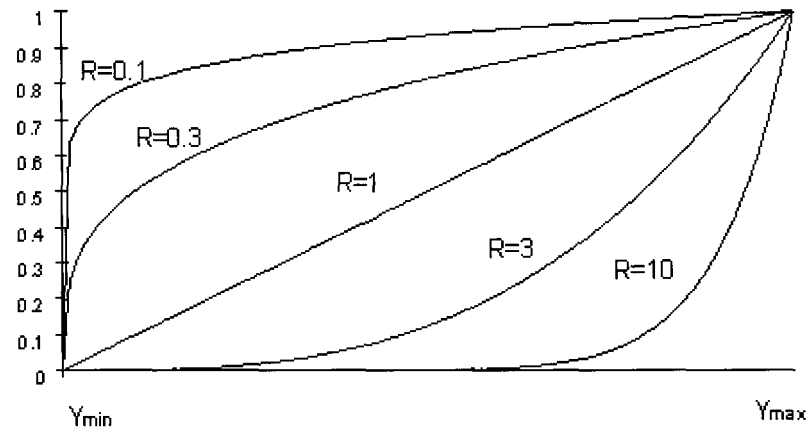
Figure 2.16 The shape of the maximization membership function with different values of the constant R.

3) The target membership function

With a specific target for Y_i, the MultiSimplex software uses a two-sided transformation to create membership functions expressed as:

$$m(y_i) = \begin{cases} \left[\dfrac{\hat{Y}_i - Y_{min}}{C_i - Y_{min}} \right]^R , & Y_{min} < \hat{Y}_i \leq C_i \\[3mm] \left[\dfrac{\hat{Y}_i - Y_{max}}{C_i - Y_{max}} \right]^R , & C_i < \hat{Y}_i < Y_{max} \\[3mm] 0, & \hat{Y}_i \leq Y_{min} \ \text{el.} \ \hat{Y}_i \geq Y_{max} \end{cases}$$

(2.6)

Where

Y_{min} is the low limit for acceptable values of Y_i.

Y_{max} is the high limit for acceptable values of Y_i.

C_i is the target value for Y_i.

R is a constant that can take different values.

By changing the constant R, it is also possible to specify many different membership functions. Values of R above 1.0 will result in a slow increase from the unacceptable limits and fast near the target value. If the constant R has the value 1.0, the function will be strictly proportional between the limits and the target value. Values of R 1.0 in Figure 2.17 will result in a fast increase from the unacceptable limits and slow near the target value.
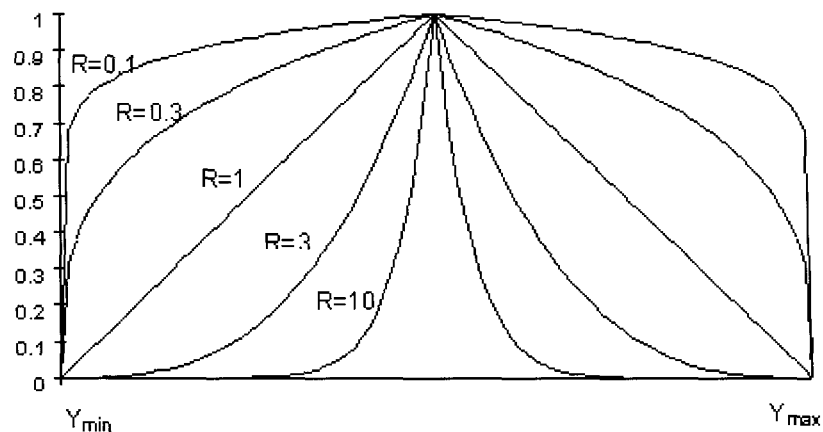
Figure 2.17   The shape of the target membership function with different values of the constant R.

4) The aggregated value of membership

MultiSimplex uses a weighted geometric average to combine the membership values of the individual response variables into an aggregated value of membership. The influence values assigned to the individual response variables are used as weights. The aggregated value of membership is expressed as:

$$M(y) = \left[m(y_1)^{\beta_1} \times m(y_2)^{\beta_i} \dots \times m(y_i)^{\beta_i} \right]^{\frac{1}{\Sigma \beta_i}}$$

(2.7)

Where

M(y) is the aggregated value of membership.

m(y_i) is the membership value for the individual response variable.

β_i is the influence value for the individual response variable.

2.5 Shape optimization method

Shape optimization of elastic structures is a very important and popular field [17, 18, 19, and 20]. In *"Une méthode de lignes de niveaux pour l'optimisation de formes"* [21] and *"A level-set method for vibration and multiple loads structural optimization"*[22] by Grégoire ALLAIRE, François JOUVE. They describe a new implementation of the level-set method for structural optimization. It is a method for shape and topology optimization to new objective functions such as eigenfrequencies and multiple loads. This method is based on a combination of the classical shape derivative and of the Osher-Sethian[23, 24] level-set algorithm for front propagation. In two and three space dimensions they maximize the first eigenfrequency or they minimize a weighted sum of compliances associated to different loading configurations. The shape derivative is used as an advection velocity in a Hamilton-Jacobi equation for changing the shape. This level-set method is a low-cost shape capturing algorithm working on a fixed Eulerian mesh and it can easily handle topology changes. It is described below:

1. Maximizing the first eigenfrequency

We start by describing the eigenvalue problem in linearized elasticity which allows computing vibration frequencies and modes. Let $\Omega \subset R^d$ (d = 2 or 3) be a bounded open set occupied by a linear isotropic elastic material with Hooke's law A and density $\rho > 0$. For any symmetric matrix ξ, A is defined by

$$A\xi = 2\mu\xi + \lambda(Tr\xi)Id \qquad (2.8)$$

where μ and λ are the Lamé moduli of the material. Id is the identity mapping from R^d into R^d. The boundary of Ω is made of two disjoint parts

$$\partial\Omega = \Gamma_N \cup \Gamma_D \qquad (2.9)$$

with Dirichlet boundary conditions on Γ_D, and Neumann boundary conditions on Γ_N. The two boundary parts Γ_D and Γ_N are allowed to vary in the optimization process, although it is possible to fix some portion of it.

We denote by $\omega \geq 0$ the vibration frequency and by u the associated mode, i.e. the corresponding displacement field in Ω, which are solution of the eigenvalue problem for the linearized elasticity system

$$\begin{cases} -div(Ae(u)) = \omega^2 \rho u & in \quad \Omega \\ \qquad u = 0 & on \quad \Gamma_D \\ (Ae(u))n = g_i & on \quad \Gamma_N \end{cases} \qquad (2.10)$$

As is well known, (3.3) admits a countable infinite family of solutions $(\omega_k,$ $u_k)k \geq 1$ in $R^+ \times H^1(\Omega)^d$, labeled by increasing order of the eigenfrequency. The eigenfunction, or modes, are normalized by imposing that $\int_\Omega \rho|u_k|^2 dx = 1$. Furthermore, the

first (i.e. smallest) eigenfrequency is characterized as the minimum value of the Rayleigh quotient, namely

$$\omega_1^2 = \min_{\substack{\upsilon\in H^1(\Omega)^d, \upsilon\neq 0 \\ \upsilon=0\,on\,\Gamma_D}} \frac{\int_\Omega Ae(\upsilon)\cdot e(\upsilon)dx}{\int_\Omega \rho|\upsilon|^2 dx} \qquad (2.11)$$

To emphasize the dependence of the eigenfrequencies on the shape, we shall often denote them by $\omega_k(\Omega)$.

The objective function is denoted by $J(\Omega)$. In rigidity maximization it is common to maximize the first eigenfrequency. Since, by convention, we always minimize the objective function J, we consider

$$J(\Omega) = -\omega_1(\Omega)^2 \qquad (2.12)$$

We introduce a working domain D (a bounded open set of R^d) which contains all admissible shapes Ω. We define a set of admissible shapes of fixed volume V

$$U_{ad} = \{\Omega \subset D \quad such \quad that \quad |\Omega| = V\}. \qquad (2.13)$$

Our model problem of shape optimization is

$$\inf_{\Omega\in U_{ad}} J(\Omega)$$

2. Multiple loads optimization

We consider $n \geq 1$ possible loading configurations for a structure Ω, indexed by i: f_i is the vector-valued function of the volume forces and g_i that of the surface

loads. The corresponding displacement field u_i in Ω is the solution of the linearized

elasticity system

$$\begin{cases} -div(Ae(u_i)) = f_i & in \quad \Omega \\ \quad u_i = 0 & on \quad \Gamma_D \\ (Ae(u_i))n = g_i & on \quad \Gamma_N \end{cases} \qquad (2.14)$$

Since Ω is varying during the optimization process, f_i and g_i must be known for

all possible configurations of Ω. Therefore, introducing a working domain $D \subset R^d$ which

contains all admissible shapes Ω, we take $f_i \in L^2(D)^d$ and $g_i \in H^1(D)^d$. We assume

further that the surface measure of Γ_D is not zero (otherwise we should impose an

equilibrium condition on f_i and g_i). In such a case it is well known that (2.14) admits a

unique solution $u_i \in H^1(\Omega)^d$. A multiple loads problem is a problem for which the

objective function $J(\Omega)$ depends on the n displacement fields u_i. For simplicity, we focus

on the sum of the compliances, i.e. we consider

$$J(\Omega) = \sum_{i=1}^{n} \left(\int_\Omega f_i \cdot u_i dx + \int_{\Gamma_N} g_i \cdot u_i ds \right) = \sum_{i=1}^{n} \int_\Omega Ae(u_i) \cdot e(u_i) dx, \qquad (2.15)$$

which is very common in rigidity maximization. The single loading case $(n = 1)$, as well as

various other objective functions. Recall definition (2.13) of the set U_{ad} of admissible

shapes, our model problem of multiple loads shape optimization is

$$\inf_{\Omega \in U_{ad}} J(\Omega)$$

3. Shape representation by the level-set method

From the previous sections, we have all the necessary theoretical ingredients to introduce a gradient method for the minimization of an objective function $J(\Omega)$. The general form of its shape derivative is

$$J'(\Omega)(\theta) = \int_{\partial\Omega} \upsilon\theta \cdot n ds, \tag{2.16}$$

where $\theta \in W^{1,\infty}(R^d, R^d)$, the function υ is given by a result (2.13) or (2.14). Ignoring smoothness issues, a descent direction is found by defining a vector field

$$\theta = -\upsilon n,$$

and then we update the shape Ω as

$$\Omega_t = (Id + t\theta)\Omega,$$

where $t > 0$ is a small descent step. Formally, we obtain

$$J(\Omega_t) = J(\Omega) - t\int_{\partial\Omega} \upsilon^2 ds + O(t^2) \tag{2.17}$$

which guarantees the decrease of the objective function. This objective function is used into shape optimization software.

A suspension triangle is tested by this method. Figure 2.18 shows the working domain, its unstructured mesh (mostly made of quadrangles but with a few triangles), the boundary conditions and the two external forces. Each load is applied separately and corresponds to different situations of driving (breaking and accelerating). The intensity of the horizontal force is 8 times larger than that of the vertical force. The three disks (at each extremity and at the corner of the part) are not subject to optimization and are made of a

stiffer material (with Young modulus 80 times larger). The middle of the corner disk is fixed while one point in the upper left part of the upper disk is fixed, only in the horizontal direction. The loads are applied at the middle the lower right disk.
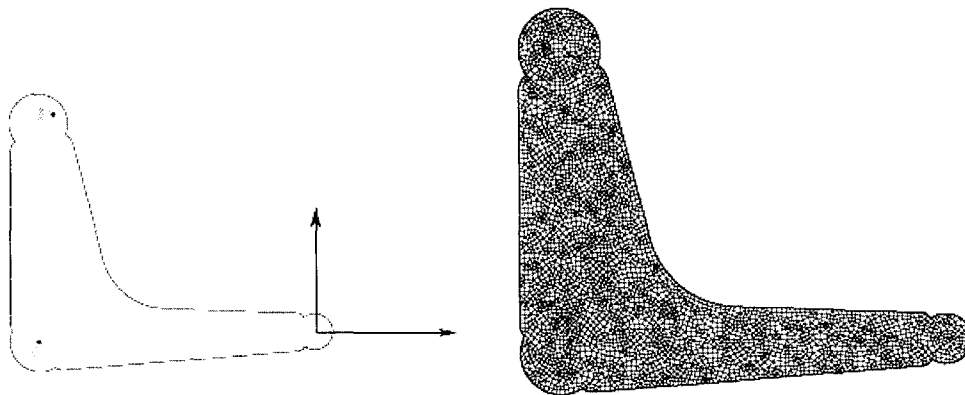
Figure 2.18   Boundary conditions and unstructured mesh of the suspension triangle.
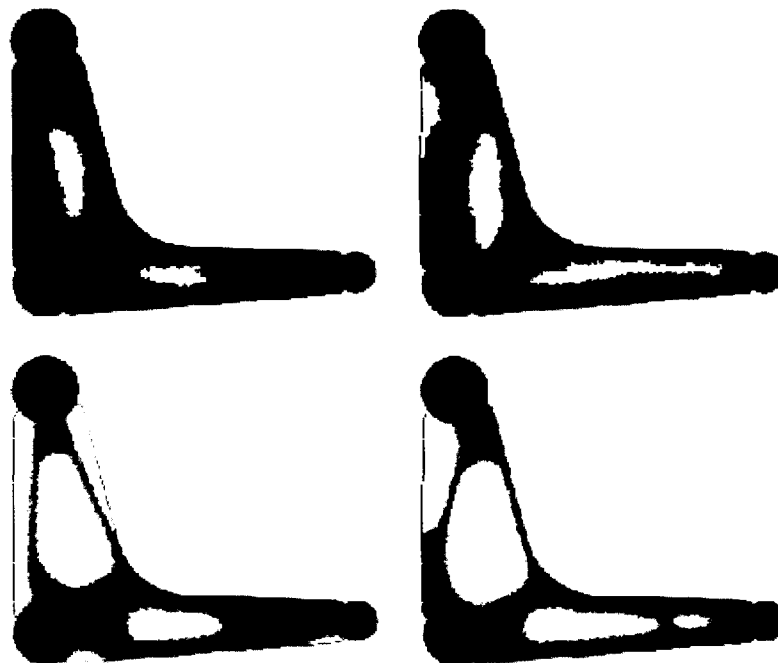
Figure 2.19   Two initializations (top) and the resulting optimal shapes (bottom) of the suspension triangle
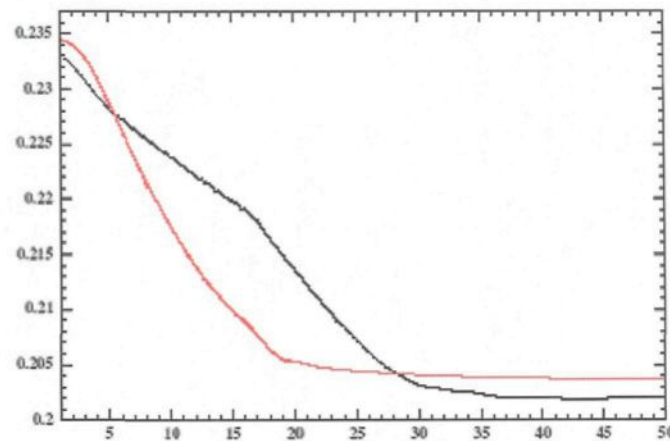
Figure 2.20   Convergence history of the objective function for the two initializations of the suspension triangle of Figure 2.19: plain line (left), dotted line (right).

According to the initial design the multiple loads optimization yields the shapes drawn on Figure 2.19. The resulting design is very sensitive to the initialization, even more in the multiple load case than for single load compliance optimization. As can be checked on Figure 2.20 the best design is obtained with the initialization of Figure 2.19 (right), which is not obvious to guess a priori.

2.6   ESO Optimization method

Evolutionary Structural Optimization (ESO) is a new technology that draws inspiration from nature to produce computer code that will always seek the optimum structure under any set of single or multiple circumstances. This new development from Australia can cater for size, shape and topology optimization.

The process of structural optimization has traditionally followed a parametric or design variable path where the shape or topology of an object was defined by a set of parameters. An optimization objective was set, such as minimum volume or maximum stiffness and the parameters adjusted, allowing for constraints, using a mathematical search engine such as sequential quadratic programming (SQP), to achieve this. After more than forty years of intensive research this still proves difficult and of limited success.

The ESO method developed in 1993 by Steven and Xie overcomes all of the difficulties associated with traditional methods and is able to cater for size, shape and topology optimization. It has also proved to be very general with its capabilities and can support: Totally general and multiple load environments including thermal loads and inertial loads. Totally general and multiple kinematics environments. Totally general structural shapes in 2D and 3D. Totally general and multiple material environments. Static, dynamic and stability optimization and combinations of these. Material and geometry non-linearity.

The process of ESO starts with a high density finite element mesh. Following multiple finite element analysis with all the load and kinematics environments catered for, each element is assessed for its effect on the optimization objectives, be theirs stress, stiffness, natural frequency or whatever, and if the element is not important to these objectives then it is removed. Elements are removed in a slow orderly way and after many analysis iterations, with tighter tolerances on the range of stress or strain, the final optimized structure evolves. Many practical situations have been examined and some have been manufactured to demonstrate the efficacy of the ESO method.

Simultaneously with the activity to make the ESO process amenable to real world situations is a parallel set of research activities directed towards establishing a formal mathematical basis for the success of the method in solving many classical problems. That the process be convex is important, that the optimums be global rather than local is important, that the algorithms be robust is important, that bench-marking be undertaken is important. It would be easy for engineers to say the answer is obvious, but has often been found there has to be a formal mathematical process by which that answer is achieved. This is where our research needs the assistance of mathematicians.

Through the literature review, we are familiarized with the properties of aluminum and its application for weight saving. We have also studied suspension systems, mechanical vibration and several optimization methods. Depending on these information and methods, we can choose the method that is the most suitable for our research. The ESO method has been chosen for this project.

CHAPTER 3

CHAPTER 3   Design of suspension control system

3.1   Kinematics study of different sub-systems

The following section presents the kinematics equations of a vehicle [25].

As we can see Figure 3.1, the vehicle is composed of three main parts: the chassis, the

suspension and the wheel. In general, there are two suspension, four bars and three bars

mechanisms.
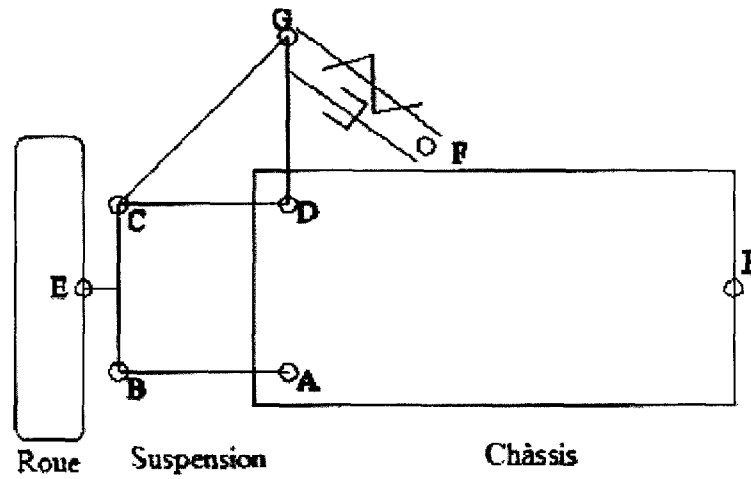
Figure 3.1   Simplified vehicle.

3.1.1 Four-bar mechanism

The four-bar mechanism is shown in Figure 3.2. It is defined by the point ABCD. Suppose the chassis rotate around the point P.
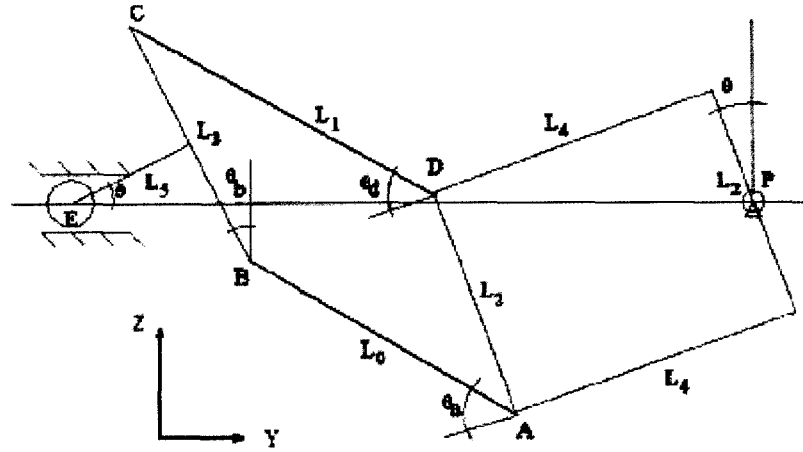
Figure 3.2   Four-bar mechanism.

The equations of position constraint:

The sum of the components at Y=0:

$$- L_2 \sin\theta - L_1 \cos(\theta_D - \theta) + L_3 \sin\theta_b + L_0 \cos(\theta_A - \theta) = 0 \qquad (3.1)$$

The sum of the components at Z=0:

$$L_2 \cos\theta + L_1 \sin(\theta_D - \theta) - L_3 \cos\theta_b - L_0 \sin(\theta_A - \theta) = 0 \qquad (3.2)$$

The sum of the components of the upper chord members at Z is equal to 0:

$$\frac{L_2}{2}\cos\theta - L_4 \sin\theta + L_1 \sin(\theta_D - \theta) - \frac{L_3}{2}\cos\theta_b - L_5 \sin\theta = 0 \qquad (3.3)$$

By solving these three equations with the Newtonian method for non-linear systems, we can find the values of θ_D, θ_b and θ_A as a function of θ .

The equations of speed constraint:

The speed at Z of the point E expressed with the superior chord members is equal to 0:

$$-\frac{L_2}{2}\sin\theta\dot{\theta} - L_4\cos\theta\dot{\theta} + L_1\cos(\theta_D - \theta)(\dot{\theta}_D - \dot{\theta}) + \frac{L_3}{2}\sin\theta_b\dot{\theta}_b - L_5\cos\theta\dot{\theta} = 0 \qquad (3.4)$$

The speed at Z of the point E expressed with the inferior chord members is equal to 0:

$$\frac{L_2}{2}\sin\theta\dot{\theta} - L_4\cos\theta\dot{\theta} + L_0\cos(\theta_A - \theta)(\dot{\theta}_A - \dot{\theta}) - \frac{L_3}{2}\sin\theta_b\dot{\theta}_b - L_5\cos\theta\dot{\theta} = 0 \qquad (3.5)$$

The sum of the speeds at Y of the two chord members is equal to:

$$-L_2\cos\theta\dot{\theta} + L_1\sin(\theta_D - \theta)(\dot{\theta}_D - \dot{\theta}) - L_0\sin(\theta_A - \theta)(\dot{\theta}_A - \dot{\theta}) + L_3\cos\theta_b\dot{\theta}_b = 0 \qquad (3.6)$$

By solving these three equations with the Newtonian method for non-linear systems, we can thus find the angular velocities values of $\dot{\theta}_D$, $\dot{\theta}_b$ and $\dot{\theta}_A$ as a function of $\dot{\theta}$.

3.1.2 Three-bar mechanism

The three-bar mechanism as shown by Figure 3.3, the sum of the components at Y=0:

Figure 3.3   Three-bar mechanism.

$$- L_7 \cos\theta_F - L_8 \sin\theta_D + L_9 = 0 \tag{3.7}$$

The sum of the components at Z=0:

$$L_7 \sin\theta_F - L_8 \cos\theta_D + L_{10} = 0 \tag{3.8}$$

By solving these two equations with the Newtonian method for non-linear system, we can find the values of $\dot{\theta}_F, L_7$ as a function of θ_D.

By finding the rate of change of L_7 as a function of time, we can find the force exerted by the mass system, spring and shock absorber.

$$\theta_H = \pi/2 - \theta_F \tag{3.9}$$

$$\theta_I = \pi/2 - \theta_D - \theta_H \tag{3.10}$$

$$L_7 = L_8 \dot{\theta}_D \cos\theta_I \tag{3.11}$$

We find that the force exerted by the mass system, spring and shock absorber is represented by the following:

$$F_7 = K(S + L_{10} - L_7) + C\dot{L}_7 \tag{3.12}$$

where S represent the initial compression of the spring and C, the dynamic viscosity coefficient of the shock absorber.

3.1.3 General suspension model

Generally, automotive suspension is represented by a two-degree of freedom systems. The suspension system is described by the equation of motion (see Figure 3.4) [13]:
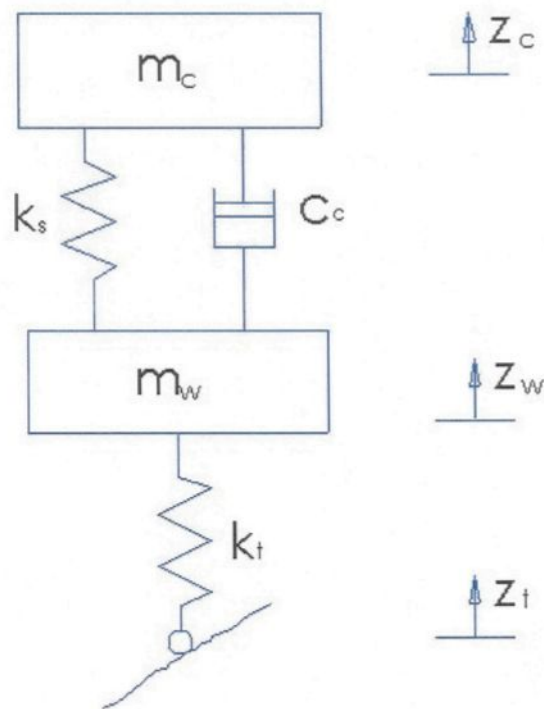
Figure 3.4   The suspension model

$$m_c \ddot{z}_c = -K_s(z_c - z_w) - C_c(\dot{z}_c - \dot{z}_w)$$
$$m_w \ddot{z}_w = K_s(z_c - z_w) + C_c(\dot{z}_c - \dot{z}_w) - K_w(z_w - z_t)$$

(3.13)

Where:

m_c : Mass of chassis;

m_w : Mass of wheel with suspension;

K_s : Coefficients of linear stiffness for spring;

C_c : Coefficients of damping for damper;

K_t : Coefficients of linear stiffness for tire;

$\left(z_c - z_w\right)$: Suspension deflection;

$\dot{z}_c$: Absolute velocity of the mass of chassis;

$\left(z_w - z_t\right)$: Tire deflection;

$\dot{z}_w$: Absolute velocity of the mass of wheel;

$\ddot{z}_c$: Absolute acceleration of the mass of chassis;

$\ddot{z}_w$: Absolute acceleration of the mass of wheel.

In this case, four springs and four dampers support a car weighing 1600 kg; the chassis weight is 1200 kg. (300 kg on each wheel) and the wheel unsprung weight is 40 kg /wheel. For illustrative purposes, we will use a simplified example as shown in Figure 3.4 that avoids suspension system kinematics complexities. we will only study a quarter vehicle model. Figure 3.5 represents suspension arm structures [14]. R_1 and R_2 are upper and lower arms. Our objective is the design of these two aluminum suspension arms that were originally in steel.
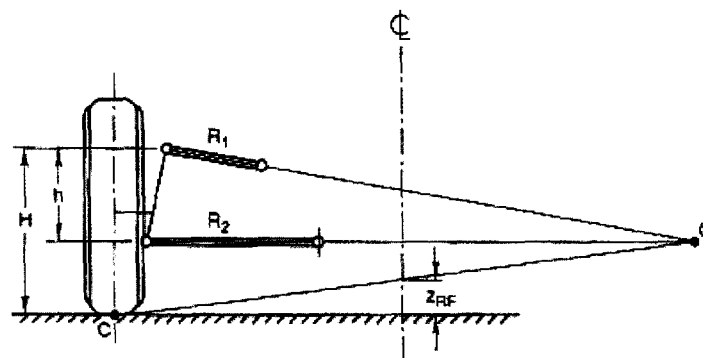
Figure 3.5   Suspension arm structures.

3.2   Design of aluminum suspension arms

Our approach to realize this design is by the numerical method. The design of upper arm is shown in Figure 3.6. The weight is 1.19 kg and the size is 320mm x 260mm x 68mm [26, 27 and 28].

We choose the thixoforming A357 for upper arm. The advantages of thixoforming A357 are: a) Dimensional precision. b) Lightweight. c) Complex net shapes. d) Low porosity. e) High volume. f) Thin wall capability. g) Competitive pricing.

The properties of A357 [29]:

Density: 2670.3 kg/m³

Heat treat: T6

Tensile strength: 330-358MPa

Yield strength: 275Mpa

Elong.:   9%

Elastic modulus: 70-80 GPa

Poisson's ratio: 0.33
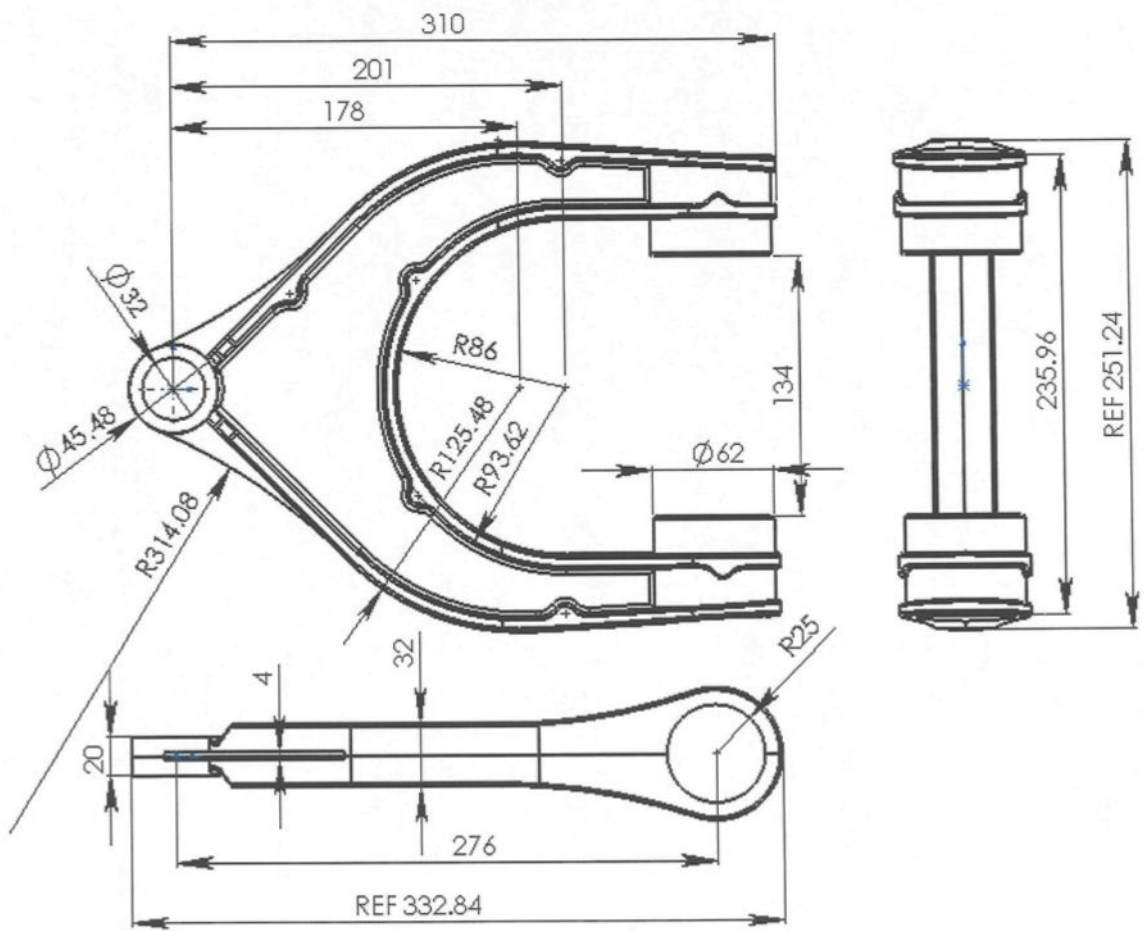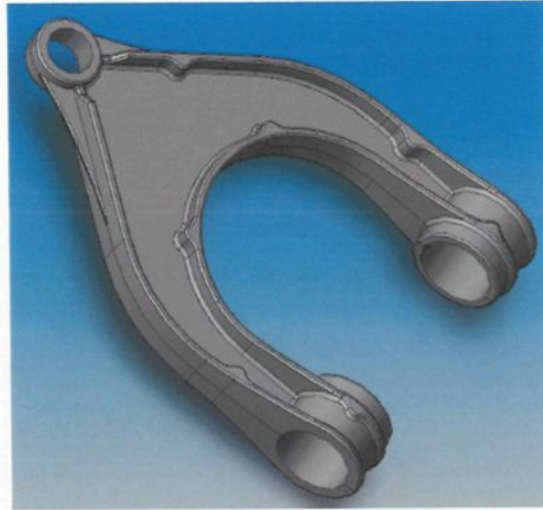
Figure 3.6 Aluminum alloy suspension upper control arm.

The suspension lower arm design is shown in Figure 3.7. The weight is 1.56 kg and the size is 335mm x 240mm x 50mm [26, 27 and 28].

We choose aluminum 6061-T6 for suspension control lower arms. The advantages of aluminum alloy 6061 [30]: Excellent joining characteristics, good acceptance of applied coatings; combines relatively high strength, good workability and high resistance to corrosion. It's also widely available.

The properties of Aluminum 6061-T6:

Density: 2700 kg/m^3

Tensile strength: 310MPa

Yield strength: 275Mpa

Elong.:   12%

Elastic modulus: 73.1GPa

Poisson's ratio: 0.33
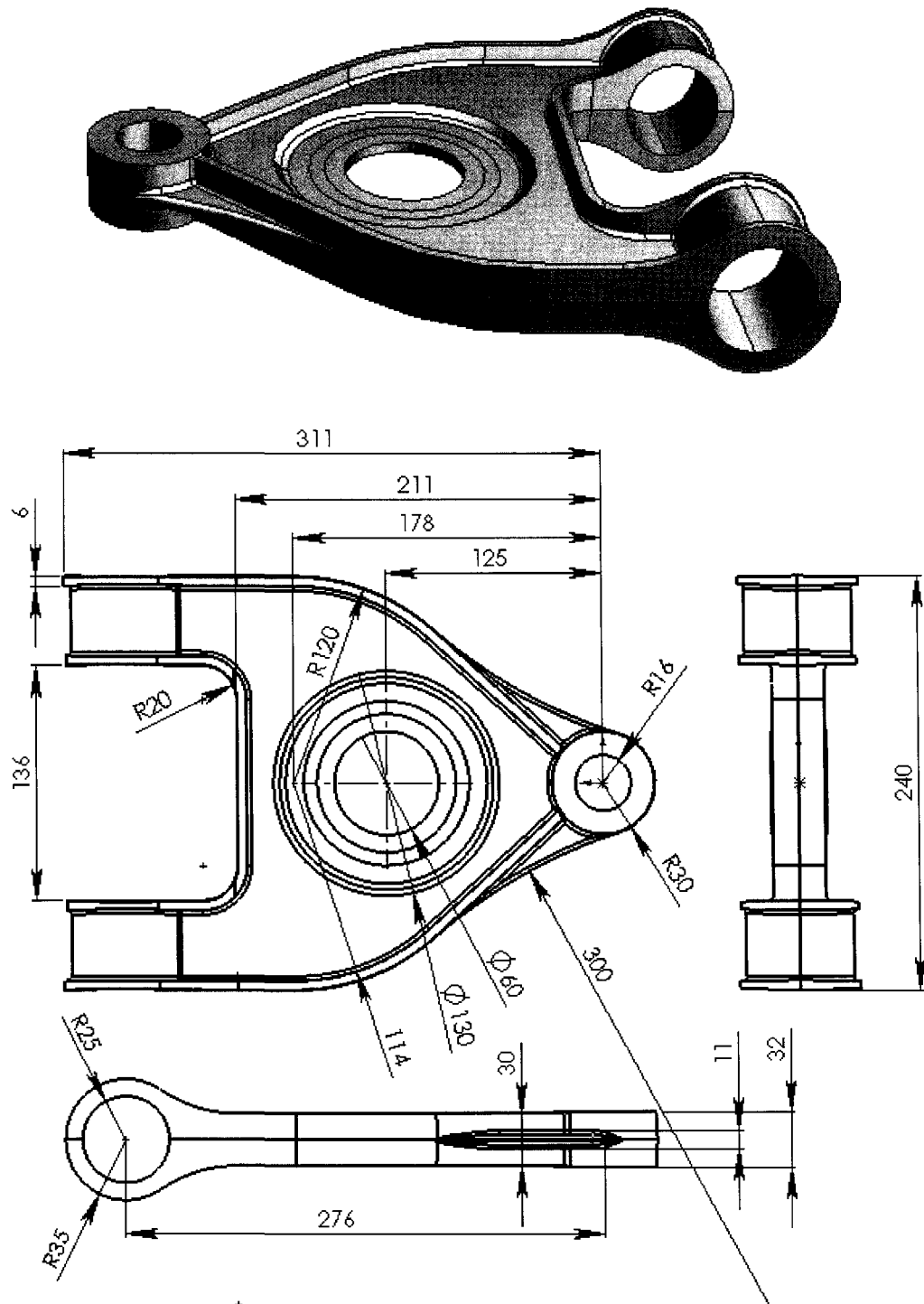
Figure 3.7   Aluminum alloy suspension lower control arm.

These typical automobile suspension arms have been chosen for the static, dynamic and vibration analysis that will allow us to cut down weight and develop shape. This takes advantage of the geometric modeling and automatic analyzing capabilities of the parametric associative CAD system. In our situation, we are doing shape development by Abaqus. This software can't to do shape optimization automatically. But it can measure the strength for each element and give us necessarily information. So we can do development parts by ESO method. The ESO is evolutionary structural optimization, it is described below:

First, we have a safety factor defined by $\dfrac{\sigma_y}{\sigma_{max}}$=k (k=1.05-1.15), σ_y is yield strength and σ_{max} is maximum strength of the part under the force. So σ_{max} should be less than σ_y .

Then we verify that the rate $\dfrac{\sigma_e}{\sigma_{max}}$<75% ($\sigma_e$<$\sigma_y$), where σ_e represent the stress of element. So the objective function can be written as $f(\sigma) = \dfrac{\sigma_e}{\sigma_{max}} < value$ (the value<75%).

In this area, we can cut the materials for reducing the weight. Depending on this function, we can reduce the weight and optimizing the shape of parts.

In this chapter, we have studied automobile suspension kinematics and structure; designed the suspension upper arms and lower arm; and introduced the objective function to develop the suspension arms.

CHAPTER 4

CHAPTER 4   Mechanical simulation and analysis of suspension arms

4.1   Theory of modelization

4.1.1   Equations of elasticity

A problem in analysis of stress and strain arises from a situation in which a body is subjected to certain actions. These may be applied forces, temperature changes, accelerations, or specified displacements of certain points of the body, and the resulting stresses, strains, and displacement are to be determined. The applied forces may act at various points on the surface of the body (concentrated forces), or they may be distributed over part of the surface of the body (distributed loads), or they may act on elements within the body (body forces) if the body is accelerating. In here, we shall derive the equations of elasticity whose solution will give the stresses, strains, and displacements of a loaded body. A statement of the conditions imposed on a problem in elasticity is as follows [31]:

1)   Every element of mass in the body is in a state of equilibrium or, more generally, Newton's second law must be satisfied.

2)   The material of which the body is composed has specified stress-strain relations.

3)   The strains are functions of the derivatives of the displacements.

4)   The stresses, strains, and displacements must be consistent with the prescribed

loading and constraints of the body.

The first of these is a physical law that must be satisfied, the second is a statement of the properties of the material, the third is a geometrical condition, and the last is the loading condition or, as it is sometimes called, the boundary condition. In order to make a stress analysis of a body, the four conditions listed above must be stated in mathematical terms. That is the equations of elasticity. For simplification reasons, we just consider plane stress and plane strain in this research. Figure 4.1 show an element dx, dy, dz with these stresses acting. In boundary conditions, the unit vector **n** normal to the surface and directed out of the body as shown in Figure 4.2. The equilibrium, compatibility and boundary conditions equations completely describe the problem, and the solution of these equations gives the stress in the body for the plane stress and plane strain problems [31].
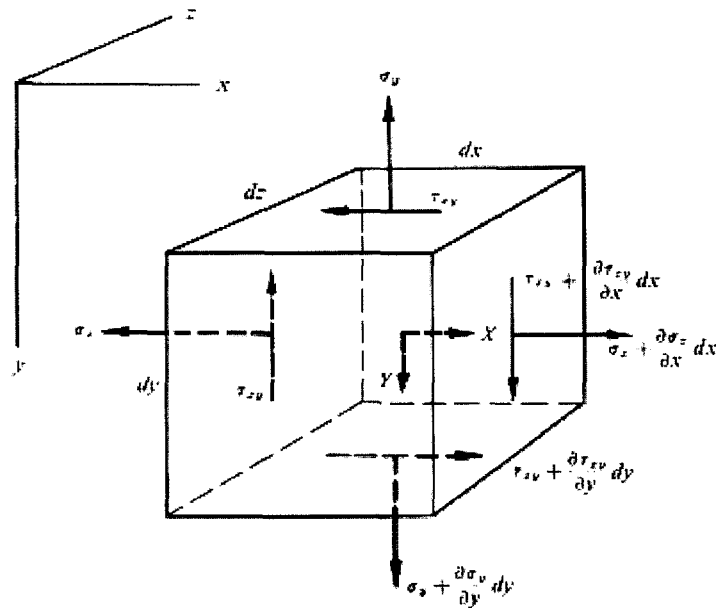
Figure 4.1   An element dx, dy, dz with these stresses acting.
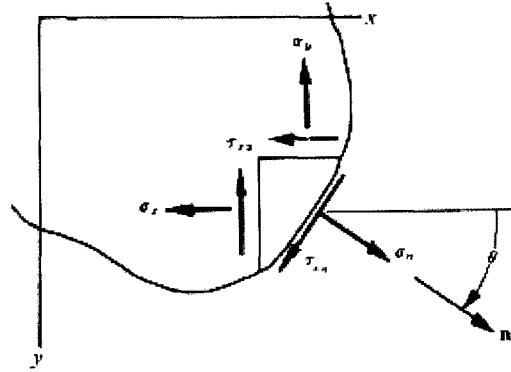
Figure 4.2 Boundary condition.

Assumed: $\sigma_z = \tau_{xy} = \tau_{yz} = 0$

$$\left.\begin{array}{l} \dfrac{\partial \sigma_x}{\partial x} + \dfrac{\partial \tau_{xy}}{\partial y} + X = 0 \\[3mm] \dfrac{\partial \sigma_y}{\partial y} + \dfrac{\partial \tau_{xy}}{\partial x} + Y = 0 \end{array}\right\} \quad \text{Equilibrium} \qquad\qquad (4.1)$$

$$\left(\dfrac{\partial^2}{\partial x^2} + \dfrac{\partial^2}{\partial y^2}\right)\left(\sigma_x + \sigma_y\right) = -\left(1 + \nu\right)\left(\dfrac{\partial X}{\partial x} + \dfrac{\partial Y}{\partial y}\right) \quad \text{Compatibility} \qquad (4.2)$$

$$\left.\begin{array}{l} \sigma_n = \dfrac{\sigma_x + \sigma_y}{2} + \dfrac{\sigma_x - \sigma_y}{2}\cos 2\theta + \tau_{xy}\sin 2\theta \\[4mm] \tau_{sn} = -\dfrac{\sigma_x - \sigma_y}{2}\sin 2\theta + \tau_{xy}\cos 2\theta \end{array}\right\} \quad \text{Boundary conditions} \quad (4.3)$$

Where

The forces X and Y are body forces per unit of volume that act in the x-and y-directions.

The vector **n** is normal to the surface.

ν is Poisson's ratio.

4.2 Procedure of simulation

4.2.1 Numerical method software

The ABAQUS suite for finite element analysis (FEA) is known for its high performance, quality and ability to solve all kinds of challenging simulations. Whether we need to understand the detailed behaviour of a complex assembly, explore some concepts for a new design, or simulate a manufacturing process. ABAQUS performs static and/or dynamic analysis and simulation on structures. It can deal with bodies with various loads, temperatures, contacts, impacts, and other environmental conditions. ABAQUS includes four functional components [32, 33]:

- Analysis Modules [34]

- Preprocessing Module

- Postprocessing Module

- Utilities

There are eight steps to do analysis stress and deformation with Abaqus software [35]:

1) The input file (In the part module): A finite element analysis in Abaqus is defined by an input file; it can be created by using a text editor or by using a graphical pre-processor. In this study, the "step" file is used as input file. Model data define the nodes, elements, materials, initial conditions, etc..

2) Material definitions (In the property module): the properties of the material must be defined.

3) Defining an assembly (In the assembly module): The geometry of a model can be defined by organizing it into parts, which are positioned relative to one another in an assembly.

4) Step definitions (In the step module): The step sequence provides a convenient way to capture changes in the loading and boundary conditions of the model. In addition, steps allow you to change the analysis procedure, the data output and various controls.

5) Load definitions (In the load module): a) Boundary conditions: Zero-valued boundary conditions (including symmetry conditions) can be imposed on individual solution variables such as displacements or rotations. b) Amplitude force can be defined for later use in specifying time-dependent loading.

6) Mesh (In the mesh module): Tools for prescribing mesh density at local and global levels; model coloring that indicates the meshing technique assigned to each region in the model; A variety of mesh controls, such as element shape, meshing technique and meshing algorithm.

7) Job (In the job module): Perform analysis.

8) Visualization (In the Visualization module): Analysis results.

4.3   Analysis of strength of aluminum upper arms for weight cutting

In this analysis process, we are doing simulation analysis steps for suspension upper arm in order to verify their stress. Furthermore, the position displacement and reaction force are analysed as well.

- **Input part:** Suspension upper arm is designed with Solidworks. It is transformed to STEP file, and then we input it to Abaqus. The overall size is 0.32mX0.26mX0.068m.

- **Property setting:** The upper control arm is made in A357, so we set the density to 2670kg/m³, Elastic young's modulus 7e+10P$_a$ and Poisson's ratio 0.33.

- **Step setting:** In simulation analysis, the step can calculate the stress response of parts, especially to verify the stress of the parts. There are kind of steps that you can choose such as static, dynamic, frequency and so on. In this step setting, we choose dynamic analysis.

- **Load setting:** 1) Boundary condition: According to the automobile suspension system developed in chapter 3, we set the boundary condition at the two holds (see Figure 4.3 and Figure 4.4). We consider two kinds of conditions: First, all direction and rotation are fixed (axes: X=Y=Z=0; Rotation: URx=URy=URz=0). We call BC fixed. The second one is axes X=Z=Free, Y=0; Rotation URz, URx=0, URy=0.52. We call BC UR2. 2) Horizontal force 2500N [36] is loaded with amplitude curve in X direction and vertical force 2500N [36] is loaded with amplitude curve in Z direction (see Figure 4.5, Figure 4.6 and Table 4.1).
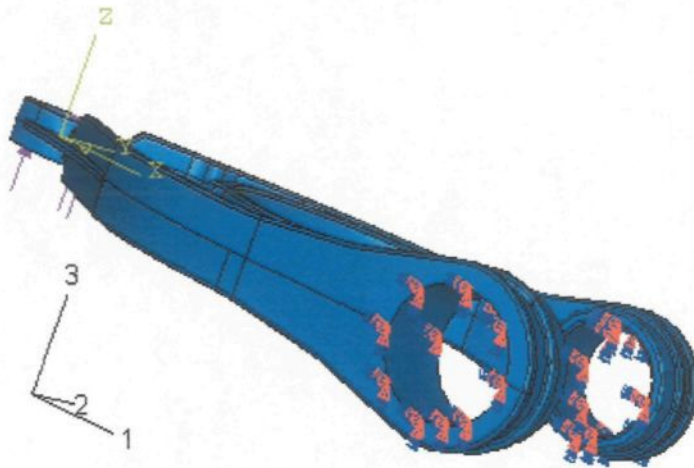
Figure 4.3   Boundary condition fixed.
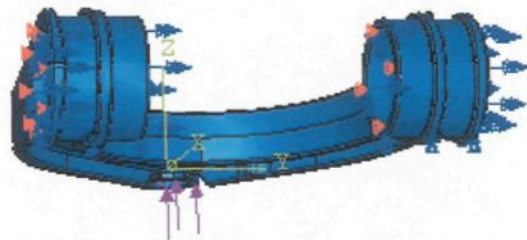
Figure 4.4   Rotation boundary condition.
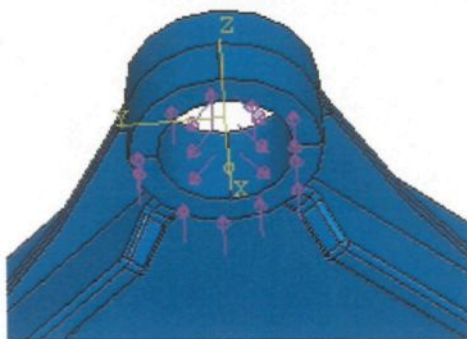
Figure 4.5   Force loading.

Time(s)	Amplitude	Time(s)	Amplitude	Time(s)	Amplitude
1.00E-02	0.12527	0.35	-0.9503651	0.69	0.6877446
2.00E-02	0.2485665	0.36	-0.9818549	0.7	0.591387
3.00E-02	0.3679469	0.37	-0.997876	0.71	0.4857123
4.00E-02	0.4815304	0.38	-0.9981758	0.72	0.3723855
5.00E-02	0.5875275	0.39	-0.9827498	0.73	0.2531918
6.00E-02	0.6842684	0.4	-0.9518409	0.74	0.1300085
7.00E-02	0.7702289	0.41	-0.905936	0.75	4.78E-03
8.00E-02	0.8440548	0.42	-0.8457586	0.76	-0.1205285
9.00E-02	0.9045828	0.43	-0.7722566	0.77	-0.2439357
1.00E-01	0.9508594	0.44	-0.6865876	0.78	-0.3634999
0.11	0.9821557	0.45	-0.5901021	0.79	-0.4773372
0.12	0.9979784	0.46	-0.4843197	0.8	-0.5836543
0.13	0.9980784	0.47	-0.3709067	0.81	-0.6807767
0.14	0.9824539	0.48	-0.2516505	0.82	-0.7671731
0.15	0.9513514	0.49	-0.1284297	0.83	-0.841483
0.16	0.9052606	0.5	-3.19E-03	0.84	-0.9025356
0.17	0.8449077	0.51	0.1221093	0.85	-0.9493692
0.18	0.7712437	0.52	0.2454799	0.86	-0.9812459
0.19	0.6854289	0.53	0.364983	0.87	-0.9976634
0.2	0.5888156	0.54	0.478736	0.88	-0.998363
0.21	0.4829256	0.55	0.5849473	0.89	-0.9833338
0.22	0.3694272	0.56	0.6819423	0.9	-0.9528126
0.23	0.2501089	0.57	0.7681936	0.91	-0.9072802
0.24	0.1268499	0.58	0.8423423	0.92	-0.847454
0.25	1.59E-03	0.59	0.9032203	0.93	-0.7742759
0.26	-0.1236898	0.6	0.9498683	0.94	-0.6888999
0.27	-0.2470234	0.61	0.9815518	0.95	-0.5926705
0.28	-0.3664656	0.62	0.997771	0.96	-0.4871038
0.29	-0.4801339	0.63	0.9982707	0.97	-0.373863
0.3	-0.5862379	0.64	0.9830431	0.98	-0.2547322
0.31	-0.6831062	0.65	0.952328	0.9899999	-0.1315881
0.32	-0.7692122	0.66	0.9066094	1	-6.37E-03
0.33	-0.8431996	0.67	0.8466074	………..	………..
0.34	-0.9039028	0.68	0.7732671	2.5	-1.59E-02

Table 4.1   Sinusoidal amplitude data of upper arm
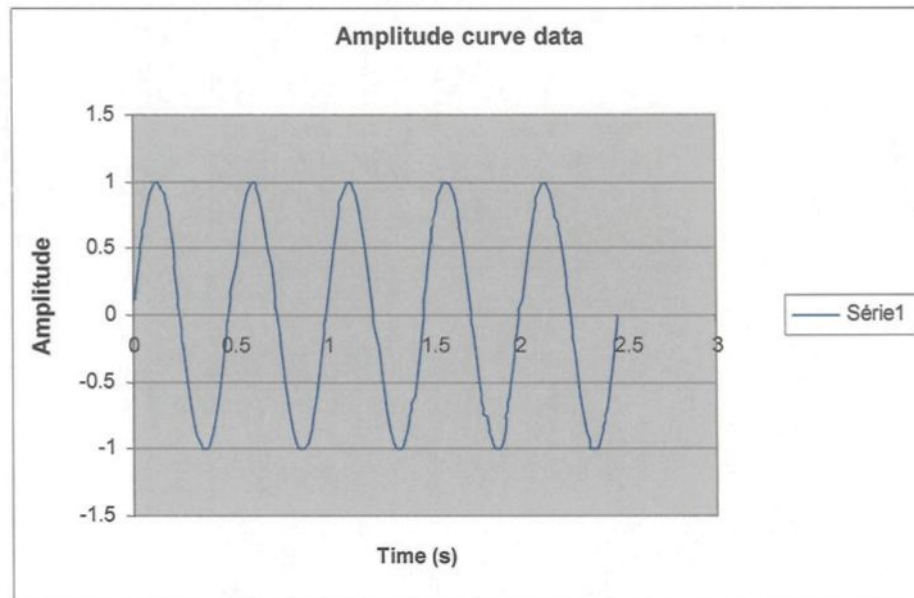
Figure 4.6   Amplitude curve data of upper arm.

- **Mesh part:** 1) Size control: Approximate global size is 0.004, minimum size is 0.2 and deviation factor is default. 2) Mesh control: element shape is Tet shape. 3) Element type is C3D4, standard and linear with 3D stress. Total number of elements is 72503 and number of nodes is 18283. Mesh part is shown in Figure 4.7

- **Job submits:** Full analysis, analysis input file processor memory is 1000.

- **Visualization:** upper arm output results: 1) Stress Mises contour is shown on Figure 4.8; boundary condition is in all directions and rotation is fixed. Maximum stress is 203.6 MPa (at element 39550, it is shown in Figure 4.9). It is less than yield strength (275 Mpa) of aluminum A357. 2) Maximum displacement at node 687 is 3.7mm (see Figure 4.10 and Figure 4.11). 3) Maximum reaction force is 488N at node 7744. It is shown in Figure 4.12 and Figure 4.13.

Figure 4.7   Mesh upper arm.

S, Mises
(Ave. Crit.: 75%)
+2.036e+08
+1.866e+08
+1.696e+08
+1.527e+08
+1.357e+08
+1.188e+08
+1.018e+08
+8.482e+07
+6.786e+07
+5.090e+07
+3.393e+07
+1.697e+07
+2.466e+03

Max +2.036e+08
 at elem ALARM-1.39550 node 5777

Min +2.466e+03
 at elem ALARM-1.20325 node 2016

Element 39550
Node 5777

ODB: Job-upperarm-fix.odb   ABAQUS/STANDARD Version 6.5-1

Step: Step-dynamic, Dynamic
Increment   12: Step Time =   0.1200
Primary Var: S, Mises
Deformed Var: CF   Deformation Scale Factor: +1.000e+00

Figure 4.8   S:Mises contour of upper arm, BC fixed.
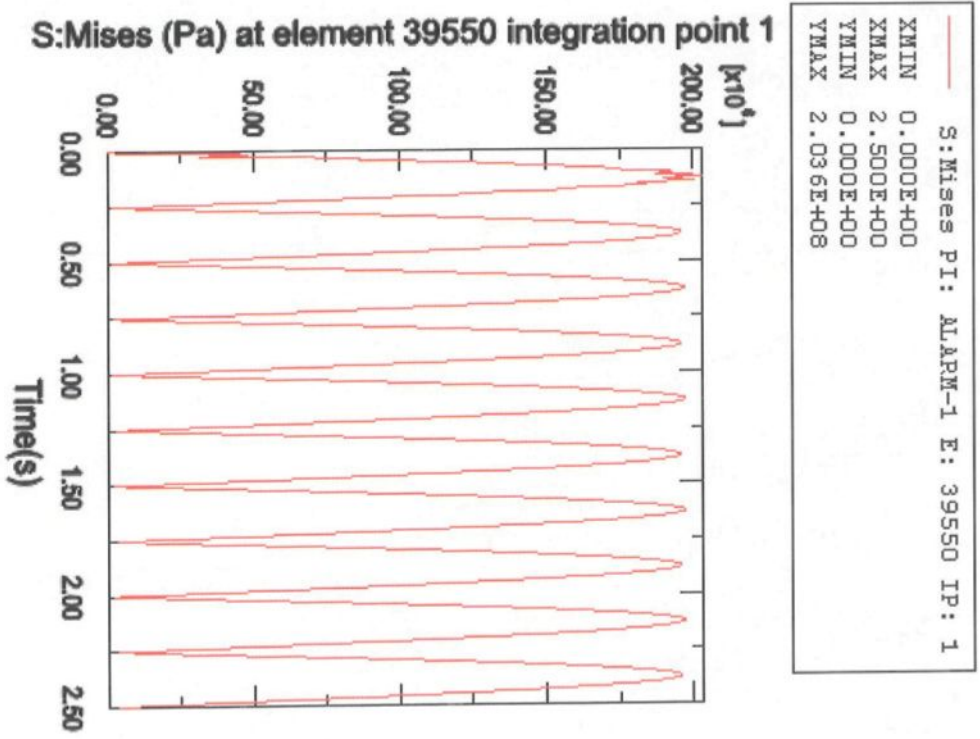
Figure 4.9   Max. S:Mises at element 39550, BC fixed.

U, Magnitude
+3.745e-03
+3.433e-03
+3.121e-03
+2.809e-03
+2.497e-03
+2.185e-03
+1.872e-03
+1.560e-03
+1.248e-03
+9.362e-04
+6.242e-04
+3.121e-04
+0.000e+00
Max +3.745e-03
  at node ALARM-1.687
Min +0.000e+00
  at node ALARM-1.145

Node 687

ODB: Job-upperarm-fix.odb   ABAQUS/STANDARD Version 6.5-1

Step: Step-dynamic, Dynamic
Increment   12: Step Time =   0.1200
Primary Var: U, Magnitude
Deformed Var: U   Deformation Scale Factor: +8.899e+00

Figure 4.10   Position displacement contour and location at node 687, BC fixed.
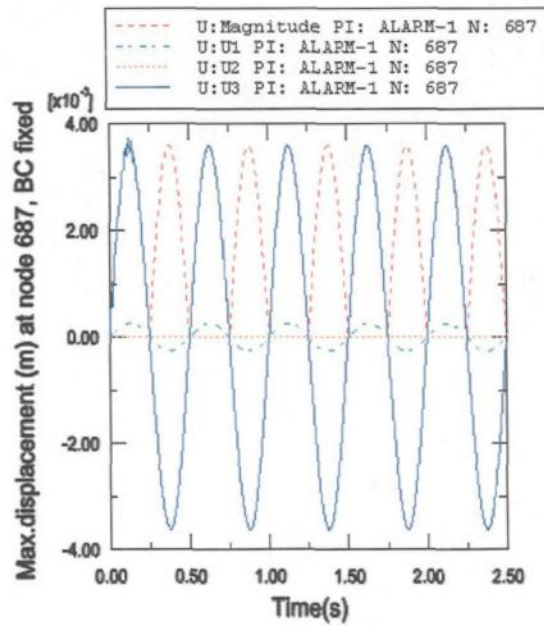
Figure 4.11   Max. Displacement at node 687, BC fixed.

RF, Magnitude
+4.884e+02
+4.477e+02
+4.070e+02
+3.663e+02
+3.256e+02
+2.849e+02
+2.442e+02
+2.035e+02
+1.628e+02
+1.221e+02
+8.139e+01
+4.070e+01
+0.000e+00
Max +4.884e+02
 at node ALARM-1.7744
Min +0.000e+00
 at node ALARM-1.1

Node 7744

ODB: Job-upperarm-fix.odb   ABAQUS/STANDARD Version 6.5-1

Step: Step-dynamic, Dynamic
Increment   12: Step Time =   0.1200
Primary Var: RF, Magnitude
Deformed Var: CF   Deformation Scale Factor: +1.000e+00

Figure 4.12   Reaction force contour and location at node 7744, BC fixed.

RF:Magnitude PI: ALARM-1 N: 7744
RF:RF1 PI: ALARM-1 N: 7744
RF:RF2 PI: ALARM-1 N: 7744
RF:RF3 PI: ALARM-1 N: 7744

[x10³]
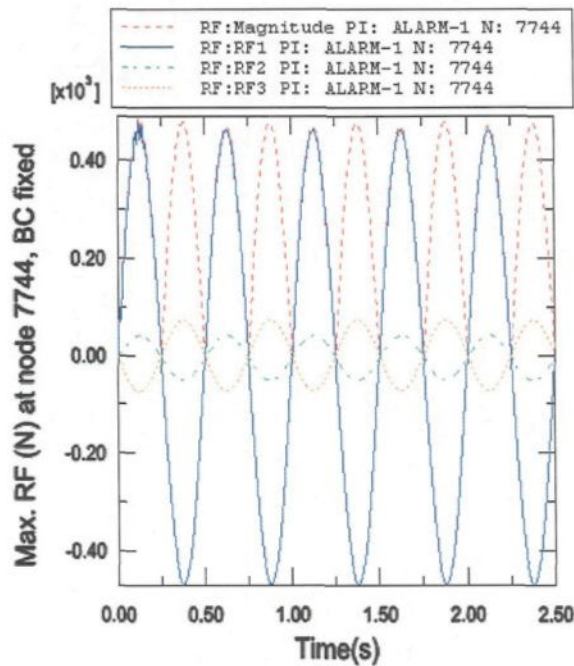
Figure 4.13   Max. Reaction force at node 7744, BC fixed.

Repeat all steps; modify the boundary condition to Rotation with axes Y. The range of rotation is from -15° to +15°. The result is shown below:

1) The boundary condition is axes X, Z free and axis Y is fixed and rotation with axes Y. Maximum stress is 109 MPa at element 39550 (see Figure 4.14) and Stress Mises contour is shown in Figure 4.15. It is less than yield strength (275 Mpa) of aluminum A357.

2) Maximum reaction force is 53N at node 3092 (See Figure 4.16 and Figure 4.17).
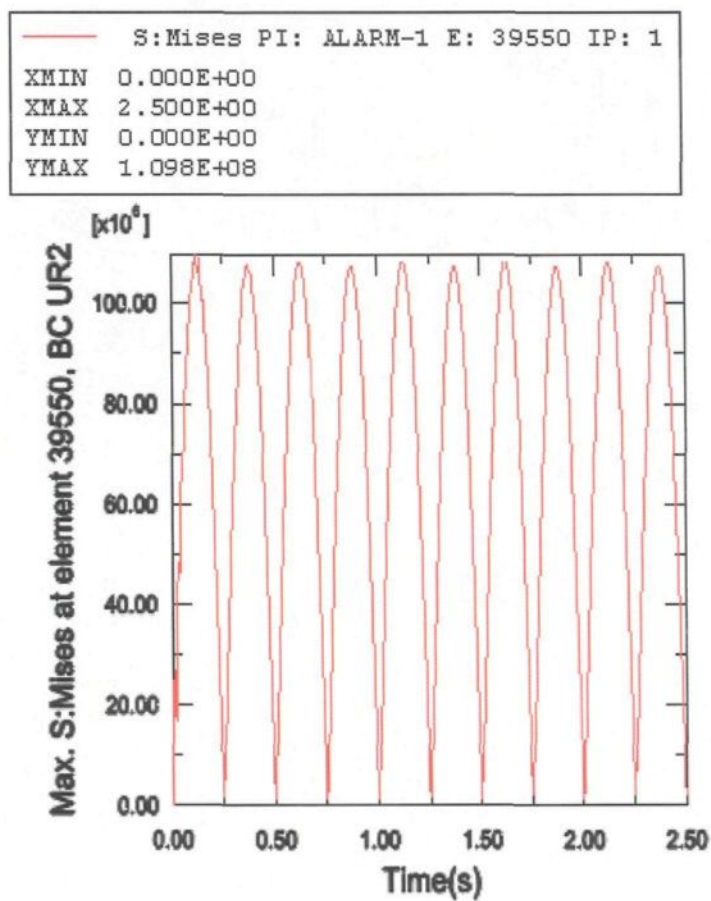
Figure 4.14   Max. S:Mises at element 39550, BC UR2.

S, Mises
(Ave. Crit.: 75%)
```
  +1.098e+08
  +1.007e+08
  +9.160e+07
  +8.247e+07
  +7.335e+07
  +6.423e+07
  +5.510e+07
  +4.598e+07
  +3.686e+07
  +2.773e+07
  +1.861e+07
  +9.487e+06
  +3.633e+05
```
Max +1.098e+08
 at elem ALARM-1.39550 node 5777

Min +3.633e+05
 at elem ALARM-1.23375 node 1702
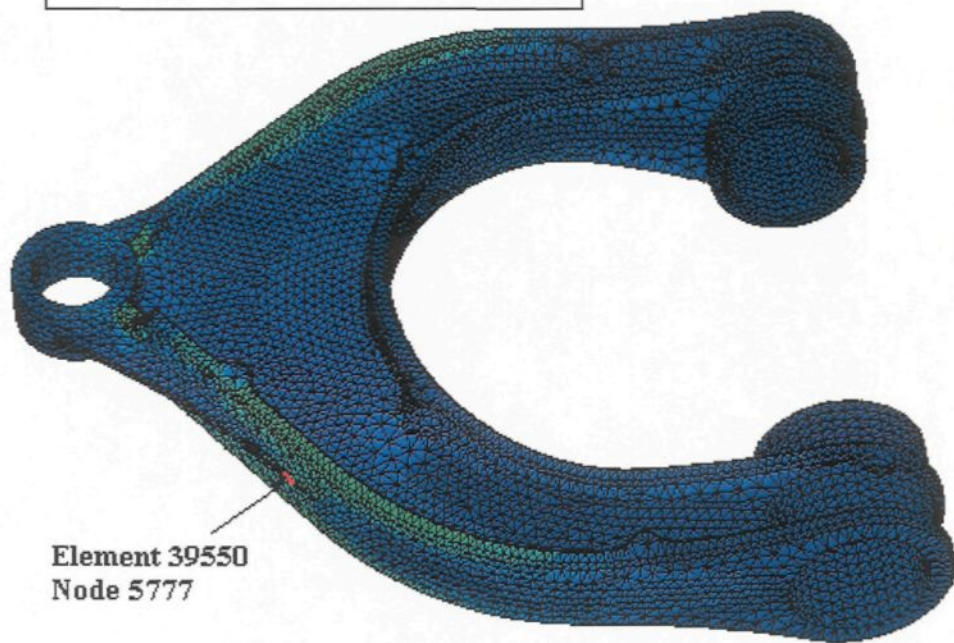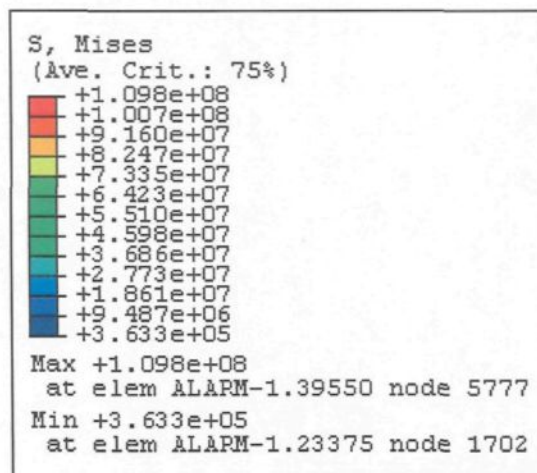
Element 39550
Node 5777

ODB: Job-upperarm-UR2.odb   ABAQUS/STANDARD Version 6.5-1

Step: Step-dynamic, Dynamic
Increment   12: Step Time =   0.1200
Primary Var: S, Mises
Deformed Var: CF   Deformation Scale Factor: +1.000e+00

Figure 4.15   S:Mises contour of upper arm, BC UR2.

```
RF, Magnitude
   +5.299e+01
   +4.857e+01
   +4.415e+01
   +3.974e+01
   +3.532e+01
   +3.091e+01
   +2.649e+01
   +2.208e+01
   +1.766e+01
   +1.325e+01
   +8.831e+00
   +4.415e+00
   +0.000e+00
Max +5.299e+01
  at node ALARM-1.3092
Min +0.000e+00
  at node ALARM-1.1
```

Node 3092

ODB: Job-upperarm-UR2.odb   ABAQUS/STANDARD Version 6.5-1

Step: Step-dynamic, Dynamic
Increment   12: Step Time =   0.1200
Primary Var: RF, Magnitude
Deformed Var: CF   Deformation Scale Factor: +1.000e+00

Figure 4.16   Reaction force contour and location at node 3092, BC UR2.
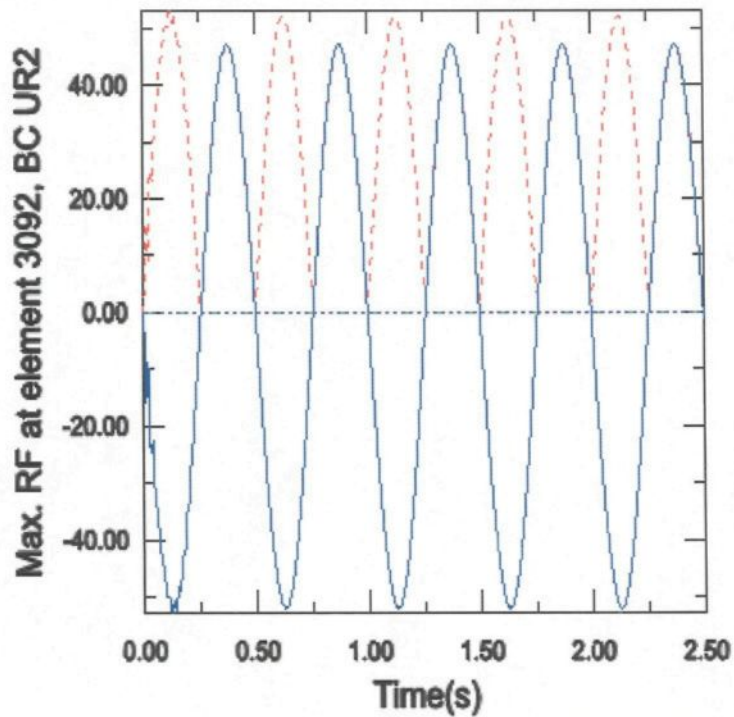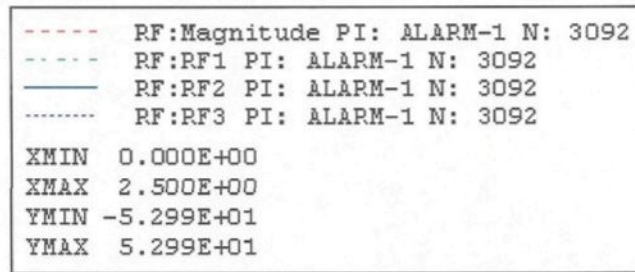
Figure 4.17   Max. Reaction force at node 3092, BC UR2.

From the results, we can see the design of aluminum suspension upper arm is successful to replace the steel one. According to ESO method, we can continue to render the aluminum piece lighter.

4.4 Shape optimization for upper arm

4.4.1 Analyse strength of optimization upper arm with sinusoidal force

Shape development for upper arm depends on our objective function (in chapter 3). The first simulation analysis is done; we change the design of upper control arm to Figure 4.18 below, then we proceed the same way as above to verify the strength of part. Repeat all steps except the mesh step, because the shape changed.

- **Mesh part:** 1) Size control: Approximate global size is 0.004, minimum size is 0.2 and deviation factor is default. 2) Mesh control: element shape set to Tet shape. 3) Element type C3D4, standard and linear with 3D stress. Total number of elements is 108996 and number of nodes is 26173 for developed upper arm.

- **Visualization:** upper arm output results after shape changed: 1) The boundary condition states that all directions and rotation fixed. Maximum stress is 152.5 MPa (at element 61192, it is shown in Figure 4.19) and the stress Mises contour is shown on Figure 4.20. It is less than yield strength (275 Mpa) of aluminum A357. 2) Maximum position displacement at node 794 is 4.2mm (see Figure 4.21 and Figure 4.22). 3) Maximum reaction force is 318N at node 13518. It is shown in Figure 4.23 and Figure 4.24.
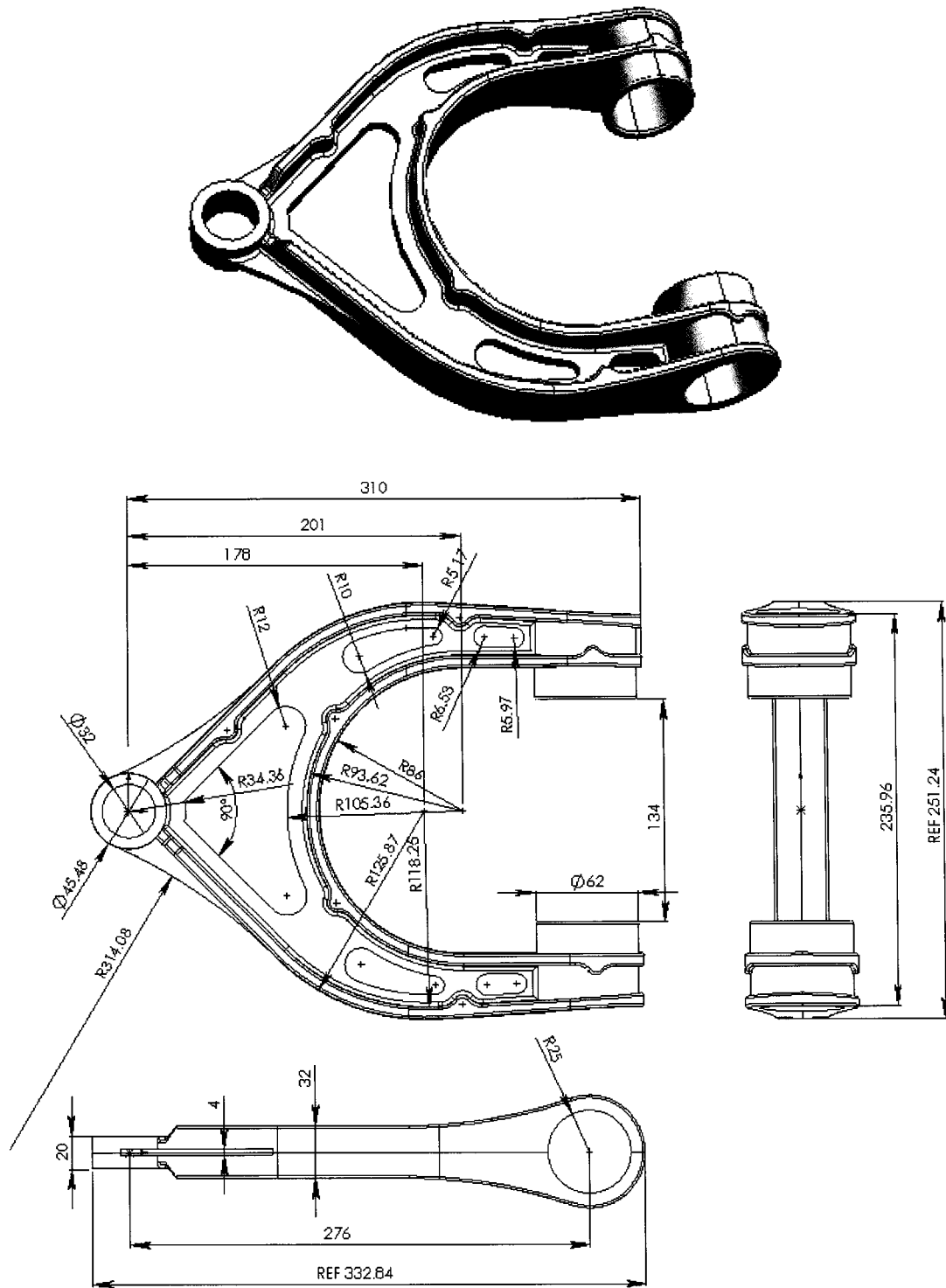
Figure 4.18 Development of design for upper arm.
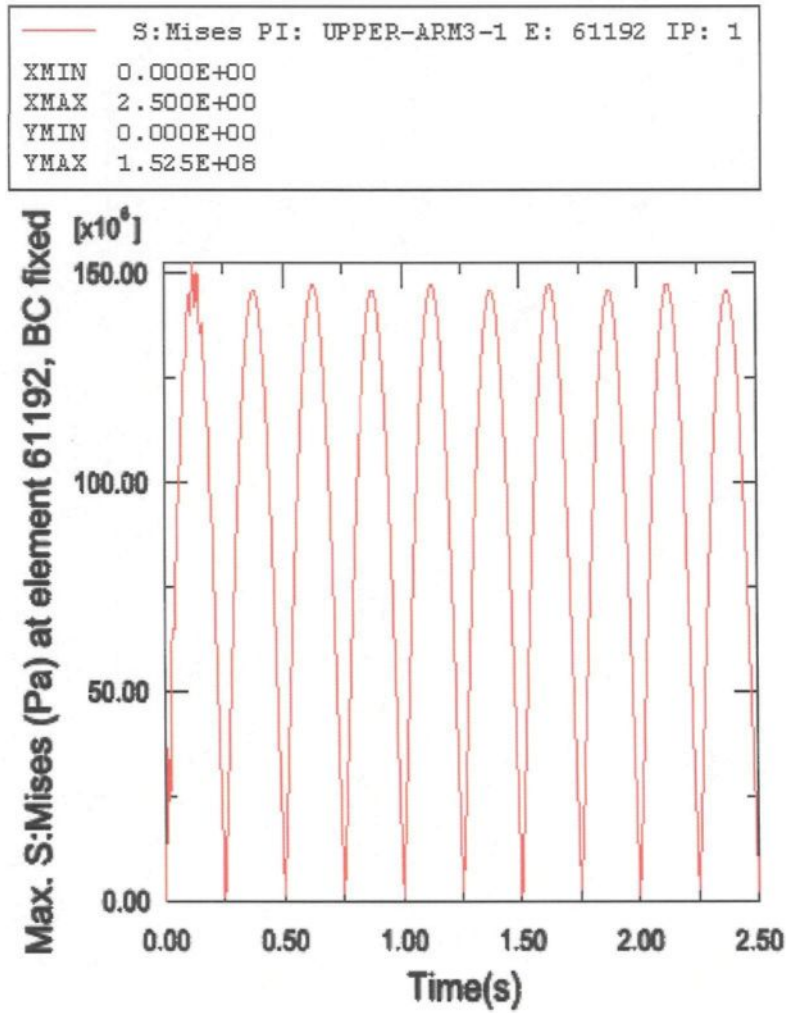
Figure 4.19 Max. S:Mises at element 61192, BC fixed.
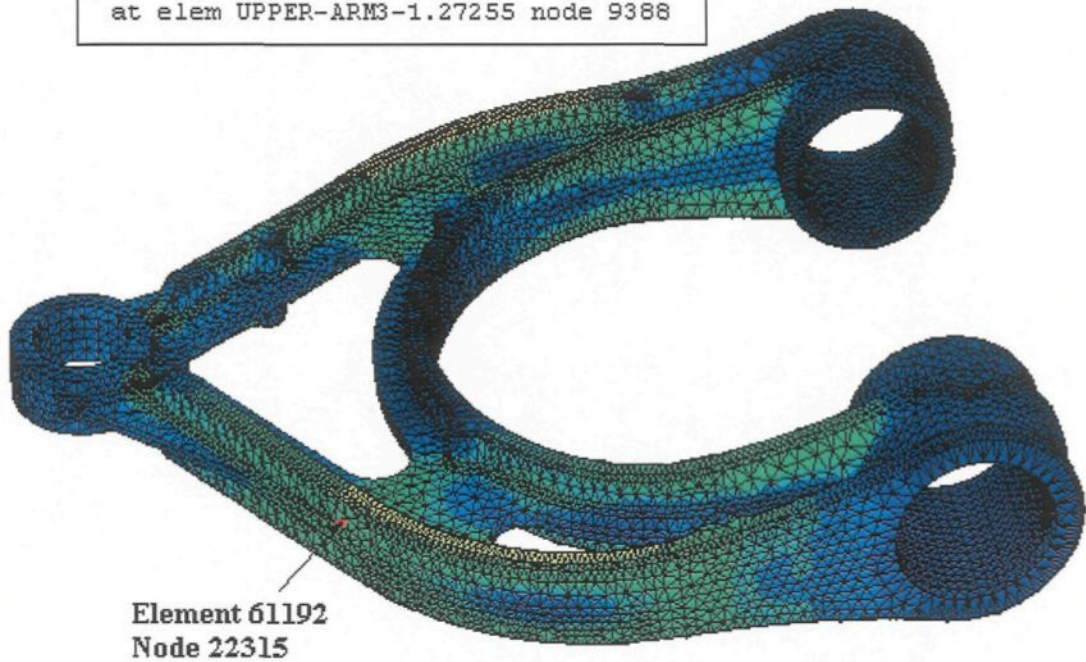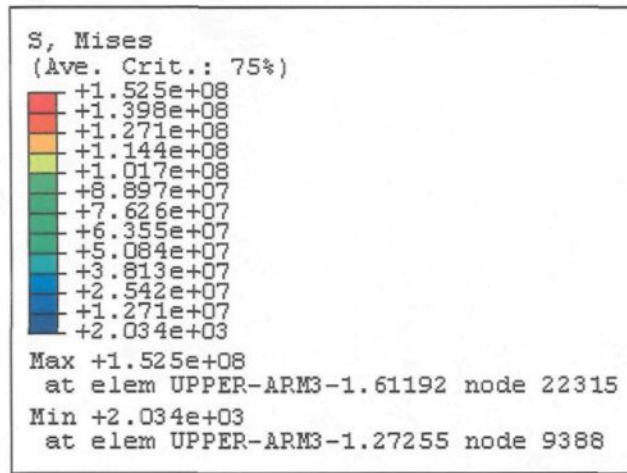
S, Mises
(Ave. Crit.: 75%)
 +1.525e+08
 +1.398e+08
 +1.271e+08
 +1.144e+08
 +1.017e+08
 +8.897e+07
 +7.626e+07
 +6.355e+07
 +5.084e+07
 +3.813e+07
 +2.542e+07
 +1.271e+07
 +2.034e+03

Max +1.525e+08
 at elem UPPER-ARM3-1.61192 node 22315

Min +2.034e+03
 at elem UPPER-ARM3-1.27255 node 9388

Element 61192
Node 22315

ODB: Job-upperarm-opt3-fix.odb   ABAQUS/STANDARD Version 6.5-1

Step: dynamic, dynamic
Increment   12: Step Time =   0.1200
Primary Var: S, Mises
Deformed Var: U   Deformation Scale Factor: +7.811e+00

Figure 4.20   S:Mises contour of development upper arm, BC fixed.

U, Magnitude
+4.267e-03
+3.912e-03
+3.556e-03
+3.200e-03
+2.845e-03
+2.489e-03
+2.134e-03
+1.778e-03
+1.422e-03
+1.067e-03
+7.112e-04
+3.556e-04
+0.000e+00
Max +4.267e-03
  at node UPPER-ARM3-1.794
Min +0.000e+00
  at node UPPER-ARM3-1.56

Node 794

ODB: Job-upperarm-opt3-fix.odb   ABAQUS/STANDARD Version 6.5-1

Step: dynamic, dynamic
Increment   12: Step Time =   0.1200
Primary Var: U, Magnitude
Deformed Var: U   Deformation Scale Factor: +7.811e+00

Figure 4.21   Displacement contour and location at node 794, BC fixed.

U:Magnitude PI: UPPER-ARM3-1 N: 794
U:U1 PI: UPPER-ARM3-1 N: 794
U:U2 PI: UPPER-ARM3-1 N: 794
U:U3 PI: UPPER-ARM3-1 N: 794

XMIN 0.000E+00
XMAX 2.500E+00
YMIN -4.104E-03
YMAX 4.267E-03
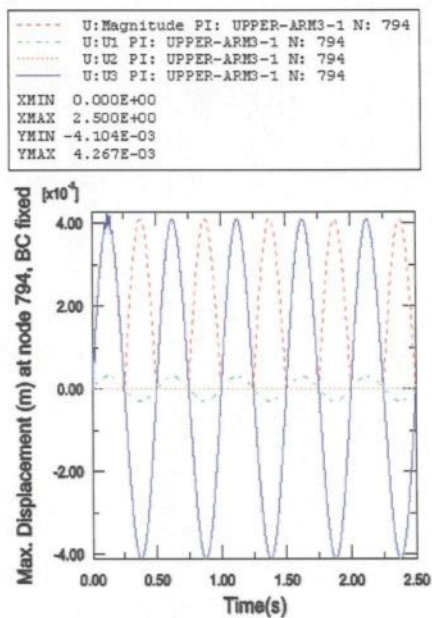
Figure 4.22   Max. Displacement at node 794, BC fixed.

```
RF, Magnitude
    +3.189e+02
    +2.924e+02
    +2.658e+02
    +2.392e+02
    +2.126e+02
    +1.861e+02
    +1.595e+02
    +1.329e+02
    +1.063e+02
    +7.974e+01
    +5.316e+01
    +2.658e+01
    +0.000e+00
Max +3.189e+02
  at node UPPER-ARM3-1.13518
Min +0.000e+00
  at node UPPER-ARM3-1.1
```

Node 13518

```
ODB: Job-upperarm-opt3-fix.odb    ABAQUS/STANDARD Version 6.5-1

Step: dynamic, dynamic
Increment    12: Step Time =   0.1200
Primary Var: RF, Magnitude
Deformed Var: CF  Deformation Scale Factor: +1.000e+00
```

Figure 4.23   Reaction force contour and location at node 13518, BC fixed.


```
----- RF:Magnitude PI: UPPER-ARM3-1 N: 13518
      RF:RF1 PI: UPPER-ARM3-1 N: 13518
----- RF:RF2 PI: UPPER-ARM3-1 N: 13518
...... RF:RF3 PI: UPPER-ARM3-1 N: 13518

XMIN  0.000E+00
XMAX  2.500E+00
YMIN -3.143E+02
YMAX  3.189E+02
```
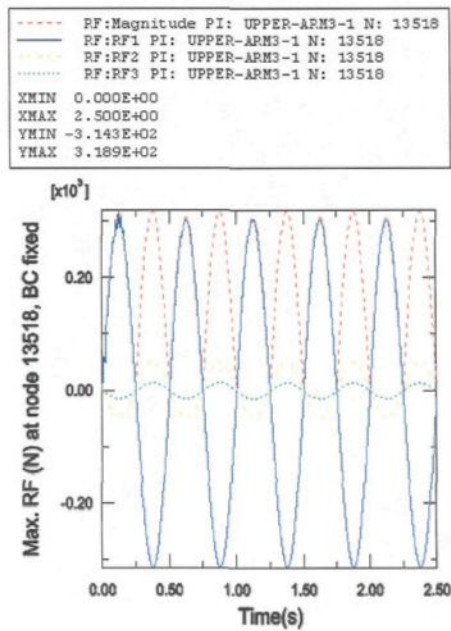
Figure 4.24   Max. Reaction force at node 13518, BC fixed.

Repeat all steps; only modift boundary condition to Rotation with respect to axis Y. The range of rotation is from -15° to +15°. The result is shown in below:

1) The boundary condition is axes X, Z free and axis Y is fixed and rotation with respect to axis Y. Maximum stress is 90 MPa at element 22571 (see Figure 4.25) and Stress Mises contour is shown in Figure 4.26. It is less than yield strength (275 MPa) of aluminum A357. 2) Maximum reaction force is 38.7N at node 2331. It is shown in Figure 4.27 and Figure 4.28.
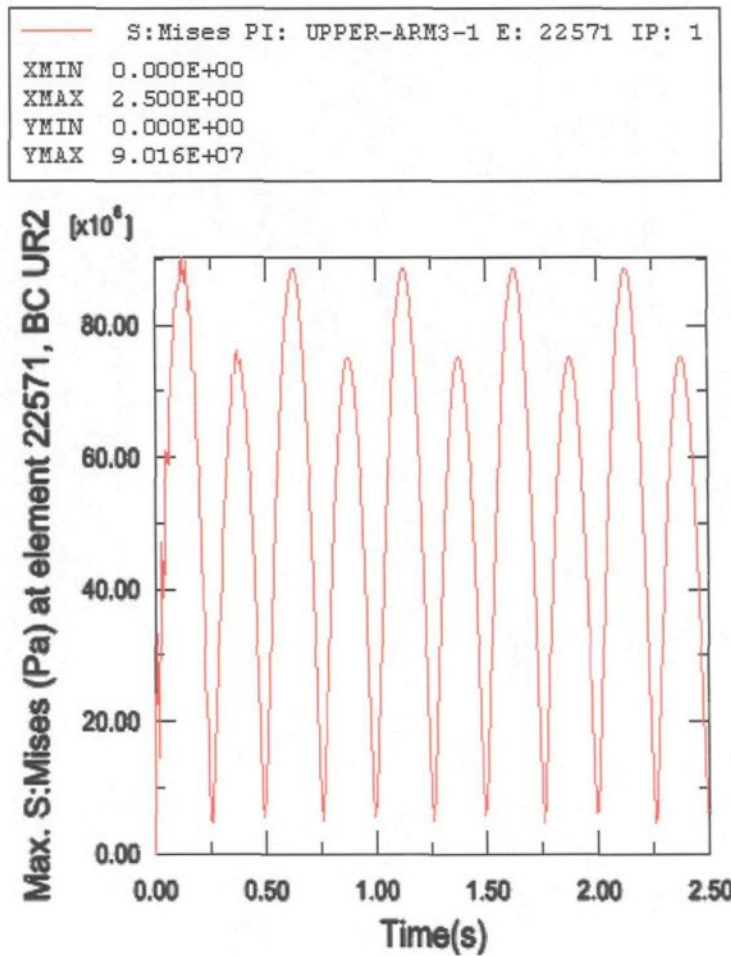
Figure 4.25   Max. S:Mises at element 22571, BC UR2.

```
S, Mises
(Ave. Crit.: 75%)
    +9.316e+07
    +8.542e+07
    +7.769e+07
    +6.996e+07
    +6.222e+07
    +5.449e+07
    +4.675e+07
    +3.902e+07
    +3.128e+07
    +2.355e+07
    +1.581e+07
    +8.080e+06
    +3.452e+05
Max +9.316e+07
  at elem UPPER-ARM3-1.22571 node 11720
Min +3.452e+05
  at elem UPPER-ARM3-1.17847 node 4612
```

Element 22571
Node 11720
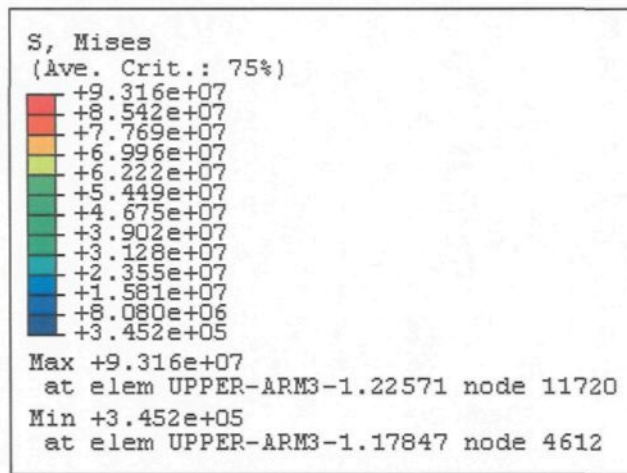
ODB: Job-upperarm-Opt3-ur.odb   ABAQUS/STANDARD Version 6.5-1

Step: dynamic, dynamic
Increment   12: Step Time =   0.1200
Primary Var: S, Mises
Deformed Var: CF   Deformation Scale Factor: +1.000e+00

Figure 4.26   S:Mises contour of development upper arm, BC UR2.

Figure 4.27   Reaction force contour and location, BC UR2.

Figure 4.28   Max. Reaction force at node 2331, BC UR2.

4.4.2 Analyse strength of optimization upper arm with random force

We replace the sinusoidal amplitude curve with random amplitude curve that represent the real case of main road excitation. They are shown in Figure 4.29 and Table 4.2. Then we verify its stress again. The stress is 156 MPa in BC fixed boundary condition (See Figure 4.30 and Figure 4.31). The stress is 103.9 MPa in BC UR2 boundary condition; they are shown in Figure 4.32 and Figure 4.33.
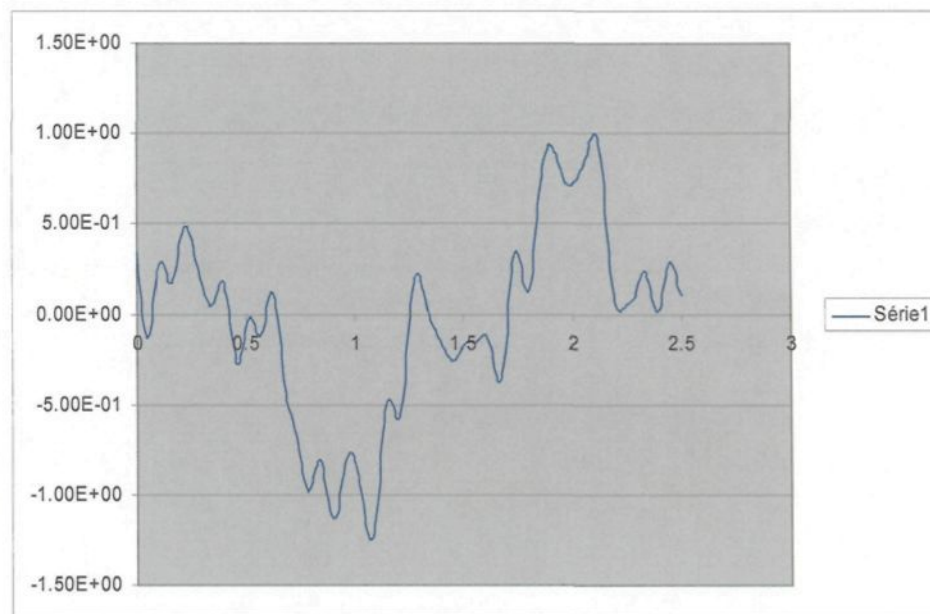
Figure 4.29 Random amplitude curve of upper arm.

Time(s)	Amplitude	Time(s)	Amplitude	Time(s)	Amplitude
0	3.54E-01	0.34	4.41E-02	6.80E-01	-4.45E-01
1.00E-02	2.15E-01	0.35	6.13E-02	0.69	-5.10E-01
0.02	7.28E-02	3.60E-01	9.52E-02	0.7	-5.55E-01
3.00E-02	-4.50E-02	0.37	1.36E-01	7.10E-01	-5.91E-01
0.04	-1.15E-01	3.80E-01	1.70E-01	0.72	-6.31E-01
5.00E-02	-1.27E-01	0.39	1.81E-01	7.30E-01	-6.86E-01
0.06	-8.12E-02	4.00E-01	1.60E-01	0.74	-7.57E-01
0.07	5.29E-03	0.41	1.02E-01	7.50E-01	-8.35E-01
8.00E-02	1.09E-01	0.42	1.51E-02	0.76	-9.08E-01
0.09	2.03E-01	4.30E-01	-8.63E-02	0.77	-9.60E-01
1.00E-01	2.68E-01	0.44	-1.81E-01	7.80E-01	-9.81E-01
0.11	2.92E-01	4.50E-01	-2.48E-01	0.79	-9.67E-01
1.20E-01	2.80E-01	0.46	-2.75E-01	8.00E-01	-9.27E-01
0.13	2.42E-01	4.70E-01	-2.57E-01	0.81	-8.75E-01
0.14	2.00E-01	0.48	-2.04E-01	8.20E-01	-8.31E-01
1.50E-01	1.73E-01	0.49	-1.34E-01	0.83	-8.11E-01
0.16	1.73E-01	5.00E-01	-6.67E-02	0.84	-8.26E-01
1.70E-01	2.06E-01	0.51	-2.22E-02	8.50E-01	-8.75E-01
0.18	2.65E-01	5.20E-01	-1.00E-02	0.86	-9.48E-01
1.90E-01	3.38E-01	0.53	-2.85E-02	8.70E-01	-1.03E+00
0.2	4.08E-01	5.40E-01	-6.55E-02	0.88	-1.09E+00
0.21	4.60E-01	0.55	-1.02E-01	8.90E-01	-1.13E+00
2.20E-01	4.85E-01	0.56	-1.20E-01	0.9	-1.13E+00
0.23	4.82E-01	5.70E-01	-1.08E-01	0.91	-1.10E+00
2.40E-01	4.55E-01	0.58	-6.34E-02	9.20E-01	-1.04E+00
0.25	4.10E-01	5.90E-01	2.10E-03	0.93	-9.60E-01
2.60E-01	3.58E-01	0.6	6.93E-02	9.40E-01	-8.85E-01
0.27	3.03E-01	6.10E-01	1.16E-01	0.95	-8.23E-01
0.28	2.49E-01	0.62	1.24E-01	9.60E-01	-7.81E-01
2.90E-01	1.97E-01	0.63	8.45E-02	0.97	-7.62E-01
0.3	1.49E-01	6.40E-01	9.34E-04	0.98	-7.66E-01
3.10E-01	1.05E-01	0.65	-1.13E-01	9.90E-01	-7.92E-01
0.32	6.90E-02	6.60E-01	-2.37E-01	....	....
3.30E-01	4.72E-02	0.67	-3.52E-01	2.5	1.05E-01

Table 4.2   Random amplitude data of upper arm.
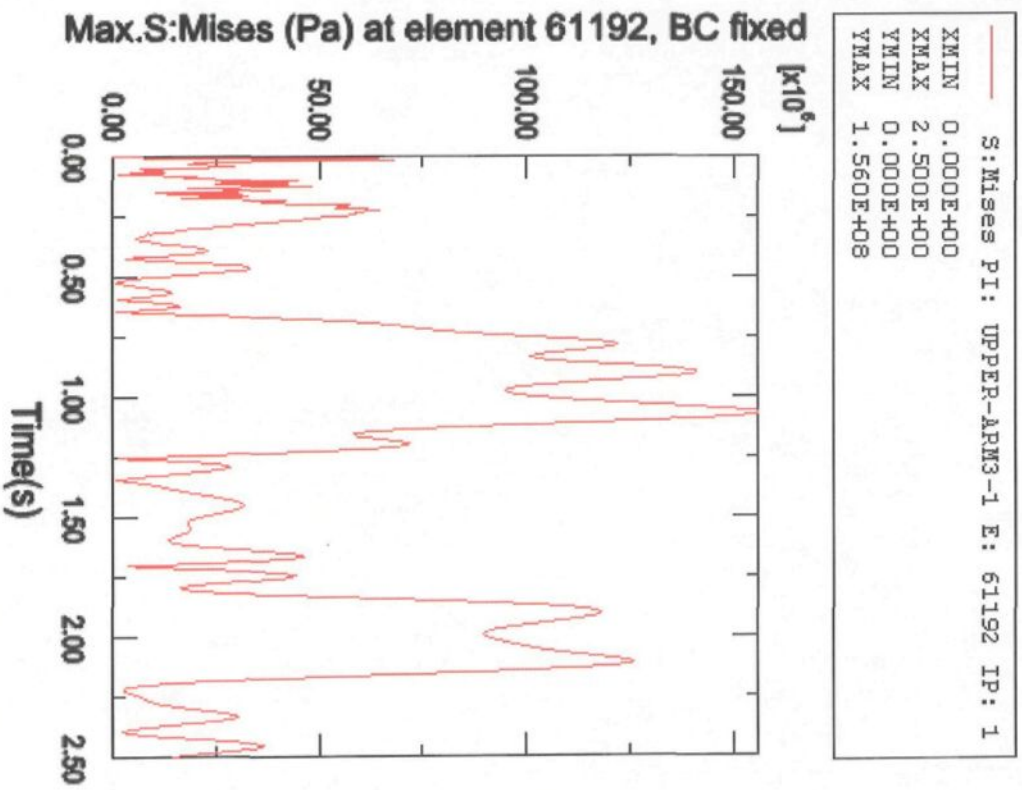
Figure 4.30 Max. S:Mises at element 61192 with random force, BC fixed.

```
S, Mises
(Ave. Crit.: 75%)
   +1.560e+08
   +1.430e+08
   +1.300e+08
   +1.170e+08
   +1.040e+08
   +9.103e+07
   +7.802e+07
   +6.502e+07
   +5.202e+07
   +3.901e+07
   +2.601e+07
   +1.301e+07
   +2.069e+03
Max +1.560e+08
  at elem UPPER-ARM3-1.61192 node 22315
Min +2.069e+03
  at elem UPPER-ARM3-1.27255 node 9388
```

Element 61192
Node 22315

ODB: Job-opt3-randonF--fix.odb   ABAQUS/STANDARD Version 6.5-1

Step: dynamic, dynamic
Increment   107: Step Time =   1.070
Primary Var: S, Mises
Deformed Var: CF   Deformation Scale Factor: +1.000e+00

Figure 4.31   S:Mises contour of development upper arm with random force, BC fixed.

S, Mises
(Ave. Crit.: 75%)
+1.039e+08
+9.523e+07
+8.660e+07
+7.798e+07
+6.935e+07
+6.072e+07
+5.209e+07
+4.346e+07
+3.483e+07
+2.620e+07
+1.757e+07
+8.936e+06
+3.065e+05

Max +1.039e+08
  at elem UPPER-ARM3-1.73666 node 22020
Min +3.065e+05
  at elem UPPER-ARM3-1.26682 node 9380

Element 73666
Node 22020
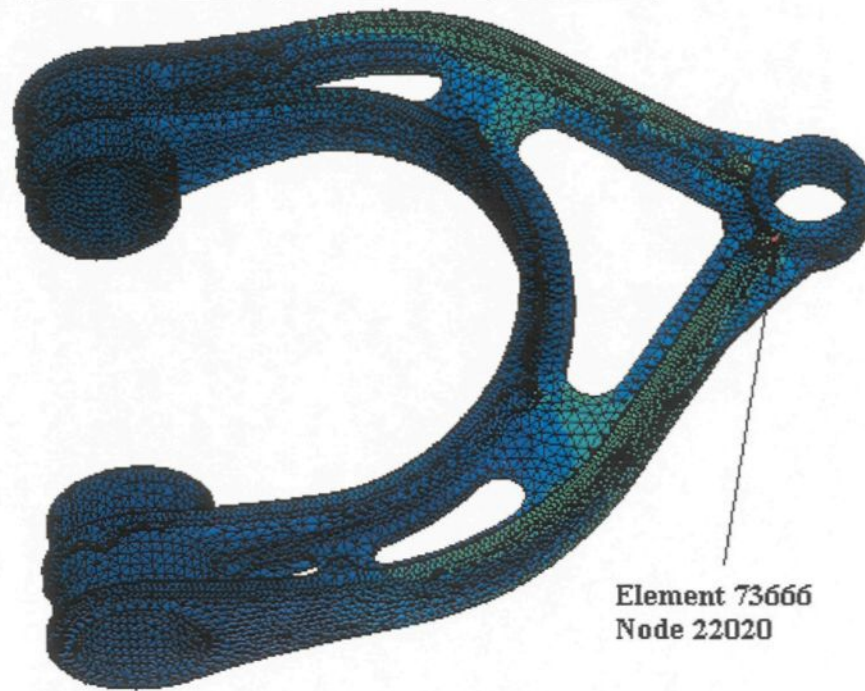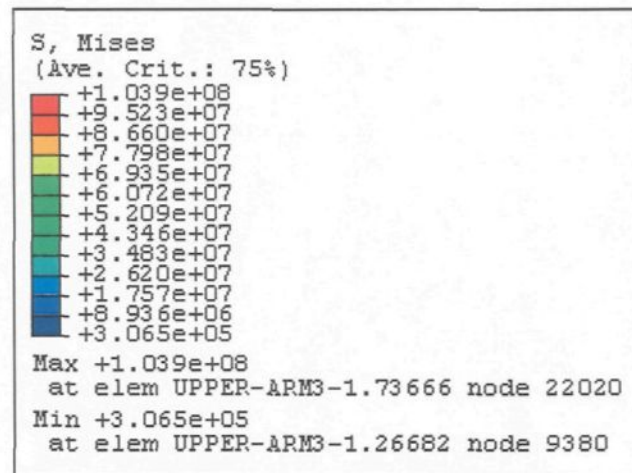
ODB: Job-Opt-randonF-ur2.odb   ABAQUS/STANDARD Version 6.5-1

Step: dynamic, dynamic
Increment   107: Step Time =   1.070
Primary Var: S, Mises
Deformed Var: CF   Deformation Scale Factor: +1.000e+00

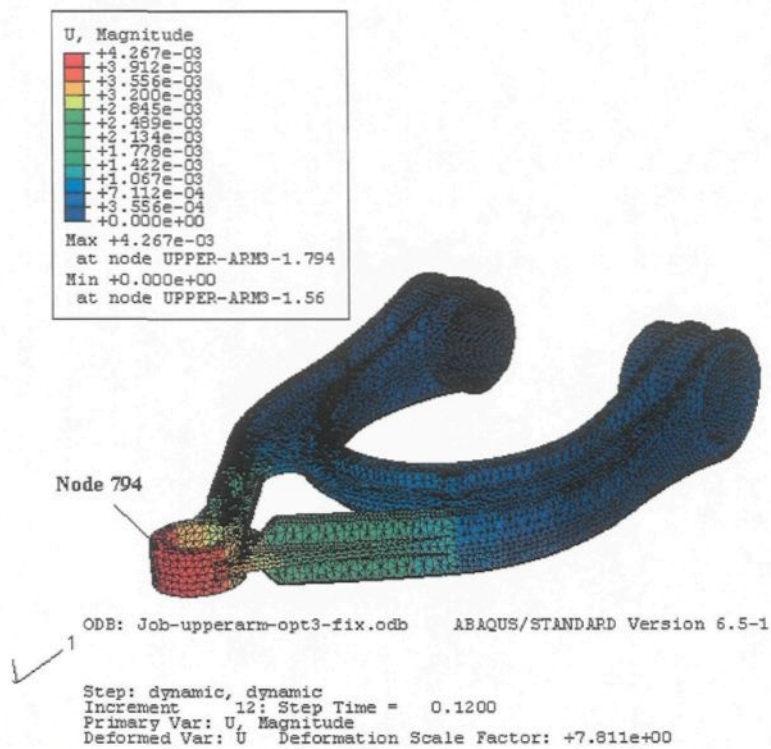**Figure 4.32**   S:Mises contour of development upper arm with random force, BC UR2.
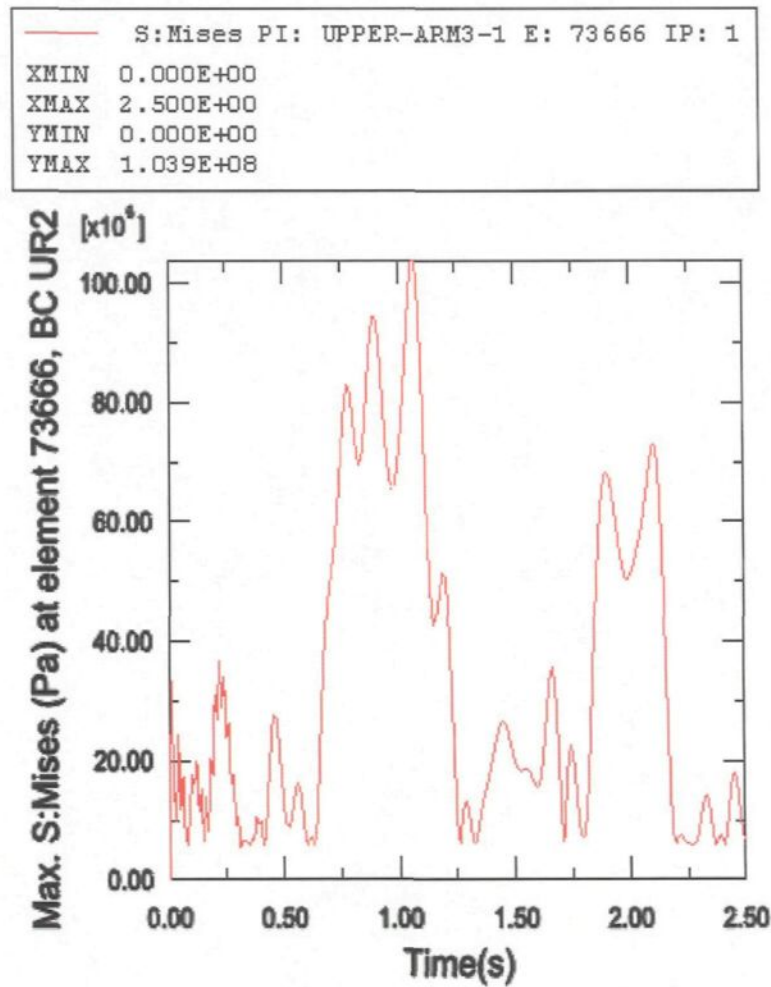
Figure 4.33 Max. S:Mises at element 73666 with random force, BC UR2.

4.5 Strength Analysis of lower arm

In this analysis process, we are doing same procedures to do simulation analysis steps for suspension lower arm in order to verify their stress.

4.5.1 Strength analysis of lower arm with sinusoidal force

- **Input part:** We input the suspension lower arm to Abaqus. The overall size is 0.32mx0.26mx0.068m.

- **Property setting:** The lower control arm is made in T6061-T6, so we set the density to 2700kg/m³, Elastic young's modulus 7.31e+10P$_a$ Poisson's ratio 0.33.

- **Step setting:** In this step setting, we setup two steps (Frequency and Dynamic). The first step in the dynamic analysis calculates the natural frequencies and mode shapes of the control arm. The second step then uses these data to calculate the dynamic response of the lower arm, especially to analyses stress of the lower arm. In the step setting, we choose dynamic analysis.

- **Load seting:** 1) Boundary condition: It is the same upper arm as section 4.3. 2) Loading: There are 3 forces loading on lower arm with amplitude in Z direction (see Table 4.3, Figure 4.34 and Figure 4.35). The vertical and lateral forces are from the tire and another one from the chassis.
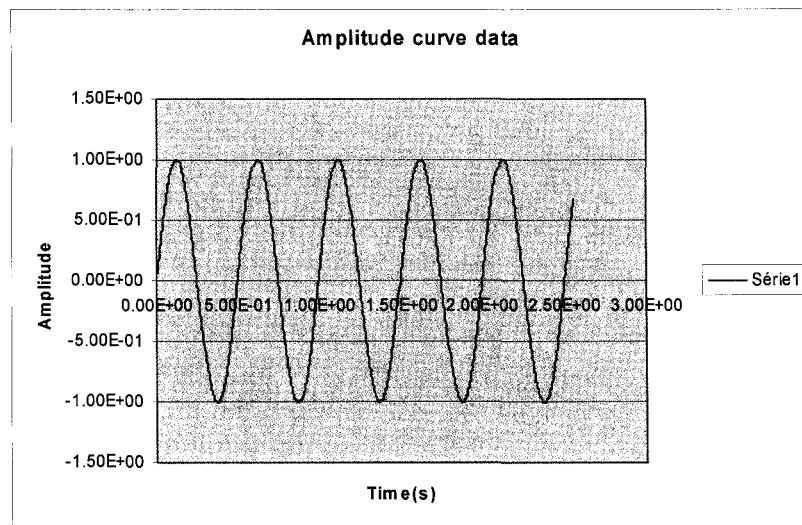
Figure 4.34 Sinusoidal amplitude curve data of lower arm.

Time(s)	Amplitude	Time(s)	Amplitude	Time(s)	Amplitude
5.00E-03	6.28E-02	0.175	0.8096718	0.345	-0.9289652
1.00E-02	0.12527	0.18	0.7712437	0.35	-0.9503651
1.50E-02	0.1872874	0.185	0.7297748	0.355	-0.9680182
2.00E-02	0.2485665	0.19	0.6854289	0.36	-0.9818549
2.50E-02	0.3088655	0.195	0.6383807	0.365	-0.9918206
3.00E-02	0.3679469	0.2	0.5888156	0.37	-0.997876
3.50E-02	0.4255776	0.205	0.536929	0.375	-0.9999971
4.00E-02	0.4815304	0.21	0.4829256	0.38	-0.9981758
4.50E-02	0.5355847	0.215	0.4270183	0.385	-0.9924191
5.00E-02	0.5875275	0.22	0.3694272	0.39	-0.9827498
5.50E-02	0.637154	0.225	0.3103799	0.395	-0.9692059
6.00E-02	0.6842684	0.23	0.2501089	0.4	-0.9518409
6.50E-02	0.7286851	0.235	0.1888516	0.405	-0.9307231
7.00E-02	0.7702289	0.24	0.1268499	0.41	-0.905936
7.50E-02	0.808736	0.245	6.43E-02	0.415	-0.8775772
8.00E-02	0.8440548	0.25	1.59E-03	0.42	-0.8457586
8.50E-02	0.8760457	0.255	-6.12E-02	0.425	-0.8106055
9.00E-02	0.9045828	0.26	-0.1236898	0.43	-0.7722566
9.50E-02	0.9295535	0.265	-0.1857227	0.435	-0.7308627
1.00E-01	0.9508594	0.27	-0.2470234	0.44	-0.6865876
0.105	0.9684166	0.275	-0.3073505	0.445	-0.6396057
0.11	0.9821557	0.28	-0.3664656	0.45	-0.5901021
0.115	0.9920226	0.285	-0.4241358	0.455	-0.538272
0.12	0.9979784	0.29	-0.4801339	0.46	-0.4843197
0.125	0.9999997	0.295	-0.5342391	0.465	-0.4284576
0.13	0.9980784	0.3	-0.5862379	0.47	-0.3709067
0.135	0.9922221	0.305	-0.6359258	0.475	-0.3118934
0.14	0.9824539	0.31	-0.6831062	0.48	-0.2516505
0.145	0.9688125	0.315	-0.7275935	0.485	-0.1904154
0.15	0.9513514	0.32	-0.7692122	0.49	-0.1284297
0.155	0.9301395	0.325	-0.8077983	0.495	-6.59E-02
0.16	0.9052606	0.33	-0.8431996	0.5	-3.19E-03
0.165	0.8768126	0.335	-0.8752765	......	....
0.17	0.8449077	0.34	-0.9039028	2.56	0.6725683

Table 4.3   Sinusoidal amplitude data of lower arm

- **Mesh part:** 1) Size control: Approximate global size is 0.004, minimum size is 0.2 and deviation factor is default. 2) Mesh control: element shape is Tet shape. 3) Element type C3D4, standard and linear with 3D stress. Total number of elements is 103697 and number of nodes is 23133. It is shown in Figure 4.36.

- **Job submit:** Full analysis, analysis input file processor memory is 1000.

- **Visualization:** upper arm output results:
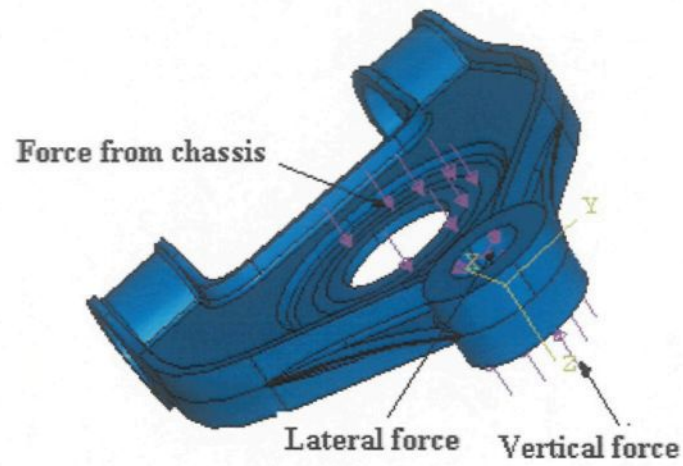
Figure 4.35   Force loading on lower arm.

Figure 4.36   Mesh lower arm.

1. Boundary condition BC fixed with 5KN sinusoidal force:

1) The boundary condition is defined in all directions and rotation with 5KN force. Maximum stress is 268 MPa at element 18744 (See Figure 4.37) and Stress Mises contour is shown on Figure 4.38. It is less than the yield strength (275 Mpa) of A357.

2) Maximum position displacement at node 238 is 9mm (see Figure 4.39).

3) Maximum reaction force is 779.2N at node 11399. It is shown in Figure 4.40.

```
        ———      S:Mises PI: LOWER-ARM-1 E: 18744 IP: 1
XMIN   1.000E-02
XMAX   2.500E+00
YMIN   3.626E+05
YMAX   2.684E+08
```
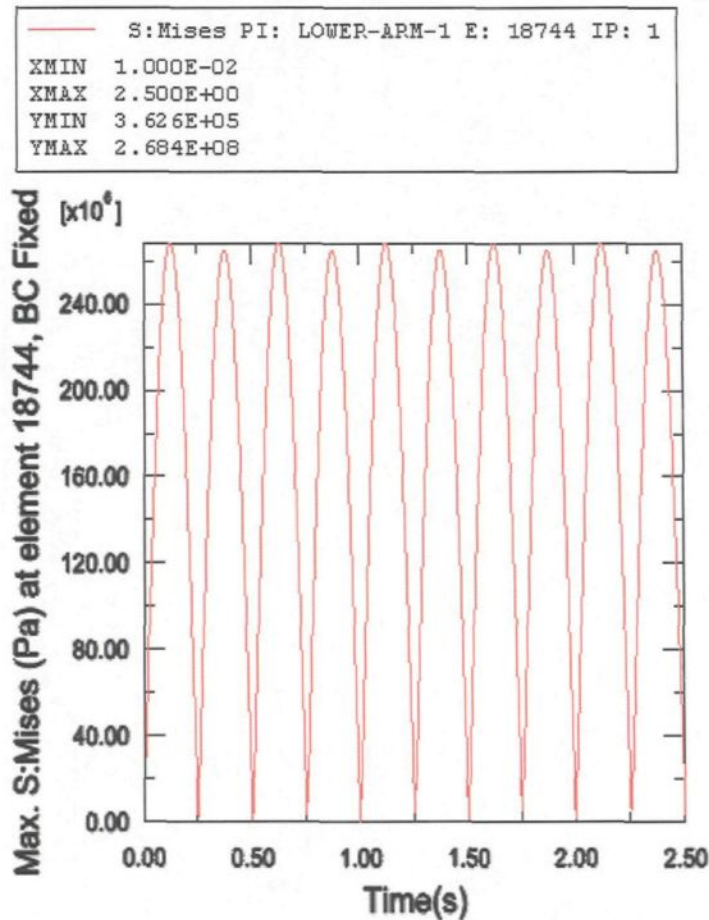
Figure 4.37   Max. S:Mises of lower arm with 5KN sinusoidal force, BC fixed.
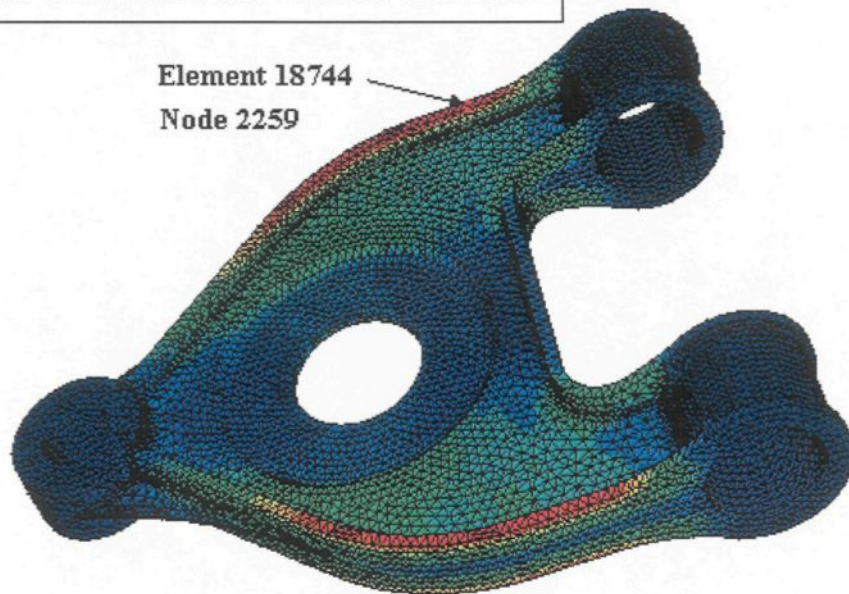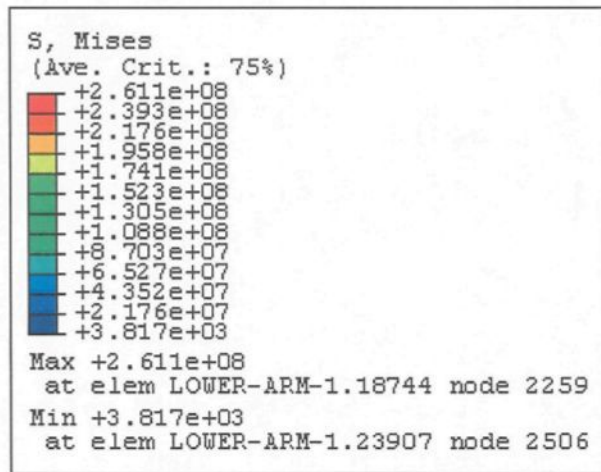
```
S, Mises
(Ave. Crit.: 75%)
    +2.611e+08
    +2.393e+08
    +2.176e+08
    +1.958e+08
    +1.741e+08
    +1.523e+08
    +1.305e+08
    +1.088e+08
    +8.703e+07
    +6.527e+07
    +4.352e+07
    +2.176e+07
    +3.817e+03
Max +2.611e+08
  at elem LOWER-ARM-1.18744 node 2259
Min +3.817e+03
  at elem LOWER-ARM-1.23907 node 2506
```

Element 18744
Node 2259

```
ODB: Job-5kfix.odb     ABAQUS/STANDARD Version 6.5-1
```

```
Step: "Modal dynamics", Modal dynamics
Increment      13: Step Time =    0.1300
Primary Var: S, Mises
Deformed Var: CF    Deformation Scale Factor: +1.000e+00
```

**Figure 4.38** S:Mises contour of lower arm with 5KN sinusoidal force, BC fixed.

Figure 4.39 Max. Displacement, 5KN sinusoidal force with BC fixed.
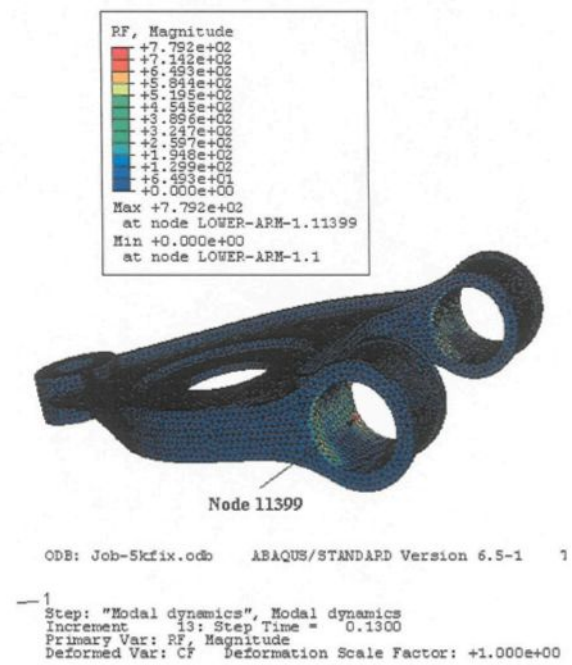
Figure 4.40 Max. Reaction force with 5KN sinusoidal force, BC fixed.

2. Boundary condition BC fixed with 4KN sinusoidal force:

1) All directions and rotation fixed with 4KN force. Stress Mises contour is shown on

Figure 4.41; Maximum stress is 189 MPa at element 4217 (See Figure 4.42). It is

less than the yield strength (275 Mpa) of aluminum A357.


```
S, Mises
(Ave. Crit.: 75%)
    +1.890e+08
    +1.733e+08
    +1.575e+08
    +1.418e+08
    +1.260e+08
    +1.103e+08
    +9.450e+07
    +7.875e+07
    +6.300e+07
    +4.725e+07
    +3.150e+07
    +1.575e+07
    +2.492e+03
Max +1.890e+08
  at elem LOWER-ARM-1.4217 node 11309
Min +2.492e+03
  at elem LOWER-ARM-1.23907 node 2506
```

Element 4217
Node 11309

ODB: Job-4kfix.odb   ABAQUS/STANDARD Version 6.5-1   T₁

Step: "Modal dynamics", Modal dynamics
Increment   13: Step Time =   0.1300
Primary Var: S, Mises
Deformed Var: CF   Deformation Scale Factor: +1.000e+00

Figure 4.41   S:Mises contour of lower arm with 4KN sinusoidal force, BC fixed.

```
        S:Mises PI: LOWER-ARM-1 E: 4217 IP: 1
XMIN  1.000E-02
XMAX  2.500E+00
YMIN  1.604E+05
YMAX  1.810E+08
```


Figure 4.42   S:Mises of lower arm with 4KN sinusoidal force, BC fixed.

2) Maximum position displacement at node 238 is 7mm (see Figure 4.43).

3) Maximum reaction force is 519.4N at node 6991. It is shown in Figure 4.44.
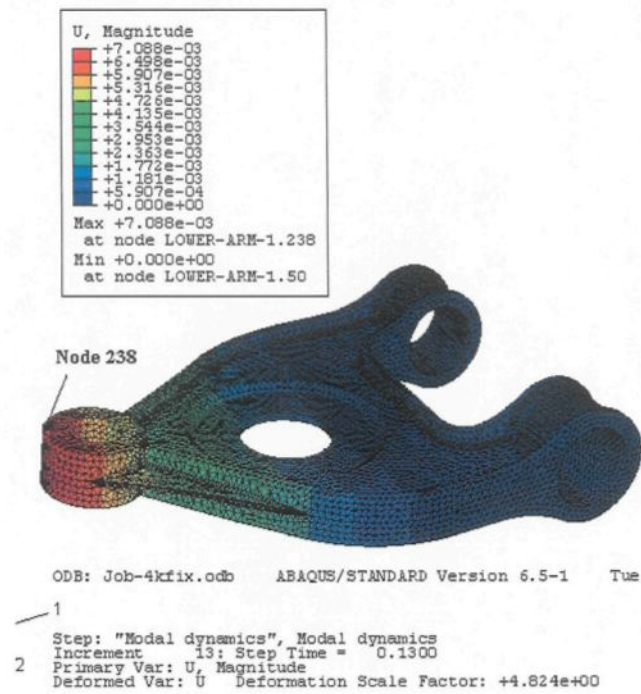
Figure 4.43   Max. Displacement, 4KN sinusoidal force with BC fixed.
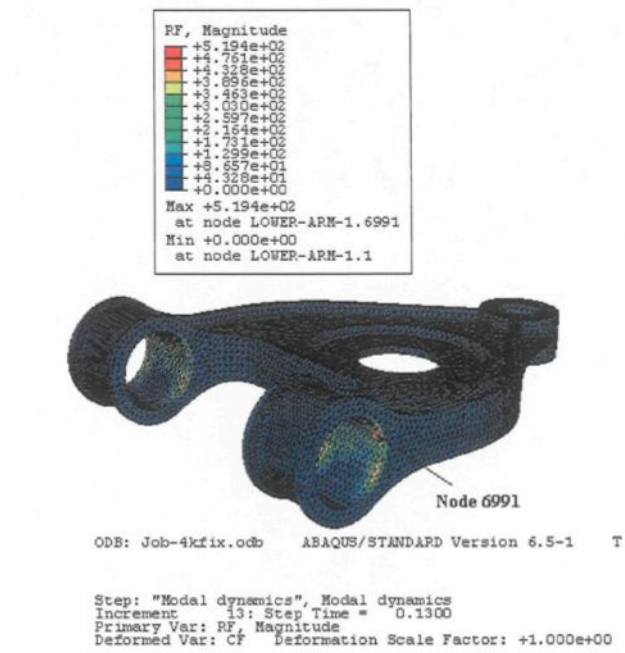
Figure 4.44   Max. Reaction force, 4KN sinusoidal force with BC fixed.

3. Boundary condition BC UR2 with 5KN sinusoidal force:

The part rotates around Y axes with 5KN force. Stress Mises contour and the maximum stress is 116.3 MPa at element 15965 (See Figure 4.45 and Figure 4.46). It is less than the yield strength (275 Mpa) of aluminum A357.


```
S, Mises
(Ave. Crit.: 75%)
    +1.163e+08
    +1.066e+08
    +9.699e+07
    +8.735e+07
    +7.770e+07
    +6.806e+07
    +5.842e+07
    +4.878e+07
    +3.914e+07
    +2.949e+07
    +1.985e+07
    +1.021e+07
    +5.695e+05
Max +1.163e+08
 at elem LOWER-ARM-1.15965 node 4367
Min +5.695e+05
 at elem LOWER-ARM-1.20289 node 2504
```

Element 15965
Node 4367
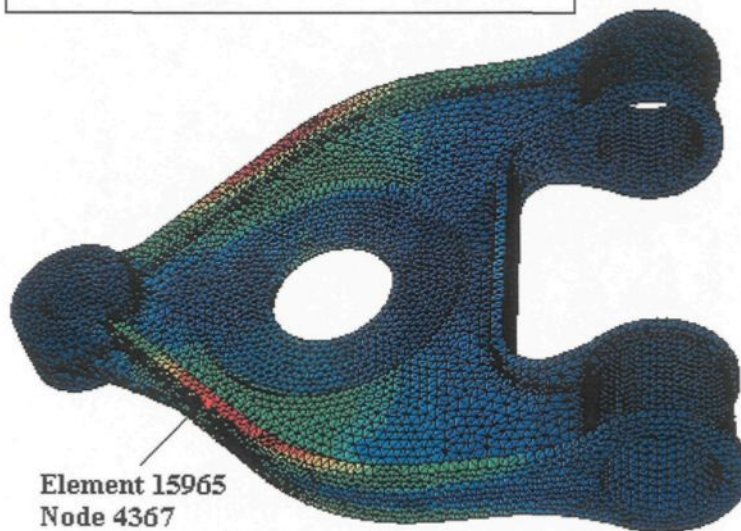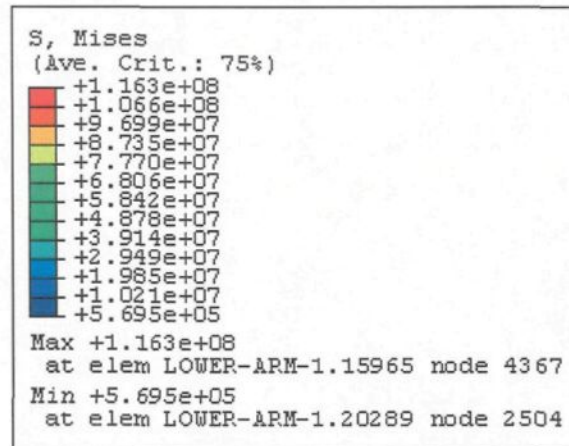
```
ODB: Job-5kur2.odb    ABAQUS/STANDARD Version 6.5-1    ]

  1
Step: "Modal dynamics", Modal dynamics
Increment    13: Step Time =    0.1300
Primary Var: S, Mises
Deformed Var: CF   Deformation Scale Factor: +1.000e+00
```

Figure 4.45   S:Mises contour of lower arm with 5KN sinusoidal force, BC UR2.
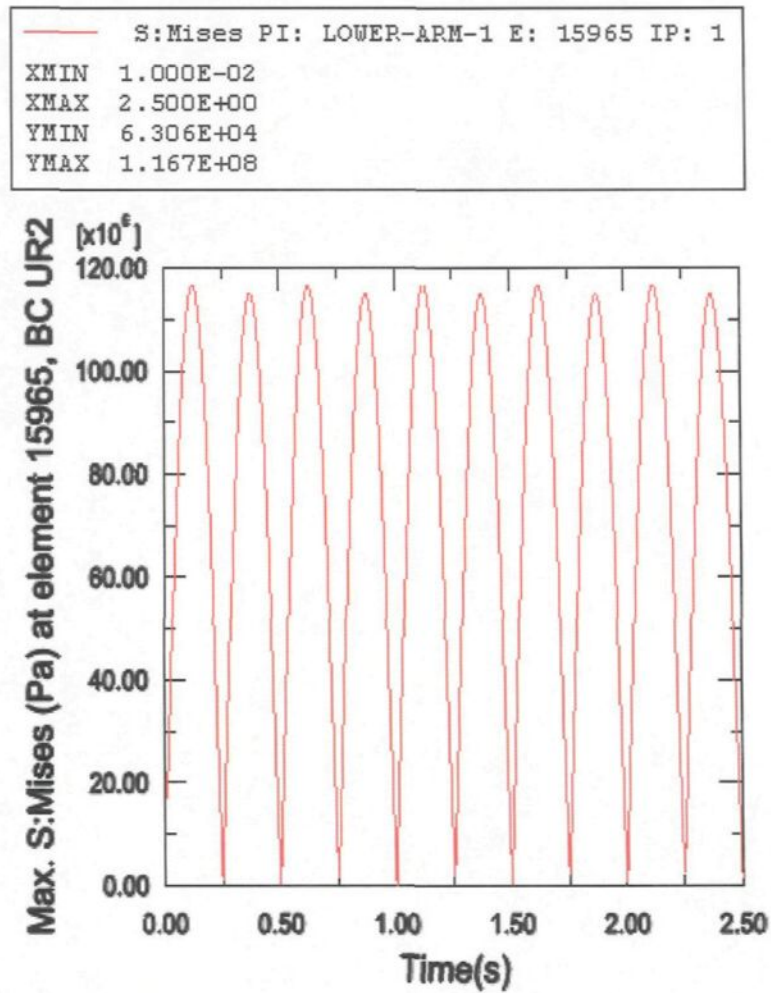
Figure 4.46   S:Mises of 5KN sinusoidal force with BC UR2.

4. Boundary condition BC UR2 with 4KN sinusoidal force:

The part rotates around Y axes with 4KN force. The maximum stress is 96.8 MPa at element 15965 (It is shown in Figure 4.47 and Figure 4.48). It is less than the yield strength (275 Mpa) of aluminum A357.

S:Mises PI: LOWER-ARM-1 E: 15965 IP: 1

XMIN 1.000E-02
XMAX 2.500E+00
YMIN 1.067E+04
YMAX 9.684E+07
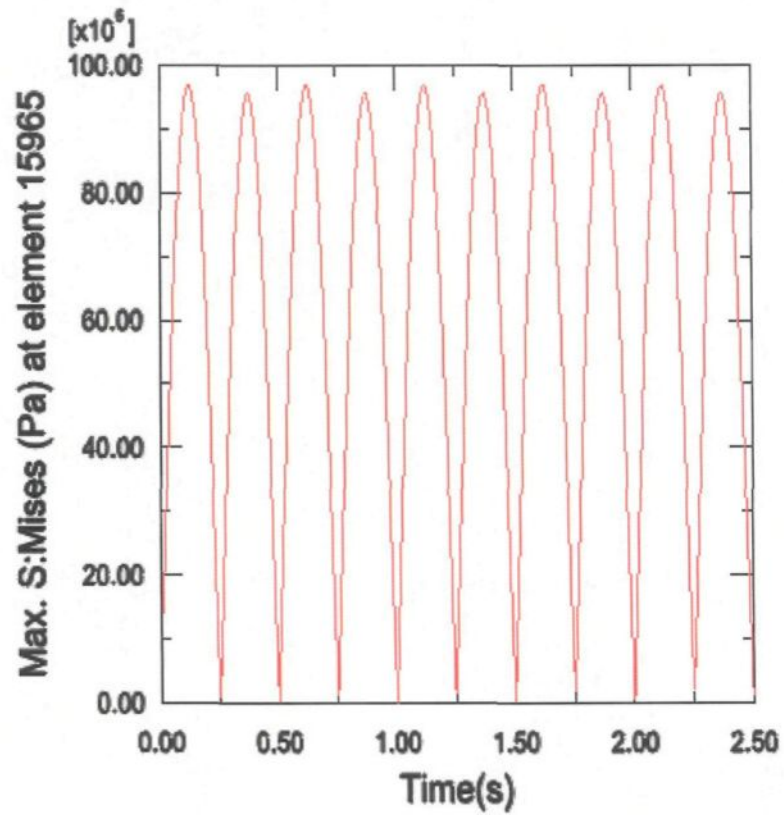
Figure 4.47   Max. S:Mises of lower arm with 4KN sinusoidal force, BC UR2.

```
S, Mises
(Ave. Crit.: 75%)
    +9.655e+07
    +8.854e+07
    +8.053e+07
    +7.252e+07
    +6.451e+07
    +5.651e+07
    +4.850e+07
    +4.049e+07
    +3.248e+07
    +2.447e+07
    +1.646e+07
    +8.452e+06
    +4.427e+05
Max +9.655e+07
  at elem LOWER-ARM-1.15965 node 4367
Min +4.427e+05
  at elem LOWER-ARM-1.14161 node 10
```

Element 15965
Node 4367

```
ODB: Job-4kur2.odb    ABAQUS/STANDARD Version 6.5-1    7

Step: "Modal dynamics", Modal dynamics
Increment    13: Step Time =    0.1300
Primary Var: S, Mises
Deformed Var: CF   Deformation Scale Factor: +1.000e+00
```

Figure 4.48   S:Mises contour of lower arm with 4KN sinusoidal force, BC UR2.

4.5.2 Analysis strength of lower arm with random force

We replace the sinusoidal amplitude curve with random amplitude curve in the same rotation boundary condition. The amplitude data and curve are shown in Table 4.2

and Figure 4.29 that represent the real case main road excitation. Then we verify its stress again.

1. *Boundary condition BC fixed with 4250N random force:*

1) All directions and rotation fixed with 4250N random force. Maximum stress is 265 MPa at element 51125 (See Figure 4.49). Stress Mises contour is shown on Figure 4.50; it is less than the yield strength (275 Mpa) of aluminum A357.
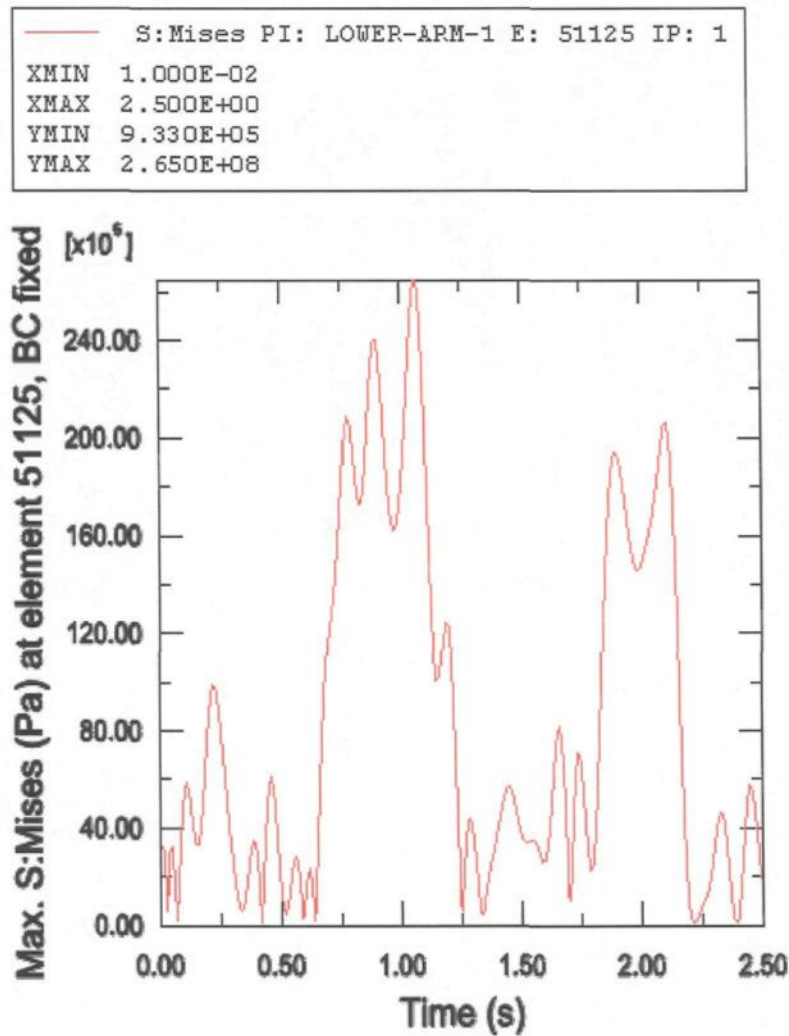
Figure 4.49 Max. S:Mises of 4250N random force with BC fixed.

```
S, Mises
(Ave. Crit.: 75%)
   ┌─ +2.650e+08
   ├─ +2.430e+08
   ├─ +2.209e+08
   ├─ +1.988e+08
   ├─ +1.767e+08
   ├─ +1.546e+08
   ├─ +1.325e+08
   ├─ +1.104e+08
   ├─ +8.835e+07
   ├─ +6.626e+07
   ├─ +4.418e+07
   ├─ +2.209e+07
   └─ +4.324e+03

Max +2.650e+08
  at elem LOWER-ARM-1.51125 node 16490

Min +4.324e+03
  at elem LOWER-ARM-1.24103 node 2505
```
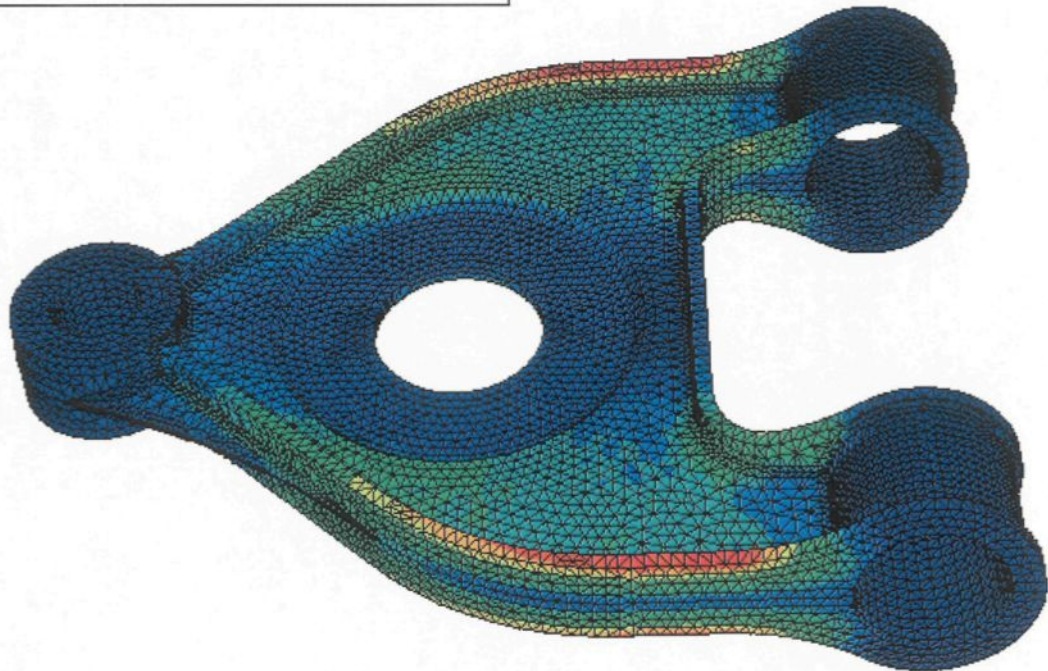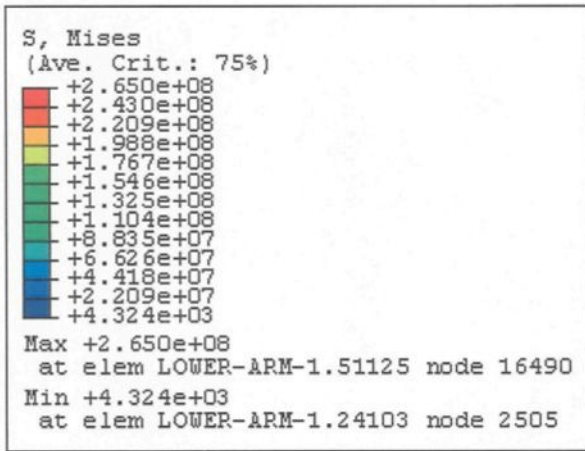

ODB: Job-425kfix-randon.odb   ABAQUS/STANDARD Version 6.5-1

Step: "Modal dynamics", Modal dynamics
Increment   107: Step Time =   1.070
Primary Var: S, Mises
Deformed Var: CF   Deformation Scale Factor: +1.000e+00

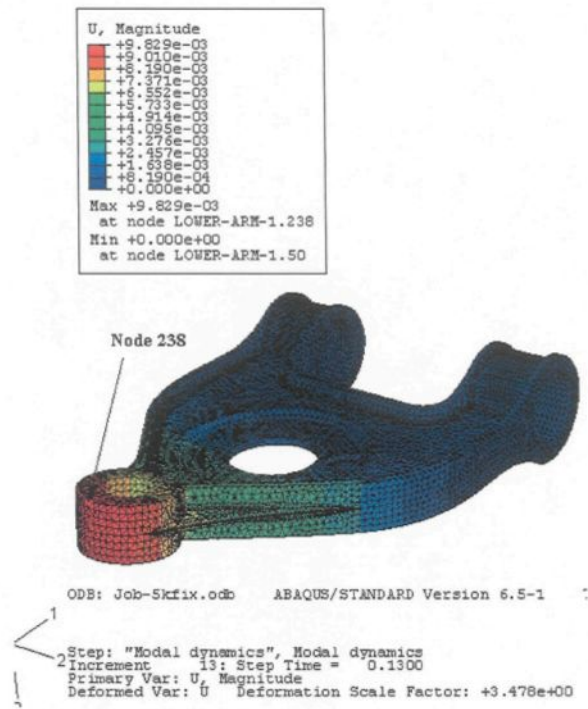**Figure 4.50** S:Mises contour of lower arm with 4250N random force, BC fixed.

2. Boundary condition BC fixed with 4KN random force:

All directions and rotation fixed with 4KN random force. Stress Mises contour is shown on Figure 4.51; Maximum stress is 249 MPa at element 51125 (See Figure 4.52). It is less than the yield strength (275 Mpa) of aluminum A357.
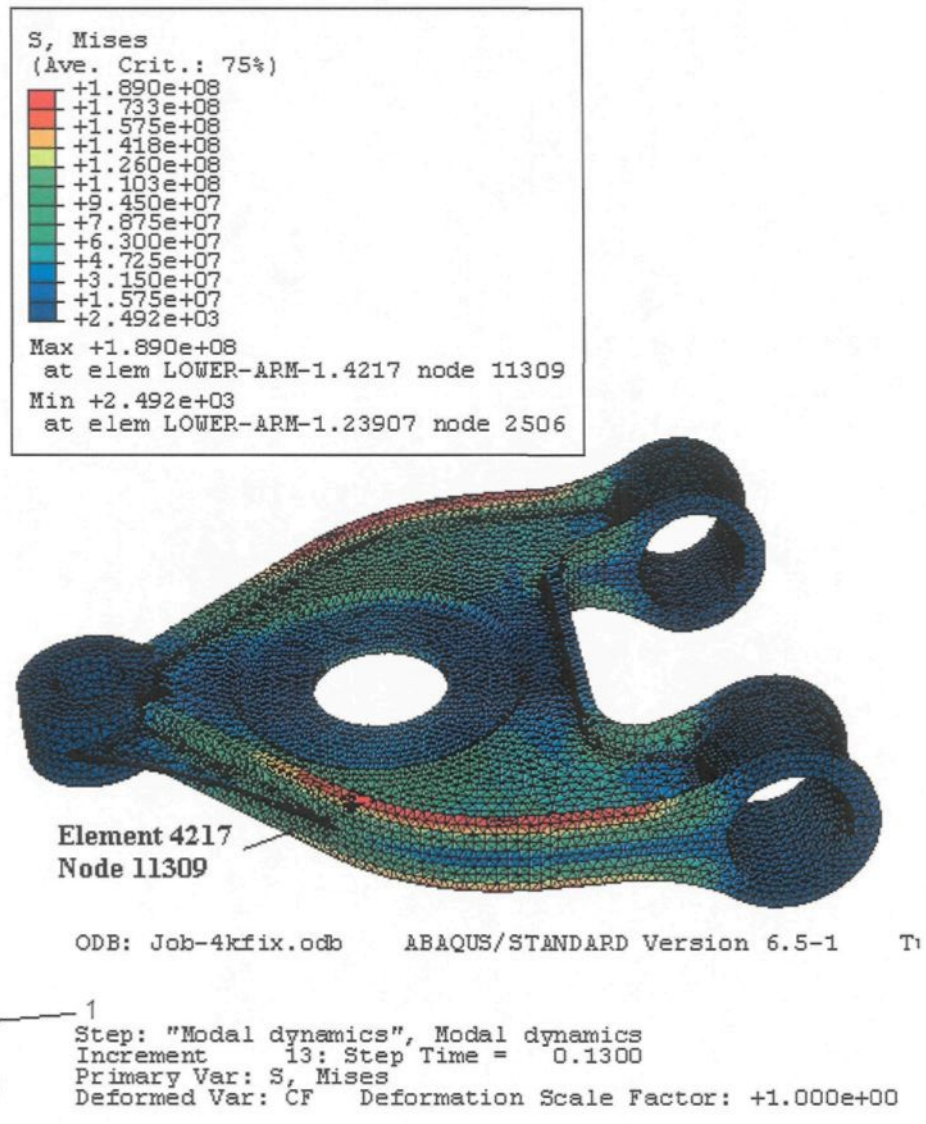


```
S, Mises
(Ave. Crit.: 75%)
   +2.492e+08
   +2.284e+08
   +2.077e+08
   +1.869e+08
   +1.661e+08
   +1.454e+08
   +1.246e+08
   +1.038e+08
   +8.307e+07
   +6.230e+07
   +4.154e+07
   +2.077e+07
   +4.063e+03
Max +2.492e+08
 at elem LOWER-ARM-1.51125 node 16490
Min +4.063e+03
 at elem LOWER-ARM-1.24103 node 2505
```

ODB: Job-4kfix-randon.odb   ABAQUS/STANDARD Version 6.5-1

```
Step: "Modal dynamics", Modal dynamics
Increment    106: Step Time =    1.060
Primary Var: S, Mises
Deformed Var: CF   Deformation Scale Factor: +1.000e+00
```

Figure 4.51 S:Mises contour of lower arm with 4KN random force, BC fixed.

```
          S:Mises PI: LOWER-ARM-1 E: 51125 IP: 1
XMIN  1.000E-02
XMAX  2.500E+00
YMIN  9.257E+05
YMAX  2.495E+08
```
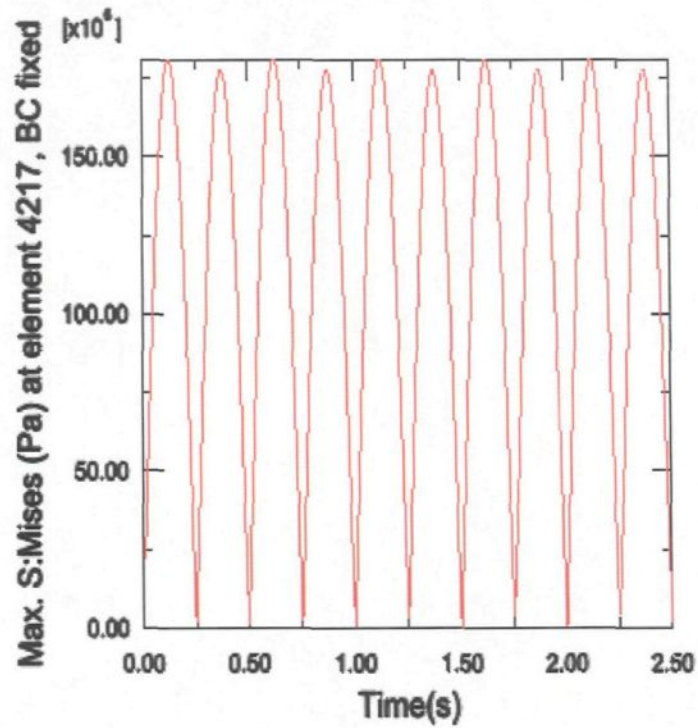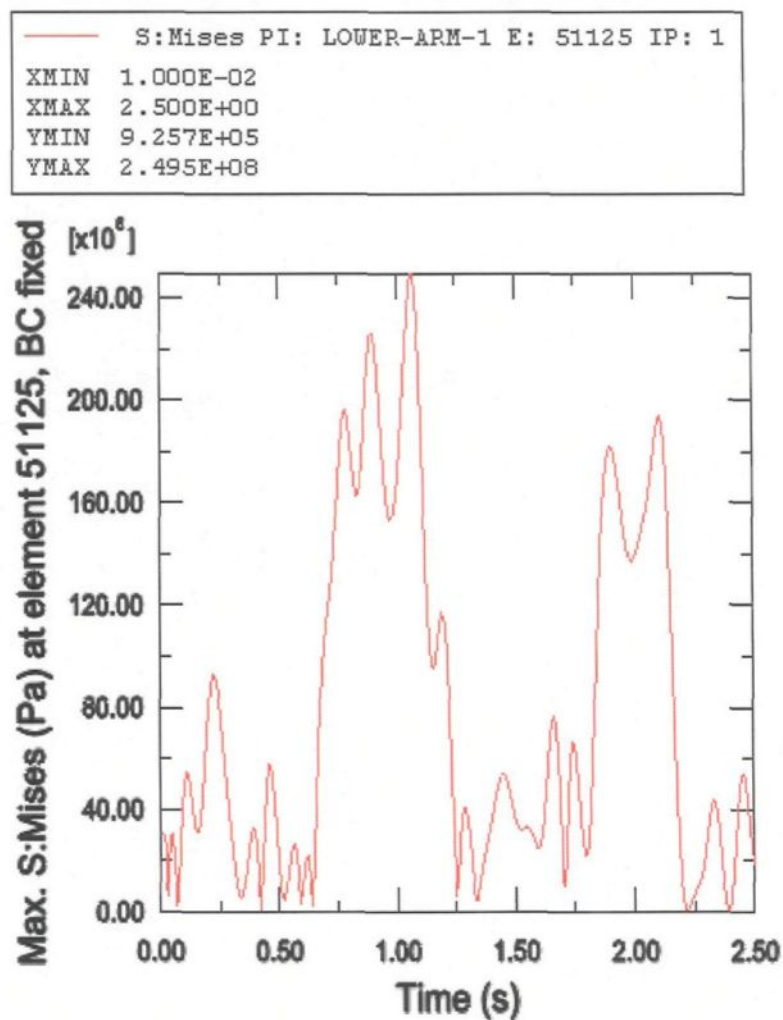

Figure 4.52   Max. S:Mises of lower arm 4KN random force, BC fixed.

3. Boundary condition BC UR2 with 5KN random force:

The part rotates around Y axes, the maximum stress is 112.2 MPa at element 15965; they

are shown in Figure 4.53 and Figure 4.54.
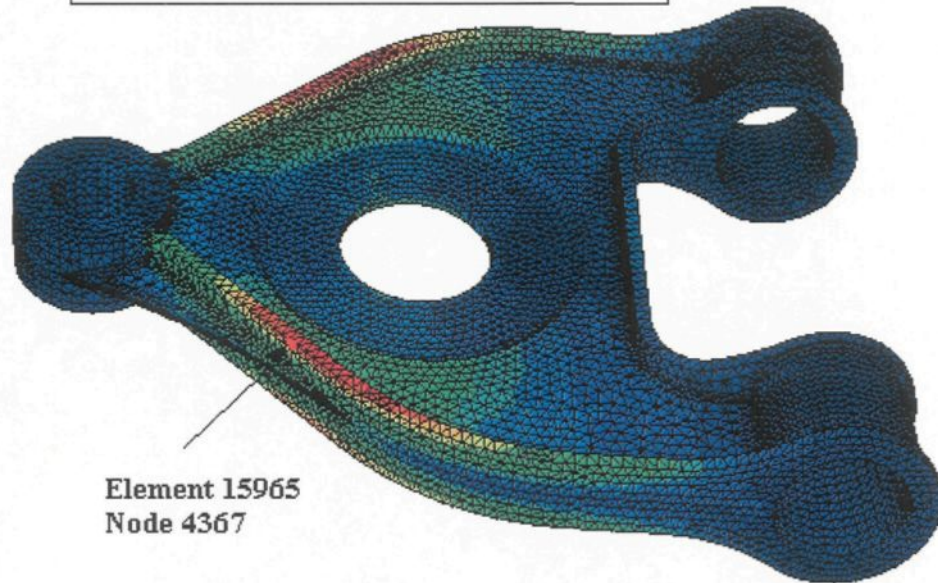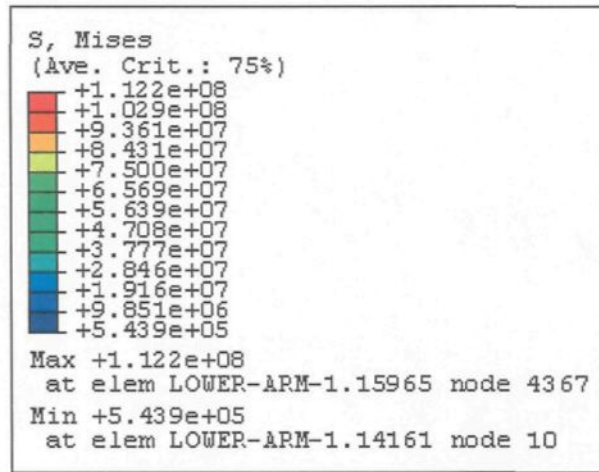
S, Mises
(Ave. Crit.: 75%)
+1.122e+08
+1.029e+08
+9.361e+07
+8.431e+07
+7.500e+07
+6.569e+07
+5.639e+07
+4.708e+07
+3.777e+07
+2.846e+07
+1.916e+07
+9.851e+06
+5.439e+05
Max +1.122e+08
  at elem LOWER-ARM-1.15965 node 4367
Min +5.439e+05
  at elem LOWER-ARM-1.14161 node 10

Element 15965
Node 4367

ODB: Job-5kur2-randon.odb   ABAQUS/STANDARD Version 6.5-1

Step: "Modal dynamics", Modal dynamics
Increment   211: Step Time =   2.110
Primary Var: S, Mises
Deformed Var: CF   Deformation Scale Factor: +1.000e+00

Figure 4.53 S:Mises contour of lower arm with 5KN random force, BC UR2.
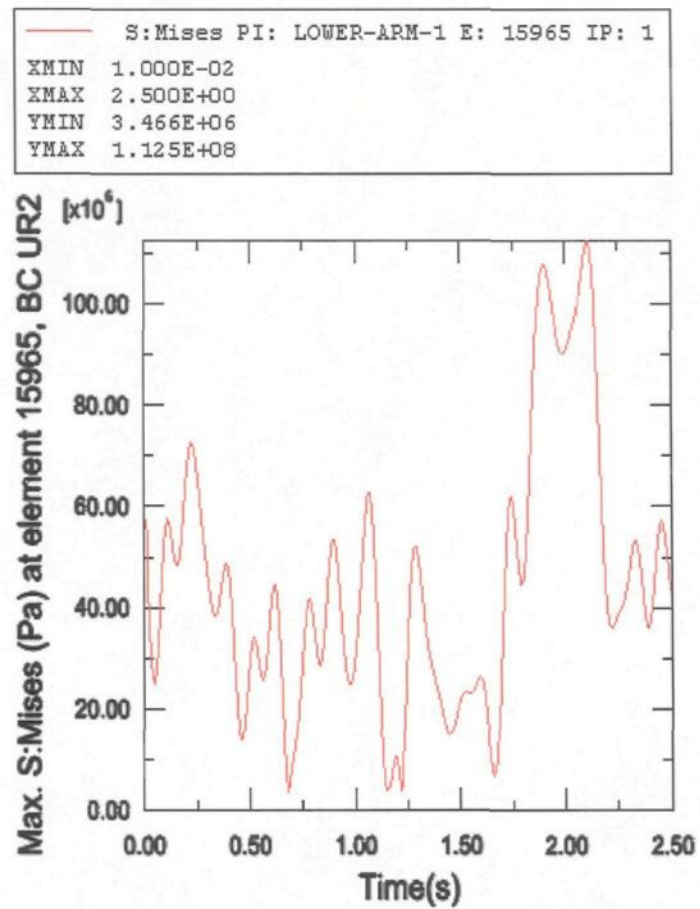
Figure 4.54   Max. S:Mises of lower arm with 5KN random force, BC UR2.

4. Boundary condition BC UR2 with 4KN random force:

The part rotates around Y axes, the maximum stress is 96.7MPa at element 15965; they are

shown in Figure 4.55 and Figure 4.56.

S, Mises
(Ave. Crit.: 75%)
+9.673e+07
+8.871e+07
+8.069e+07
+7.266e+07
+6.464e+07
+5.661e+07
+4.859e+07
+4.056e+07
+3.254e+07
+2.452e+07
+1.649e+07
+8.468e+06
+4.435e+05

Max +9.673e+07
  at elem LOWER-ARM-1.15965 node 4367
Min +4.435e+05
  at elem LOWER-ARM-1.14161 node 10

Element 15965
Node 4367

ODB: Job-4kur2-randon.odb   ABAQUS/STANDARD Version 6.5-1

Step: "Modal dynamics", Modal dynamics
Increment   211: Step Time =   2.110
Primary Var: S, Mises
Deformed Var: CF   Deformation Scale Factor: +1.000e+00

Figure 4.55   S:Mises contour of lower arm with 4KN random force, BC UR2.
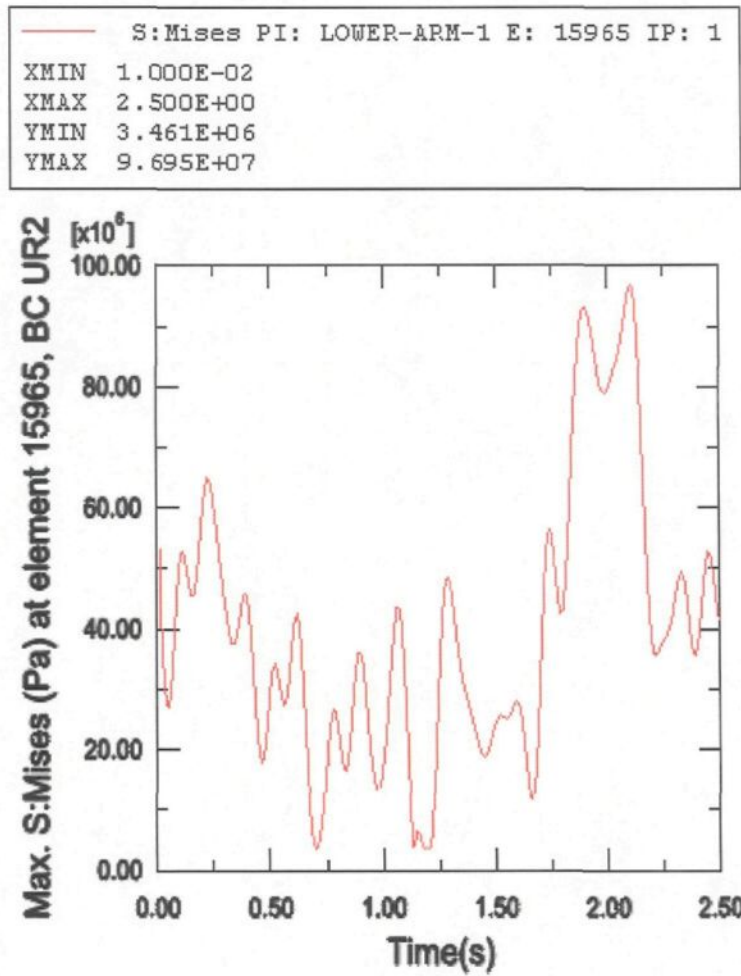
Figure 4.56 Max. S:Mises of lower arm with 4KN random force, BC UR2.

In this chapter, we studied the theory of modelization to analyse stress and establish the simulation procedure. We have loaded different sinusoidal and random forces under fixed and rotation boundary conditions. Through analysis and depending on the result of the simulation, we can cut the weight of suspension arms by the ESO method. Finally we verified the stresses and improved the upper and lower suspension arms. This method efficiently helps us to quickly design parts, save time and process steps. Today it is a very popular and useful method in optimization area.

CHAPTER 5

CHAPTER 5 Mechanical vibration analysis of suspension arms

5.1 Analysis of the vibration of lower arm

ABAQUS/Standard offers the Lanczos and the subspace iteration eigenvalue extraction methods. The Lanczos method is generally faster when a large number of eigenmodes is required for a system with many degrees of freedom. The subspace iteration method may be faster when only a few (less than 20) eigenmodes are needed. We use the Lanczos eigensolver in this analysis and request the first 30 eigenvalues. Instead of specifying the number of modes required, it is also possible to specify the minimum and maximum frequencies of interest so that the step will complete once ABAQUS/Standard has found all of the eigenvalues inside the specified range. In lower arm dynamic analysis, the response is usually associated with the lower modes. However, enough modes should be extracted to provide a good representation of the dynamic response of the structure. One way of checking that a sufficient number of eigenvalues has been extracted is to look at the total effective mass in each degree of freedom, which indicates how much of the mass is active in each direction of the extracted modes. The effective masses are tabulated in the data file under the eigenvalue output. Ideally, the sum of the modal effective masses for each mode in each direction should be at least 90% of the total mass. Specify direct modal

damping and enter a critical damping fraction of 0.05 [32] for modes 1 through 10. The time period is 2.5 and time increment is 0.01. During the simulation, we found that first 10 modes are enough in this case. Therefore, the results of frequency are just shown 10 modes and several deformation shapes.

5.1.1 Analysis of the vibration with 5KN sinusoidal force

1. Frequency of lower arm in boundary condition BC fixed:

The primary results for step Frequency with boundary condition fixed are the extracted eigenvalues, it is shown by Table 5.1. We can visualize the deformation mode associated with a given natural frequency by plotting the mode shape associated with that frequency (See Figure 5.1).

E I G E N V A L U E   O U T P U T

MODE NO	EIGENVALUE	FREQUENCY		GENERALIZED MASS	COMPOSITE MODAL DAMPING
		(RAD/TIME)	(CYCLES/TIME)		
1	1.94390E+06	1394.2	221.90	0.20368	0.0000
2	3.76458E+07	6135.6	976.51	0.25525	0.0000
3	4.46407E+07	6681.4	1063.4	0.22431	0.0000
4	1.62449E+08	12746.	2028.5	0.42107	0.0000
5	1.75955E+08	13265.	2111.2	0.10822	0.0000
6	2.56975E+08	16030.	2551.3	0.15941	0.0000
7	2.98513E+08	17278.	2749.8	0.21291	0.0000
8	5.08110E+08	22541.	3587.6	0.10162	0.0000
9	6.05708E+08	24611.	3917.0	0.11285	0.0000
10	7.22424E+08	26878.	4277.8	0.40529	0.0000

Table 5.1   The extracted eigenvalues step frequency with BC fixed
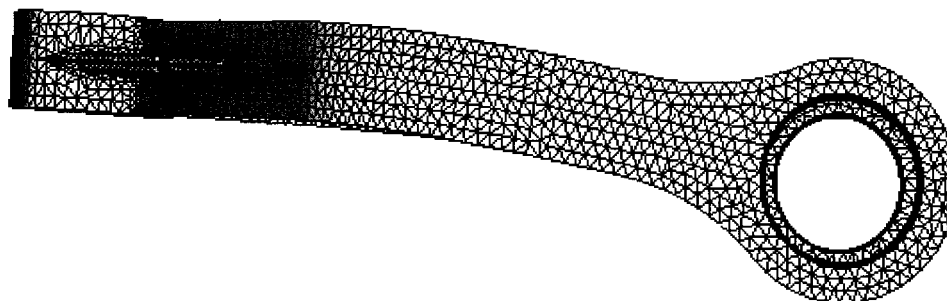
ODB: Job-lowarm4-5k.odb   ABAQUS/STANDARD Version 6.5-1   Fri

Step: "Extract Frequencies", First 10 modes
Mode   1: Value = 1.94390E+06 Freq =   221.90   (cycles/time)

Deformed Var: U   Deformation Scale Factor: +3.410e-02

(a) Mode 1
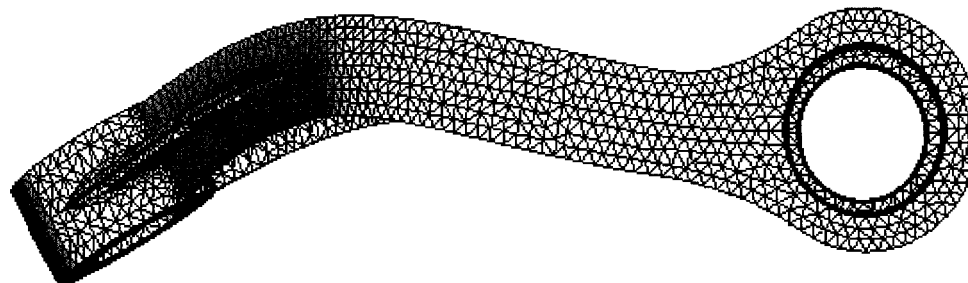
ODB: Job-lowarm4-5k.odb   ABAQUS/STANDARD Version 6.5-1   Fri I

Step: "Extract Frequencies", First 10 modes
Mode   3: Value = 4.46407E+07 Freq =   1063.4   (cycles/time)

Deformed Var: U   Deformation Scale Factor: +3.410e-02

(b) Mode 3
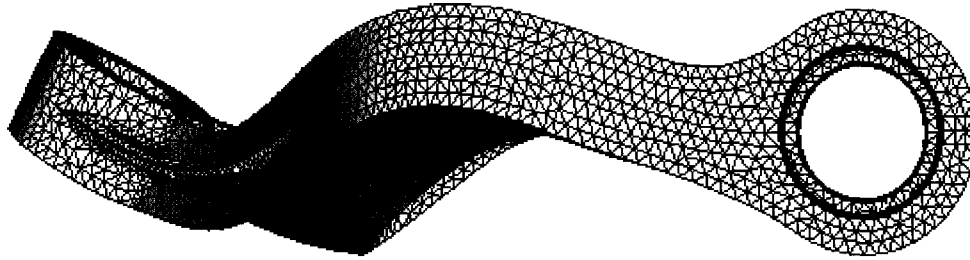
ODB: Job-lowarm4-5k.odb   ABAQUS/STANDARD Version 6.5-1   Fri :

Step: "Extract Frequencies", First 10 modes
Mode   6: Value = 2.56975E+08 Freq =   2551.3   (cycles/time)

Deformed Var: U   Deformation Scale Factor: +3.410e-02

(c) Mode 6
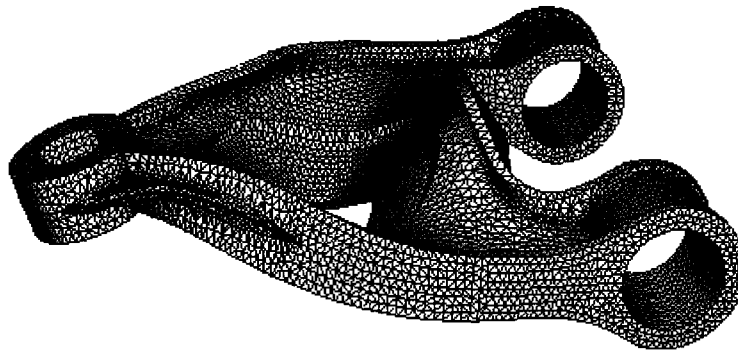
ODB: Job-5kfix.odb   ABAQUS/STANDARD Version 6.5-1   Tue May 3

Step: "Extract Frequencies", First 10 modes
Mode   9: Value = 6.05708E+08 Freq =   3917.0   (cycles/time)

Deformed Var: U   Deformation Scale Factor: +3.410e-02

(d) Mode 9

Figure 5.1   (a), (b), (c) and (d) are frequency modes with force 5KN, BC fixed.

2. Frequency of lower arm in boundary condition BC UR2:

The Step Frequency with boundary condition UR2 are the extracted eigenvalues (Table 5.2), participation factors (Table 5.3), and effective mass (Table 5.4), as shown below. The mode shape associated with that frequency are shown by Figure 5.2.

```
E I G E N V A L U E     O U T P U T

MODE NO      EIGENVALUE              FREQUENCY         GENERALIZED MASS   COMPOSITE MODAL DAMPING
                              (RAD/TIME)    (CYCLES/TIME)


     1      -2.11588E-05      0.0000          0.0000           1.1079        0.0000
     2       1.39265E-07      3.73183E-04     5.93939E-05      0.62834       0.0000
     3       4.92787E-05      7.01988E-03     1.11725E-03      1.0481        0.0000
     4       4.29955E+06      2073.5          330.01           0.35675       0.0000
     5       6.52889E+06      2555.2          406.67           0.42193       0.0000
     6       1.18273E+07      3439.1          547.35           0.35668       0.0000
     7       1.66808E+07      4084.2          650.02           0.24324       0.0000
     8       1.14633E+08      10707.          1704.0           0.31420       0.0000
     9       1.36840E+08      11698.          1861.8           0.31516       0.0000
    10       1.75553E+08      13250.          2108.7           0.14801       0.0000
```

Table 5.2   The extracted eigenvalues step frequency with BC UR2
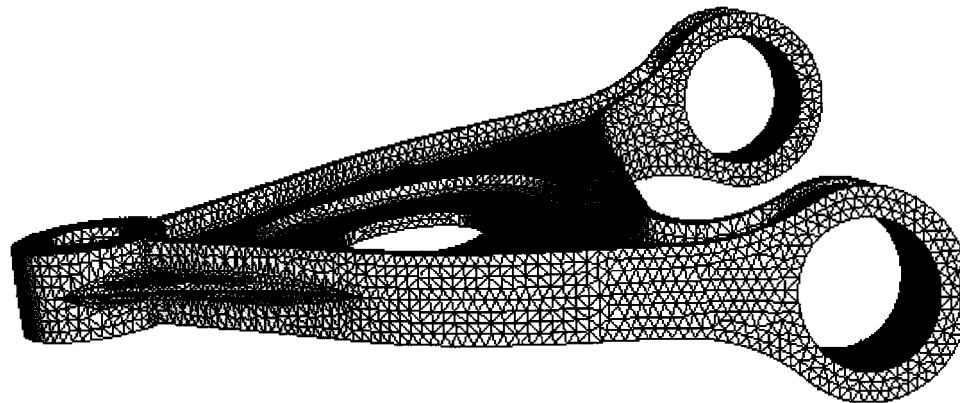

```
ODB: Job-lowarm4-5k.odb     ABAQUS/STANDARD Version 6.5-1     Fri F
```

```
    1
    Step: "Extract Frequencies", First 10 modes
    Mode    4: Value =   4.29955E+06 Freq =    330.01      (cycles/time)

    Deformed Var: U   Deformation Scale Factor: +3.410e-02
```

(a) Mode 4
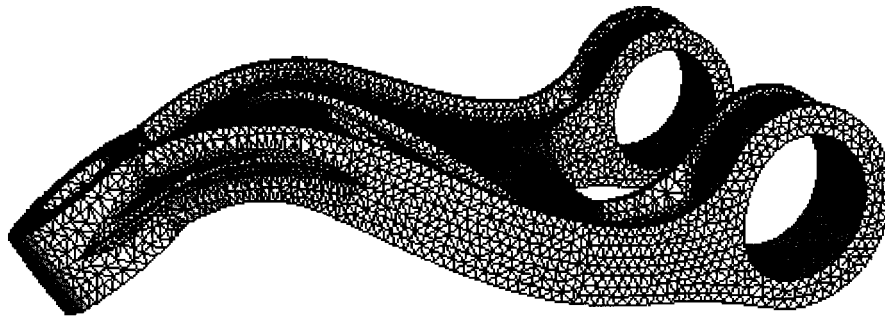
```
ODB: Job-5kur2.odb      ABAQUS/STANDARD Version 6.5-1      Tue May 30
```

```
Step: "Extract Frequencies", First 10 modes
Mode   8: Value =  1.14633E+08 Freq =    1704.0      (cycles/time)

Deformed Var: U   Deformation Scale Factor: +3.410e-02
```

(b) Mode 8


```
ODB: Job-lowarm4-5k.odb      ABAQUS/STANDARD Version 6.5-1      Fri
```

```
Step: "Extract Frequencies", First 10 modes
Mode  10: Value =  1.75553E+08 Freq =    2108.7      (cycles/time)

Deformed Var: U   Deformation Scale Factor: +3.410e-02
```
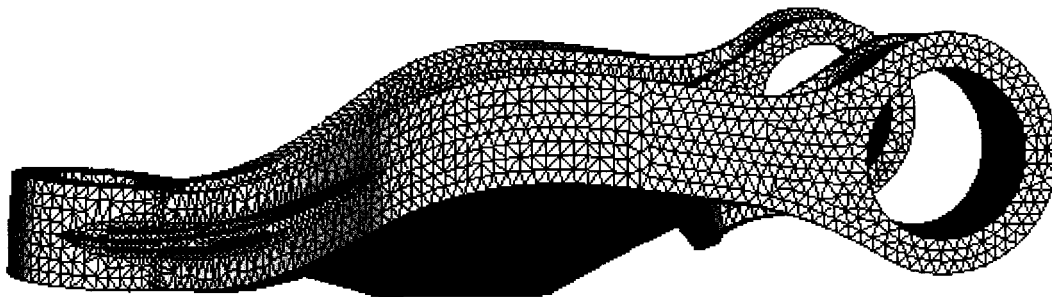
(c) Mode 10

Figure 5.2   (a), (b) and (c) are frequency modes with force 5KN and BC UR2.

The column for generalized mass lists the mass of a single degree of freedom system associated with that mode. The table of participation factors indicates the predominant degrees of freedom in which the modes act. The results indicate, for example, that mode 3 acts predominantly in the 3(Z)-direction.

```
P A R T I C I P A T I O N   F A C T O R S
```

MODE NO	X-COMPONENT	Y-COMPONENT	Z-COMPONENT	X-ROTATION	Y-ROTATION	Z-ROTATION
1	-0.99725	-2.05173E-12	0.11473	-1.09165E-07	4.01797E-02	-3.42366E-09
2	-0.80174	3.34801E-13	0.31801	1.55339E-07	-0.17283	-3.64768E-07
3	0.23016	-9.16007E-13	1.1895	-1.75569E-07	-0.17555	5.88105E-08
4	1.48318E-13	2.90910E-02	-6.54319E-12	0.14409	1.53147E-12	-1.78111E-03
5	-3.79941E-12	1.2151	2.78280E-12	-5.32717E-03	-1.08106E-13	1.84059E-02
6	-2.80837E-13	3.84206E-02	-1.75824E-12	5.82187E-02	-4.90857E-14	3.15688E-03
7	7.09997E-13	4.30444E-04	-8.16007E-12	2.88696E-04	1.11369E-12	1.51298E-05
8	1.53840E-13	-6.96475E-04	-1.46834E-13	6.95579E-05	-4.77115E-14	-1.38476E-04
9	-8.84144E-14	-7.58959E-02	2.87199E-13	9.08287E-03	-3.83325E-14	-1.79082E-02
10	-1.01822E-13	-1.93781E-03	-7.81271E-13	-1.36581E-05	1.44957E-13	-4.75653E-04

Table 5.3   Participation factors

The table of effective mass indicates the amount of mass active in each degree of freedom for any one mode. The results indicate that the 3 modes with significant mass in the 3 directions is mode 3. The total modal effective mass is 1.5612 kg.

```
E F F E C T I V E   M A S S
```

MODE NO	X-COMPONENT	Y-COMPONENT	Z-COMPONENT	X-ROTATION	Y-ROTATION	Z-ROTATION
1	1.1018	4.66364E-24	1.45821E-02	1.32024E-14	1.78853E-03	1.29857E-17
2	0.40389	7.04321E-26	6.35440E-02	1.51621E-14	1.87696E-02	8.36045E-14
3	5.55222E-02	8.79430E-25	1.4831	3.23071E-14	3.22984E-02	3.62504E-15
4	7.84780E-27	3.01910E-04	1.52735E-23	7.40637E-03	8.36716E-25	1.13172E-06
5	6.09071E-24	0.62298	3.26737E-24	1.19737E-05	4.93098E-27	1.42939E-04
6	2.81308E-26	5.26505E-04	1.10263E-24	1.20892E-03	8.59374E-28	3.55460E-06
7	1.22619E-25	4.50689E-08	1.61969E-23	2.02733E-08	3.01697E-25	5.56815E-11
8	7.43602E-27	1.52411E-07	6.77418E-27	1.52019E-09	7.15237E-28	6.02499E-09
9	2.46362E-27	1.81536E-03	2.59952E-26	2.60000E-05	4.63085E-28	1.01072E-04
10	1.53452E-27	5.55788E-07	9.03422E-26	2.76100E-11	3.11003E-27	3.34864E-08
TOTAL	1.5612	0.62563	1.5612	8.65329E-03	5.28565E-02	2.48736E-04

Table 5.4   Effective mass

The total mass of the model is given earlier in the data file and is 1.56 kg. To ensure that enough modes have been used, the total effective mass in each direction should be a large proportion of the mass of the model (say 90%). The total effective mass in the 1- and

3-directions is above the 90% recommended; the total effective mass in the 2-direction is much lower. However, since the loading is applied in the 3-direction, the response in the 2-direction is not significant.

5.1.2 Vibration analysis with sinusoidal force 4KN

1. Frequency of lower arm in boundary condition BC fixed:

Repeat the frequency step with a new loading. The results for step Frequency with boundary condition fixed are the extracted eigenvalues, it is shown by Table 5.5. They are visualized the deformation mode associated with a given natural frequency by plotting the mode shape associated with that frequency (see Figure 5.3).

```
                       E I G E N V A L U E    O U T P U T

MODE NO     EIGENVALUE          FREQUENCY        GENERALIZED MASS   COMPOSITE MODAL DAMPING
                            (RAD/TIME)  (CYCLES/TIME)


    1      1.94390E+06      1394.2       221.90        0.20368         0.0000
    2      3.76458E+07      6135.6       976.51        0.25525         0.0000
    3      4.46407E+07      6681.4       1063.4        0.22431         0.0000
    4      1.62449E+08      12746.       2028.5        0.42107         0.0000
    5      1.75955E+08      13265.       2111.2        0.10822         0.0000
    6      2.56975E+08      16030.       2551.3        0.15941         0.0000
    7      2.98513E+08      17278.       2749.8        0.21291         0.0000
    8      5.08110E+08      22541.       3587.6        0.10162         0.0000
    9      6.05708E+08      24611.       3917.0        0.11285         0.0000
   10      7.22424E+08      26878.       4277.8        0.40529         0.0000
```

Table 5.5   The extracted eigenvalues step frequency with BC fixed
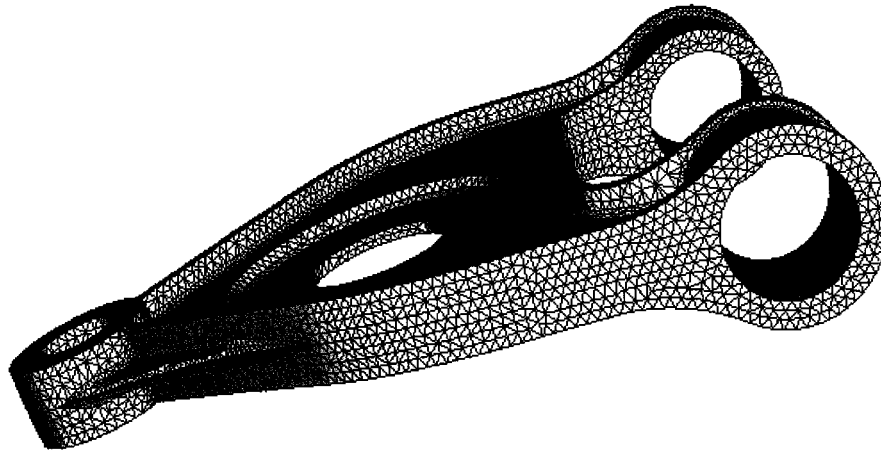
Lower arm dynamic with frequency
ODB: Job-lowerarm4.odb   ABAQUS/STANDARD Version 6.5-1   Thu F

Step: "Extract Frequencies", First 10 modes
Mode   1: Value = 1.94390E+06 Freq =   221.90   (cycles/time)

Deformed Var: U   Deformation Scale Factor: +3.410e-02

(a) Mode 1

Lower arm dynamic with frequency
ODB: Job-lowerarm4.odb   ABAQUS/STANDARD Version 6.5-1   Thu F

Step: "Extract Frequencies", First 10 modes
Mode   2: Value = 3.76458E+07 Freq =   976.51   (cycles/time)

Deformed Var: U   Deformation Scale Factor: +3.410e-02

(b) Mode 2

Lower arm dynamic with frequency
ODB: Job-lowerarm4.odb   ABAQUS/STANDARD Version 6.5-1   Thu Fe

Step: "Extract Frequencies", First 10 modes
Mode   6: Value = 2.56975E+08 Freq =   2551.3   (cycles/time)

Deformed Var: U   Deformation Scale Factor: +3.410e-02

(c) Mode 6

Figure 5.3   (a), (b) and (c) frequency modes, force 4KN, BC fixed.

2. Frequency of lower arm in boundary condition BC UR2:

The results for step Frequency with boundary condition UR2 are the extracted eigenvalues, participation factors, and effective mass (Table 5.6), as shown below. The mode shape associated with that frequency (see Figure 5.4).

EIGENVALUE OUTPUT

MODE NO	EIGENVALUE	FREQUENCY (RAD/TIME)	(CYCLES/TIME)	GENERALIZED MASS	COMPOSITE MODAL DAMPING
1	-2.11588E-05	0.0000	0.0000	1.1079	0.0000
2	1.39265E-07	3.73183E-04	5.93939E-05	0.62834	0.0000
3	4.92787E-05	7.01988E-03	1.11725E-03	1.0481	0.0000
4	4.29955E+06	2073.5	330.01	0.35675	0.0000
5	6.52889E+06	2555.2	406.67	0.42193	0.0000
6	1.18273E+07	3439.1	547.35	0.35668	0.0000
7	1.66808E+07	4084.2	650.02	0.24324	0.0000
8	1.14633E+08	10707.	1704.0	0.31420	0.0000
9	1.36840E+08	11698.	1861.8	0.31516	0.0000
10	1.75553E+08	13250.	2108.7	0.14801	0.0000

PARTICIPATION FACTORS

MODE NO	X-COMPONENT	Y-COMPONENT	Z-COMPONENT	X-ROTATION	Y-ROTATION	Z-ROTATION
1	-0.99725	-2.05173E-12	0.11473	-1.09165E-07	4.01797E-02	-3.42366E-09
2	-0.80174	3.34801E-13	0.31801	1.55339E-07	-0.17283	-3.64768E-07
3	0.23016	-9.16007E-13	1.1895	-1.75569E-07	-0.17555	5.88105E-08
4	1.48318E-13	2.90910E-02	-6.54319E-12	0.14409	1.53147E-12	-1.78111E-03
5	-3.79941E-12	1.2151	2.78280E-12	-5.32717E-03	-1.08106E-13	1.84059E-02
6	-2.80837E-13	3.84206E-02	-1.75824E-12	5.82187E-02	-4.90857E-14	3.15688E-03
7	7.09997E-13	4.30444E-04	-8.16007E-12	2.88696E-04	1.11369E-12	1.51298E-05
8	1.53840E-13	-6.96475E-04	-1.46834E-13	6.95579E-05	-4.77115E-14	-1.38476E-04
9	-8.84144E-14	-7.58959E-02	2.87199E-13	9.08287E-03	-3.83325E-14	-1.79082E-02
10	-1.01822E-13	-1.93781E-03	-7.81271E-13	-1.36581E-05	1.44957E-13	-4.75653E-04

EFFECTIVE MASS

MODE NO	X-COMPONENT	Y-COMPONENT	Z-COMPONENT	X-ROTATION	Y-ROTATION	Z-ROTATION
1	1.1018	4.66364E-24	1.45821E-02	1.32024E-14	1.78853E-03	1.29857E-17
2	0.40389	7.04321E-26	6.35440E-02	1.51621E-14	1.87696E-02	8.36045E-14
3	5.55222E-02	8.79430E-25	1.4831	3.23071E-14	3.22984E-02	3.62504E-15
4	7.84780E-27	3.01910E-04	1.52735E-23	7.40637E-03	8.36716E-25	1.13172E-06
5	6.09071E-24	0.62298	3.26737E-24	1.19737E-05	4.93098E-27	1.42939E-04
6	2.81308E-26	5.26505E-04	1.10263E-24	1.20892E-03	8.59374E-28	3.55460E-06
7	1.22619E-25	1.61969E-23	1.61969E-23	2.02733E-08	3.01697E-25	5.56815E-11
8	7.43602E-27	1.52411E-07	6.77418E-27	1.52019E-09	7.15237E-28	6.02499E-09
9	2.46362E-27	1.81536E-03	2.59952E-26	2.60000E-05	4.63085E-28	1.01072E-04
10	1.53452E-27	5.55788E-07	9.03422E-26	2.76100E-11	3.11003E-27	3.34864E-08
TOTAL	1.5612	0.62563	1.5612	8.65329E-03	5.28565E-02	2.48736E-04

Table 5.6 The extracted eigenvalues, participation factors and effective mass of step frequency with BC UR2
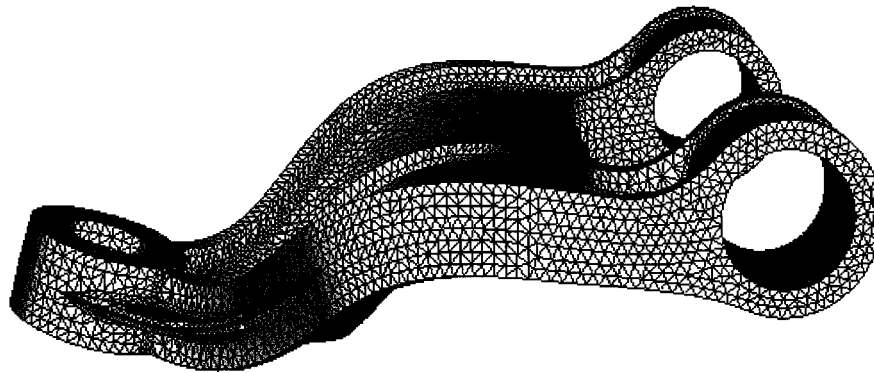
Lower arm dynamic with frequency
ODB: Job-lowerarm4.odb   ABAQUS/STANDARD Version 6.5-1   Fri F
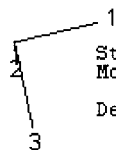
Step: "Extract Frequencies", First 10 modes
Mode   4: Value =   4.29955E+06 Freq =   330.01   (cycles/time)

Deformed Var: U   Deformation Scale Factor: +3.410e-02

(a) Mode 4

ODB: Job-4kur2.odb   ABAQUS/STANDARD Version 6.5-1   Tue May 3

Step: "Extract Frequencies", First 10 modes
Mode   8: Value =   1.14633E+08 Freq =   1704.0   (cycles/time)

Deformed Var: U   Deformation Scale Factor: +3.410e-02

(b) Mode 8

Lower arm dynamic with frequency
ODB: Job-lowerarm4.odb   ABAQUS/STANDARD Version 6.5-1   Fri Fe

Step: "Extract Frequencies", First 10 modes
Mode 10: Value =   1.75553E+08 Freq =   2108.7   (cycles/time)

Deformed Var: U   Deformation Scale Factor: +3.410e-02
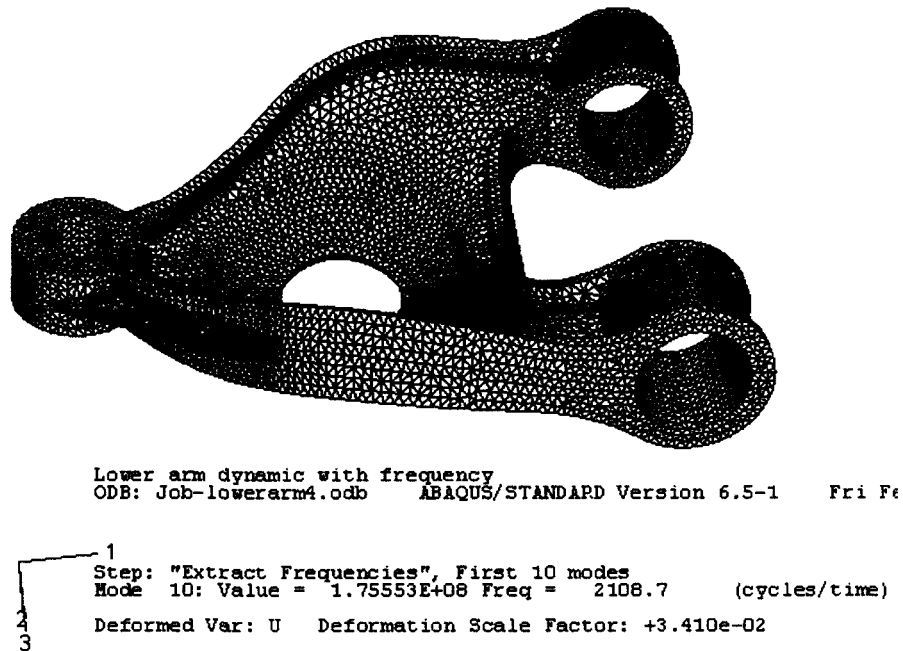
(c) Mode 10

Figure 5.4   (a), (b) and (c) are frequency modes with force 4KN, BC UR2.

5.1.3 Vibration analysis with random force 5KN

We use the random force amplitude instead of sinusoidal amplitude. Then repeat paragraph 5.1.1 analyse vibration of lower arm again. The results of step Frequency with boundary condition UR2 are the extracted eigenvalues, participation factors, and effective mass as Table 5.7 shown below. The mode shapes associated with those frequencies are represented by Figure 5.5.

ODB: Job-5kur2-randon.odb   ABAQUS/STANDARD Version 6.5-1

Step: "Extract Frequencies", First 10 modes
Mode   1: Value = -2.11588E-05 Freq =   0.0000   (cycles/time)

Deformed Var: U   Deformation Scale Factor: +3.410e-02

(a) Mode 1
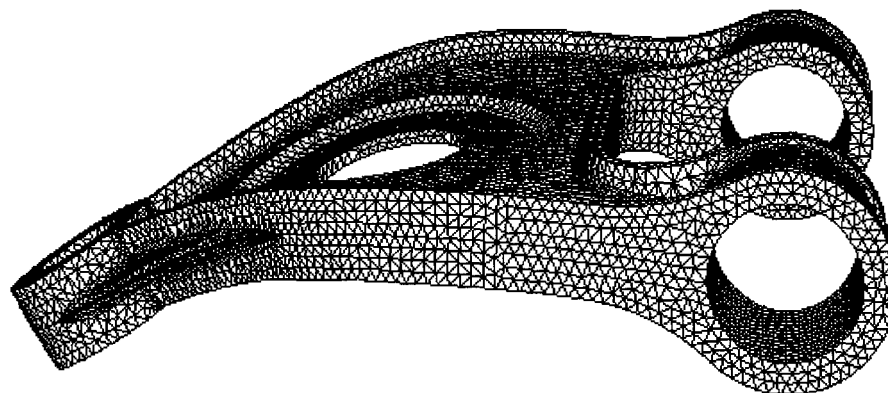
ODB: Job-5kur2-randon.odb   ABAQUS/STANDARD Version 6.5-1   We

Step: "Extract Frequencies", First 10 modes
Mode   7: Value = 1.66808E+07 Freq =   650.02   (cycles/time)

Deformed Var: U   Deformation Scale Factor: +3.410e-02

(b) Mode 7

ODB: Job-5kur2-randon.odb   ABAQUS/STANDARD Version 6.5-1   We

1

Step: "Extract Frequencies", First 10 modes
Mode   8: Value = 1.14633E+08 Freq =   1704.0   (cycles/time)

Deformed Var: U   Deformation Scale Factor: +3.410e-02

(c) Mode 8

ODB: Job-5kur2-randon.odb   ABAQUS/STANDARD Version 6.5-1   We

1

Step: "Extract Frequencies", First 10 modes
Mode   10: Value = 1.75553E+08 Freq =   2108.7   (cycles/time)

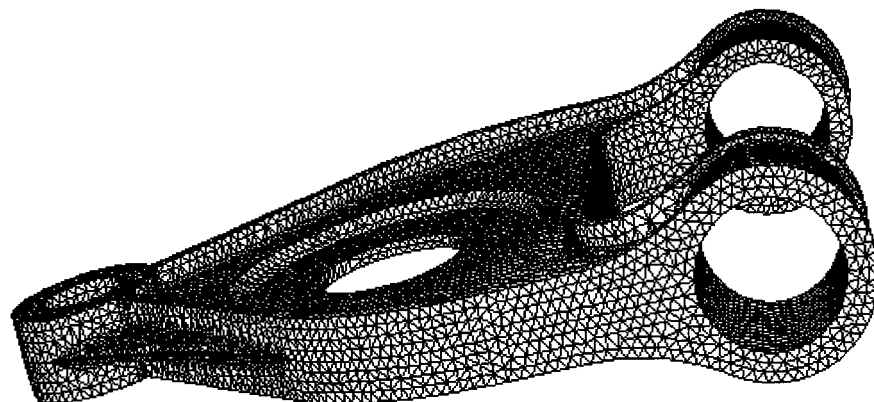Deformed Var: U   Deformation Scale Factor: +3.410e-02

(d) Mode 10

Figure 5.5   (a), (b), (c) and (d) are frequency modes with force 5KN, BC UR2.

E I G E N V A L U E   O U T P U T

MODE NO	EIGENVALUE	FREQUENCY (RAD/TIME)	FREQUENCY (CYCLES/TIME)	GENERALIZED MASS	COMPOSITE MODAL DAMPING
1	-2.11588E-05	0.0000	0.0000	1.1079	0.0000
2	1.39265E-07	3.73183E-04	5.93939E-05	0.62834	0.0000
3	4.92787E-05	7.01988E-03	1.11725E-03	1.0481	0.0000
4	4.29955E+06	2073.5	330.01	0.35675	0.0000
5	6.52889E+06	2555.2	406.67	0.42193	0.0000
6	1.18273E+07	3439.1	547.35	0.35668	0.0000
7	1.66808E+07	4084.2	650.02	0.24324	0.0000
8	1.14633E+08	10707.	1704.0	0.31420	0.0000
9	1.36840E+08	11698.	1861.8	0.31516	0.0000
10	1.75553E+08	13250.	2108.7	0.14801	0.0000

P A R T I C I P A T I O N   F A C T O R S

MODE NO	X-COMPONENT	Y-COMPONENT	Z-COMPONENT	X-ROTATION	Y-ROTATION	Z-ROTATION
1	-0.99725	-2.05173E-12	0.11473	-1.09165E-07	4.01797E-02	-3.42366E-09
2	-0.80174	3.34801E-13	0.31801	1.55339E-07	-0.17283	-3.64768E-07
3	0.23016	-9.16007E-13	1.1895	-1.75569E-07	-0.17555	5.88105E-08
4	1.48318E-13	2.90910E-02	-6.54319E-12	0.14409	1.53147E-12	-1.78111E-03
5	-3.79941E-12	1.2151	2.78280E-12	-5.32717E-03	-1.08106E-13	1.84059E-02
6	-2.80837E-13	3.84206E-02	-1.75824E-12	5.82187E-02	-4.90857E-14	3.15688E-03
7	7.09997E-13	4.30444E-04	-8.16007E-12	2.88696E-04	1.11369E-12	1.51298E-05
8	1.53840E-13	-6.96475E-04	-1.46834E-13	6.95579E-05	-4.77115E-14	-1.38476E-04
9	-8.84144E-14	-7.58959E-02	2.87199E-13	9.08287E-03	-3.83325E-14	-1.79082E-02
10	-1.01822E-13	-1.93781E-03	-7.81271E-13	-1.36581E-05	1.44957E-13	-4.75653E-04

E F F E C T I V E   M A S S

MODE NO	X-COMPONENT	Y-COMPONENT	Z-COMPONENT	X-ROTATION	Y-ROTATION	Z-ROTATION
1	1.1018	4.66364E-24	1.45821E-02	1.32024E-14	1.78853E-03	1.29857E-17
2	0.40389	7.04321E-26	6.35440E-02	1.51621E-14	1.87696E-02	8.36045E-14
3	5.55222E-02	8.79430E-25	1.4831	3.23071E-14	3.22984E-02	3.62504E-15
4	7.84780E-27	3.01910E-04	1.52735E-23	7.40637E-03	8.36716E-25	1.13172E-06
5	6.09071E-24	0.62298	3.26737E-24	1.19737E-05	4.93098E-27	1.42939E-04
6	2.81308E-26	5.26505E-04	1.10263E-24	1.20892E-03	8.59374E-28	3.55460E-06
7	1.22619E-25	4.50689E-08	1.61969E-23	2.02733E-08	3.01697E-25	5.56815E-11
8	7.43602E-27	1.52411E-07	6.77418E-27	1.52019E-09	7.15237E-28	6.02499E-09
9	2.46362E-27	1.81536E-03	2.59952E-26	2.60000E-05	4.63085E-28	1.01072E-04
10	1.53452E-27	5.55788E-07	9.03422E-26	2.76100E-11	3.11003E-27	3.34864E-08
TOTAL	1.5612	0.62563	1.5612	8.65329E-03	5.28565E-02	2.48736E-04

Table 5.7 The extracted eigenvalues, participation factors and effective mass of step frequency with 5KN random force, BC UR2

5.1.4   Vibration analysis with random force 4KN

We use random amplitude replace sinusoidal amplitude. Then repeat paragraph 5.1.2 analyse vibration of lower arm again. The results for step Frequency with boundary condition UR2 are the extracted eigenvalues, participation factors, and effective mass (Table 5.8), as shown below. The mode shape associated with that frequency are represented by Figure 5.6.
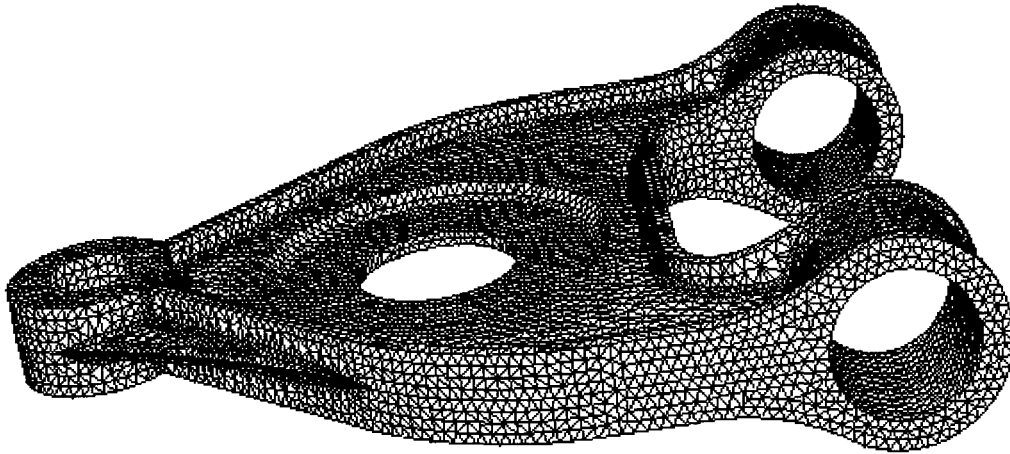
ODB: Job-4kur2-randon.odb   ABAQUS/STANDARD Version 6.5-1

Step: "Extract Frequencies", First 10 modes
Mode   1: Value = -2.11588E-05 Freq =   0.0000   (cycles/time)

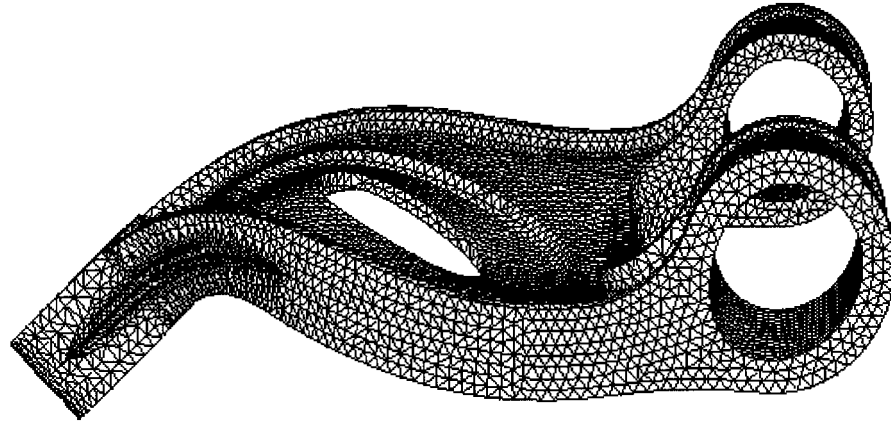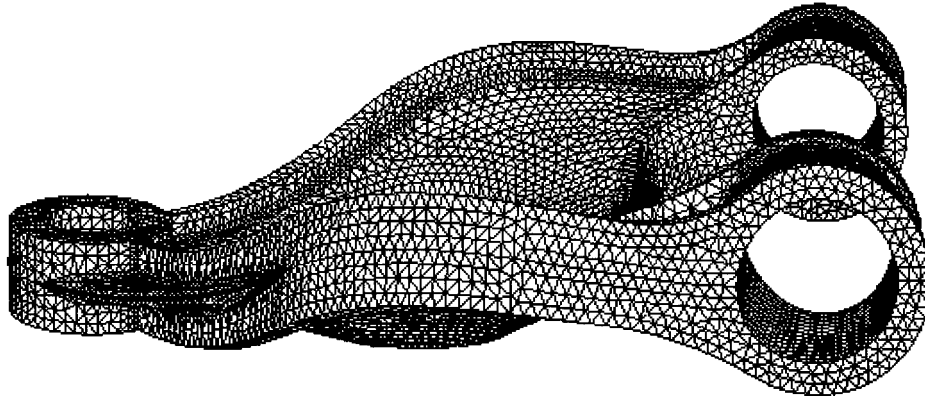Deformed Var: U   Deformation Scale Factor: +3.410e-02

(a) Mode 1
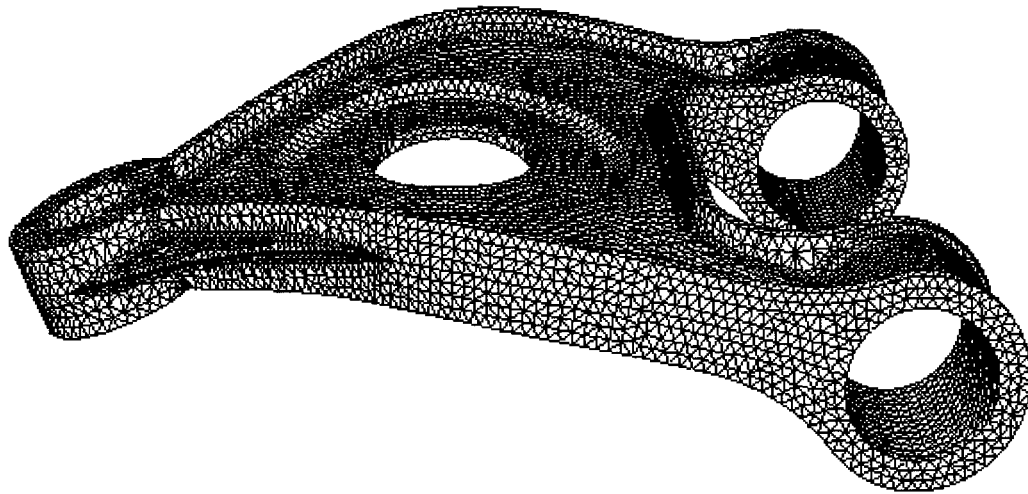
ODB: Job-4kur2-randon.odb   ABAQUS/STANDARD Version 6.5-1

Step: "Extract Frequencies", First 10 modes
Mode   7: Value = 1.66808E+07 Freq =   650.02   (cycles/time)

Deformed Var: U   Deformation Scale Factor: +3.410e-02

(b) Mode 7
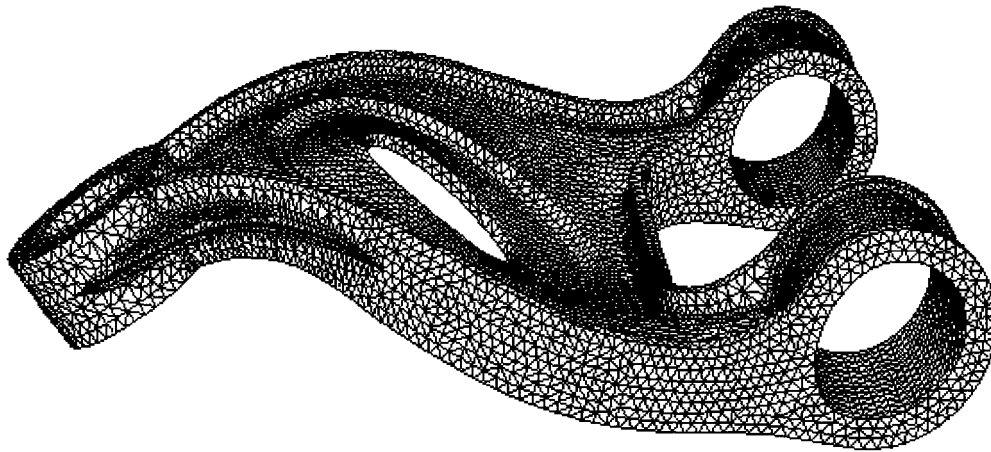
ODB: Job-4kur2-randon.odb   ABAQUS/STANDARD Version 6.5-1   Wi

Step: "Extract Frequencies", First 10 modes
Mode   8: Value =   1.14633E+08 Freq =   1704.0   (cycles/time:

Deformed Var: U   Deformation Scale Factor: +3.410e-02

(c) Mode 8
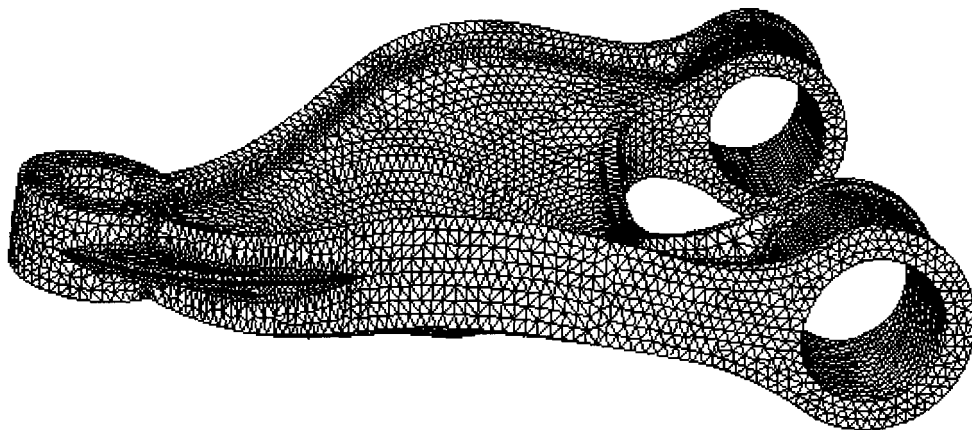
ODB: Job-4kur2-randon.odb   ABAQUS/STANDARD Version 6.5-1   We

Step: "Extract Frequencies", First 10 modes
Mode   10: Value =   1.75553E+08 Freq =   2108.7   (cycles/time)

Deformed Var: U   Deformation Scale Factor: +3.410e-02

(d) Mode 10

Figure 5.6   (a), (b), (c) and (d) are frequency modes with force 4KN, BC UR2.

```
                        E I G E N V A L U E    O U T P U T
```

MODE NO	EIGENVALUE	FREQUENCY (RAD/TIME)	(CYCLES/TIME)	GENERALIZED MASS	COMPOSITE MODAL DAMPING
1	-2.11588E-05	0.0000	0.0000	1.1079	0.0000
2	1.39265E-07	3.73183E-04	5.93939E-05	0.62834	0.0000
3	4.92787E-05	7.01988E-03	1.11725E-03	1.0481	0.0000
4	4.29955E+06	2073.5	330.01	0.35675	0.0000
5	6.52889E+06	2555.2	406.67	0.42193	0.0000
6	1.18273E+07	3439.1	547.35	0.35668	0.0000
7	1.66808E+07	4084.2	650.02	0.24324	0.0000
8	1.14633E+08	10707.	1704.0	0.31420	0.0000
9	1.36840E+08	11698.	1861.8	0.31516	0.0000
10	1.75553E+08	13250.	2108.7	0.14801	0.0000

```
        P A R T I C I P A T I O N    F A C T O R S
```

MODE NO	X-COMPONENT	Y-COMPONENT	Z-COMPONENT	X-ROTATION	Y-ROTATION	Z-ROTATION
1	-0.99725	-2.05173E-12	0.11473	-1.09165E-07	4.01797E-02	-3.42366E-09
2	-0.80174	3.34801E-13	0.31801	1.55339E-07	-0.17283	-3.64768E-07
3	0.23016	-9.16007E-13	1.1895	-1.75569E-07	-0.17555	5.88105E-08
4	1.48318E-13	2.90910E-02	-6.54319E-12	0.14409	1.53147E-12	-1.78111E-03
5	-3.79941E-12	1.2151	2.78280E-12	-5.32717E-03	-1.08106E-13	1.84059E-02
6	-2.80837E-13	3.84206E-02	-1.75824E-12	5.82187E-02	-4.90857E-14	3.15688E-03
7	7.09997E-13	4.30444E-04	-8.16007E-12	2.88696E-04	1.11369E-12	1.51298E-05
8	1.53840E-13	-6.96475E-04	-1.46834E-13	6.95579E-05	-4.77115E-14	-1.38476E-04
9	-8.84144E-14	-7.58959E-02	2.87199E-13	9.08287E-03	-3.83325E-14	-1.79082E-02
10	-1.01822E-13	-1.93781E-03	-7.81271E-13	-1.36581E-05	1.44957E-13	-4.75653E-04

```
        E F F E C T I V E    M A S S
```

MODE NO	X-COMPONENT	Y-COMPONENT	Z-COMPONENT	X-ROTATION	Y-ROTATION	Z-ROTATION
1	1.1018	4.66364E-24	1.45821E-02	1.32024E-14	1.78853E-03	1.29857E-17
2	0.40389	7.04321E-26	6.35440E-02	1.51621E-14	1.87696E-02	8.36045E-14
3	5.55222E-02	8.79430E-25	1.4831	3.23071E-14	3.22984E-02	3.62504E-15
4	7.84780E-27	3.01010E-04	1.52735E-23	7.40637E-03	8.36716E-25	1.13172E-06
5	6.09071E-24	0.62298	3.26737E-24	1.19737E-05	4.93098E-27	1.42939E-04
6	2.81308E-26	5.26505E-04	1.10263E-24	1.20892E-03	8.59374E-28	3.55460E-06
7	1.22619E-25	4.50689E-08	1.61969E-23	2.02733E-08	3.01697E-25	5.56815E-11
8	7.43602E-27	1.52411E-07	6.77418E-27	1.52019E-09	7.15237E-28	6.02499E-09
9	2.46362E-27	1.81536E-03	2.59952E-26	2.60000E-05	4.63085E-28	1.01072E-04
10	1.53452E-27	5.55788E-07	9.03422E-26	2.76100E-11	3.11003E-27	3.34864E-08
TOTAL	1.5612	0.62563	1.5612	8.65329E-03	5.28565E-02	2.48736E-04

1

Table 5.8 The extracted eigenvalues, participation factors and effective mass of step frequency with 4KN random force, BC UR2

In the simulations above, we have loaded different sinusoidal and random forces under the fixed and rotation boundary condition. We can visualize that part deformation shape associated with its frequency by the simulation. To analyse the load deformation with the eigenvalues and effective mass avoid the range of resonance in the design of parts. Through the simulation of vibrations, we verified vibrations and improved the suspension arms. The results of the vibration analysis for the arms are not shown in all condition of them, but it is satisfy enough.

CHAPTER 6

CHAPTER 6 Results and discussion

6.1 Comparing results of upper arm with different boundary conditions and constant force

We can compare the result of the upper arm in fixed boundary condition (axes X=Y=Z=UR1=UR2=UR3=0) and boundary condition rotation with respect to the Y-axis (UR2=0.52, axes Y=UR1=UR3=0). The stress of the part in BC fixed is higher than the stress of part in BC UR2 (See Figure 6.1 to Figure 6.3). However, their maximum stresses are less than average yield strength 275MPa. Therefore the upper control arm is successfully developed.

$$Force \quad 2500N \begin{cases} BC \quad Fixed \\ BC \quad Rotation(UR2) \end{cases}$$

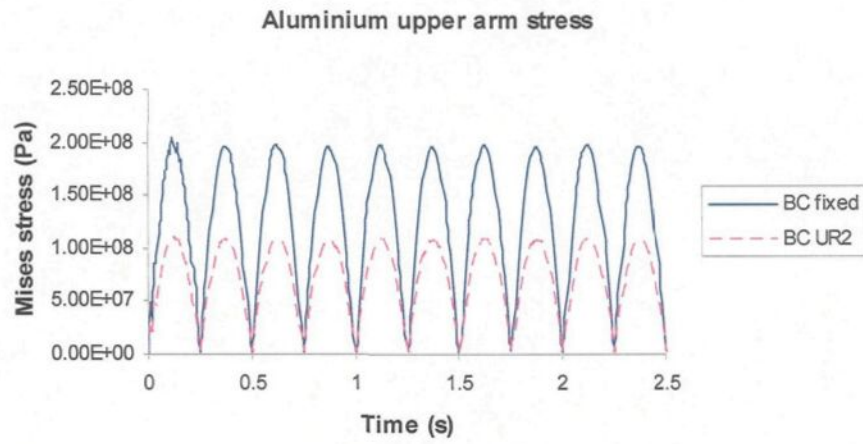**a) Comparing the stress of the upper arms with sinusoidal force:**

Aluminium upper arm stress

Figure 6.1   Compare stress of aluminum upper arm.

b) Comparing the stress of the shape developed upper arm with sinusoidal force:
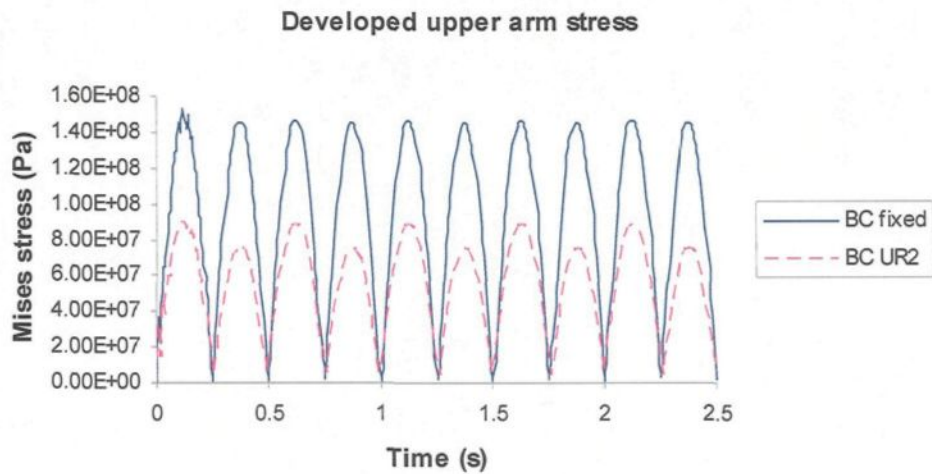
Developed upper arm stress

Figure 6.2   Comparing the stress of developed upper arm with sinusoidal forces.

c) Comparing the stress of the developed upper arm with random force:

Developed upper arm stress with random force
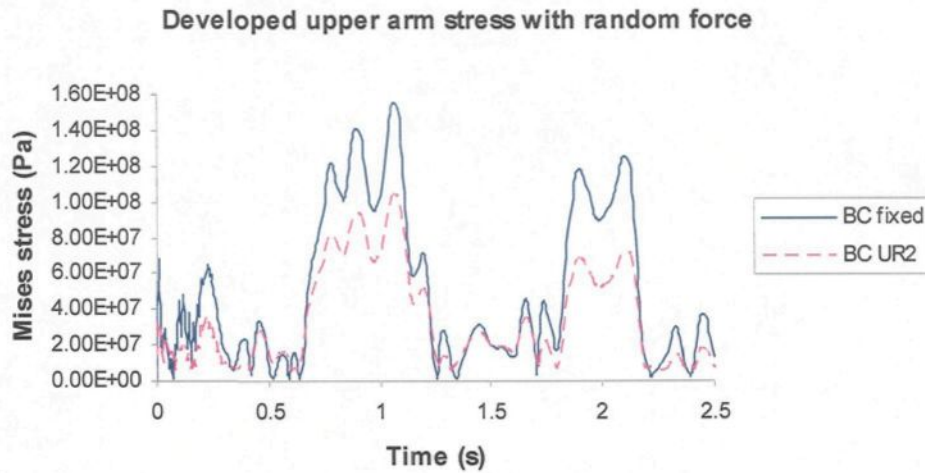
Figure 6.3 Comparing the stress of developed upper arm with random forces.

6.2 Comparing the stress of the lower arm with different force in same boundary condition

We compare results of the stress under different forces with the same boundary conditions. Higher forces are associated with higher stress; lower force, with lower stress (See Figure 6.4 to Figure 6.7). The maximum stress of the aluminum lower arm is less than the average yield strength 275MPa. Therefore, the aluminum suspension lower arm is successfully developed.

a) Boundary condition fixed with sinusoidal force:

$$BC \quad fixed \begin{cases} force = 5250N \\ force = 4000N \end{cases}$$
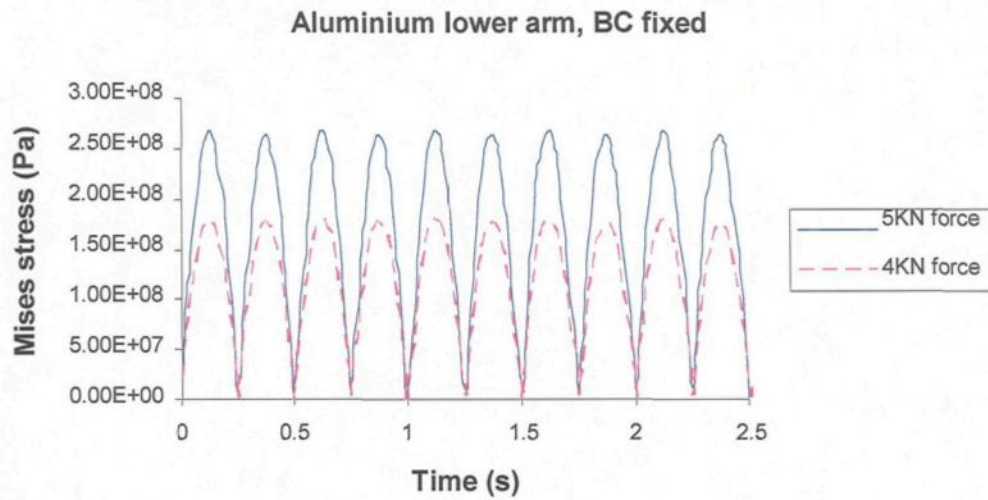
Figure 6.4   Comparing stress of lower arms, BC fixed.

b) Boundary condition of rotation with sinusoidal force:

$$BC \quad rotation(UR2) \begin{cases} force = 5250N \\ force = 4000N \end{cases}$$
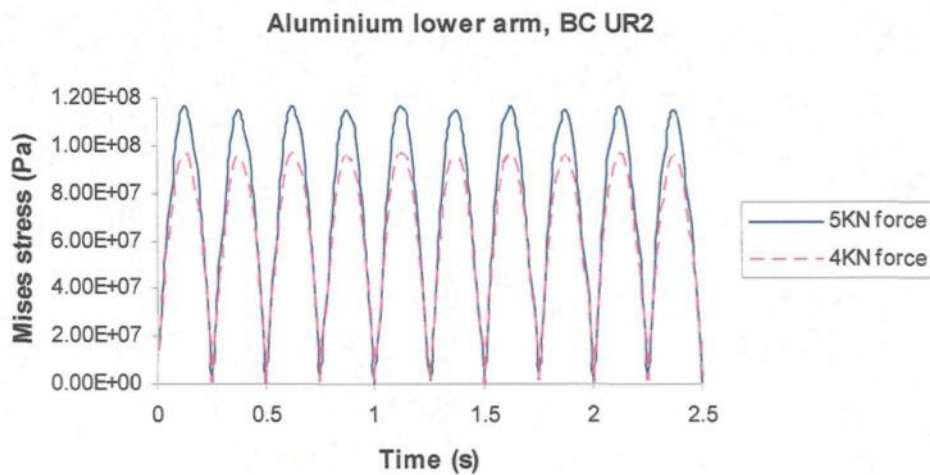
Figure 6.5   Comparing the stress of lower arms with sinusoidal force, BC UR2.

c) Boundary condition fixed with random force:

$$BC \quad fixed \begin{cases} force = 4250N \\ force = 4000N \end{cases}$$

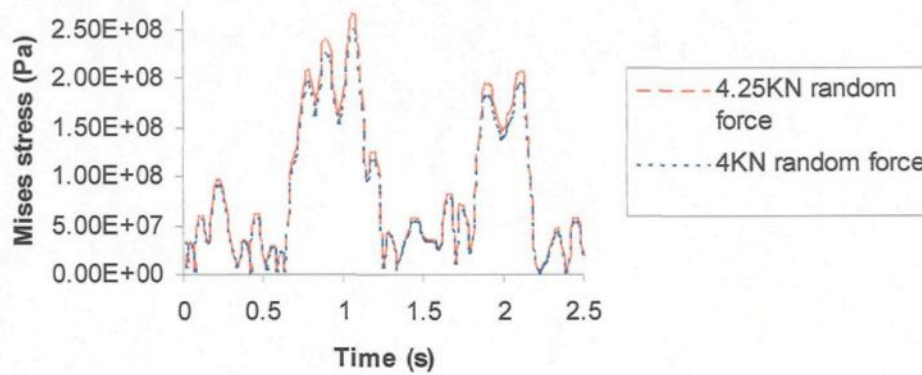**Aluminium lower arm with random force, BC fixed**

Figure 6.6   Compare the stress of lower arms with random force, BC fixed.

d) Boundary condition of rotation with random force:

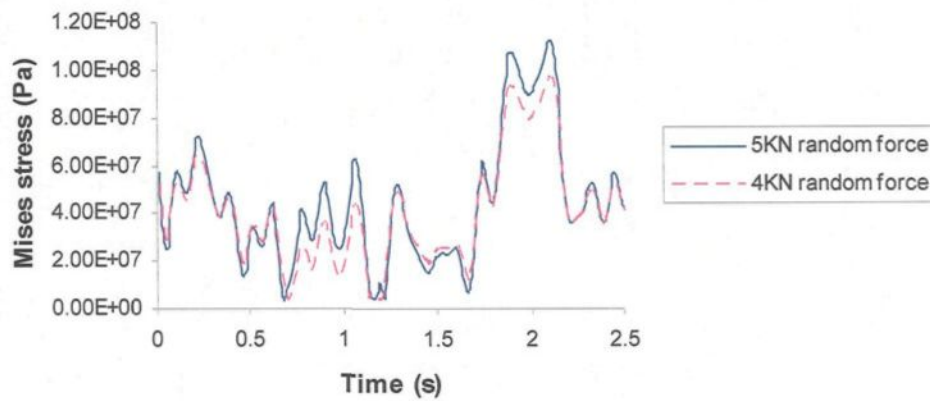**Aluminium lower arm with random force, BC UR2**

Figure 6.7   Compare the stress of lower arms with random force, BC UR2.

6.3 Comparing frequencies under different forces

We load different forces (sinusoidal and random are same) 4KN to 5KN on the lower arm and obtained the same frequency data. It is shown in table 6.1 and table 6.2. The frequency is a natural frequency, because the natural frequency just relates part mass but not the force on the part. This result indicates that the part is designed well and its natural frequency is same.

a) The frequencies of force from 4000N to 5250N with BC fixed

EIGENVALUE OUTPUT

MODE NO	EIGENVALUE	FREQUENCY (RAD/TIME)	(CYCLES/TIME)	GENERALIZED MASS	COMPOSITE MODAL DAMPING	
1	1.94390E+06	1394.2	221.90	0.20368	0.0000	
2	3.76458E+07	6135.6	976.51	0.25525	0.0000	
3	4.46407E+07	6681.4	1063.4	0.22431	0.0000	← 5250N, BC fixed
4	1.62449E+08	12746.	2028.5	0.42107	0.0000	
5	1.75955E+08	13265.	2111.2	0.10822	0.0000	
6	2.56975E+08	16030.	2551.3	0.15941	0.0000	
7	2.98513E+08	17278.	2749.8	0.21291	0.0000	
8	5.08110E+08	22541.	3587.6	0.10162	0.0000	
9	6.05708E+08	24611.	3917.0	0.11285	0.0000	
10	7.22424E+08	26878.	4277.8	0.40529	0.0000	

EIGENVALUE OUTPUT

MODE NO	EIGENVALUE	FREQUENCY (RAD/TIME)	(CYCLES/TIME)	GENERALIZED MASS	COMPOSITE MODAL DAMPING	
1	1.94390E+06	1394.2	221.90	0.20368	0.0000	
2	3.76458E+07	6135.6	976.51	0.25525	0.0000	
3	4.46407E+07	6681.4	1063.4	0.22431	0.0000	
4	1.62449E+08	12746.	2028.5	0.42107	0.0000	← 4250N, BC fixed
5	1.75955E+08	13265.	2111.2	0.10822	0.0000	
6	2.56975E+08	16030.	2551.3	0.15941	0.0000	
7	2.98513E+08	17278.	2749.8	0.21291	0.0000	
8	5.08110E+08	22541.	3587.6	0.10162	0.0000	
9	6.05708E+08	24611.	3917.0	0.11285	0.0000	
10	7.22424E+08	26878.	4277.8	0.40529	0.0000	

EIGENVALUE OUTPUT

MODE NO	EIGENVALUE	FREQUENCY (RAD/TIME)	(CYCLES/TIME)	GENERALIZED MASS	COMPOSITE MODAL DAMPING	
1	1.94390E+06	1394.2	221.90	0.20368	0.0000	
2	3.76458E+07	6135.6	976.51	0.25525	0.0000	
3	4.46407E+07	6681.4	1063.4	0.22431	0.0000	
4	1.62449E+08	12746.	2028.5	0.42107	0.0000	
5	1.75955E+08	13265.	2111.2	0.10822	0.0000	← 4000N, BC fixed
6	2.56975E+08	16030.	2551.3	0.15941	0.0000	
7	2.98513E+08	17278.	2749.8	0.21291	0.0000	
8	5.08110E+08	22541.	3587.6	0.10162	0.0000	
9	6.05708E+08	24611.	3917.0	0.11285	0.0000	
10	7.22424E+08	26878.	4277.8	0.40529	0.0000	

Table 6.1 Comparing frequencies with different forces under BC fixed

b) The frequencies of force 5250N and 4000N with BC UR2

EIGENVALUE OUTPUT

MODE NO	EIGENVALUE	FREQUENCY (RAD/TIME)	(CYCLES/TIME)	GENERALIZED MASS	COMPOSITE MODAL DAMPING
1	-2.11588E-05	0.0000	0.0000	1.1079	0.0000
2	1.39265E-07	3.73183E-04	5.93939E-05	0.62834	0.0000
3	4.92787E-05	7.01988E-03	1.11725E-03	1.0481	0.0000
4	4.29955E+06	2073.5	330.01	0.35675	0.0000
5	6.52889E+06	2555.2	406.67	0.42193	0.0000
6	1.18273E+07	3439.1	547.35	0.35668	0.0000
7	1.66808E+07	4084.2	650.02	0.24324	0.0000
8	1.14633E+08	10707.	1704.0	0.31420	0.0000
9	1.36840E+08	11698.	1861.8	0.31516	0.0000
10	1.75553E+08	13250.	2108.7	0.14801	0.0000

← 5250N, BC UR2

EIGENVALUE OUTPUT

MODE NO	EIGENVALUE	FREQUENCY (RAD/TIME)	(CYCLES/TIME)	GENERALIZED MASS	COMPOSITE MODAL DAMPING
1	-2.11588E-05	0.0000	0.0000	1.1079	0.0000
2	1.39265E-07	3.73183E-04	5.93939E-05	0.62834	0.0000
3	4.92787E-05	7.01988E-03	1.11725E-03	1.0481	0.0000
4	4.29955E+06	2073.5	330.01	0.35675	0.0000
5	6.52889E+06	2555.2	406.67	0.42193	0.0000
6	1.18273E+07	3439.1	547.35	0.35668	0.0000
7	1.66808E+07	4084.2	650.02	0.24324	0.0000
8	1.14633E+08	10707.	1704.0	0.31420	0.0000
9	1.36840E+08	11698.	1861.8	0.31516	0.0000
10	1.75553E+08	13250.	2108.7	0.14801	0.0000

← 4000N, BC UR2

Table 6.2 Comparing frequencies with different forces under BC UR2

6.4 Comparing weight of aluminum suspension control arm vs steel.

Suspension upper control arm	Material	Yield strength (Pa)	Density (kg/m^3)	Mass (kg)	Weight save (%)
	Steel	2.9e+008	7800	2.04	N/A
	A357	2.75e+08	2670.3	0.996	51.2
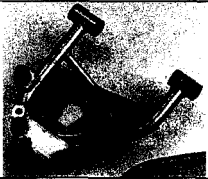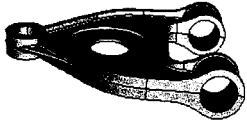
Suspension lower control arm	Material	Yield strength (Pa)	Density (kg/m^3)	Mass (kg)	Weight save (%)
	Steel	3.45+008	7800	2.6	N/A
	T6061-T6	2.75e+08	2700	1.56	40

Table 6.4　Comparing suspension lower control arms

In these results, we have modify the shape and weight of the part under given stress conditions through the use of modelization and simulation software and the ESO method. It can help engineer to do per-design efficiently, save time, materials and reduce the cost of productions. Now we have successfully designed the suspension arms and achieved 51.2% weight saving for upper arm and 40% weight saving for lower arm. Therefore, the more and more aluminum is possible to instead of the steel in transportation area. It will make a good condition environment to the world. However, it should be noted that mechanical design of the parts are only theoretical, it must be verified with performance test and road test in real life.

CHAPTER 7

CHAPTER 7 Conclusion

Through this research, we have shown that modelization and simulation software with ESO method is efficient and timesaving tools in helping engineer to design mechanical parts and systems. It is far more economical than the traditional experimental method which is more consuming in material, cost and time. The method is very flexible and their many parameters enable us to closely imitate real life conditions and make accurate predictions based on the set boundaries. Through this research, the use of modelization and simulation software with ESO method allowed us to compare the properties and advantages of aluminum alloy versus steel in the manufacturing of an automobile control arm. The results based on those models demonstrated that the aluminum alloy under specific designs is able to sustain efficiently the stress acting on the control arm with the advantage of being lighter than steel parts. The simulation and modelization software with ESO method also enables us to optimize the shape of the part with respect to the stress constraints in order to reduce the amount of material required and thus the weight of the part as well. This advantage is significant since it will not only allow considerable savings in the manufacturing process, but a lighter car also improves its energy consumption and driving performances, leading to a reduction in cost for both the manufacturer and the consumer and a better and safer driving experience. On the other hand, through this automobile suspension arms design, we studied kinematics mechanism

systems, aluminum properties and application of aluminum parts in automobile. We did complex part design with the CAD system and the knowledge of mechanical design. This research also enables us to study the vibration movement of a dynamic system and the amount of stress it induces on a mechanical part, this is important to analyze in order to prevent failures of the part which is crucial in ensuring the safety of the passengers. We simply present the conclusions by point below:

1. Dynamic behavior of automobile was studied.

2. Evaluated stress analysis for two aluminum automobile parts with advanced methods.

3. Dynamic analysis of vibrations for aluminum lower control arms was simulated.

4. We reduced the weight through material comparison between steel and aluminum parts.

6. We demonstrated that the aluminum suspension complex parts with advanced design can be used for automobile applications.

7. Through this research, the use of modelization and simulation software with ESO method allowed us to compare the properties and advantages of aluminum alloy versus steel in the manufacturing of the automobile.

8. Through this research, we can accomplish weight reduction and shape development with advanced method. This method is one of the best ways for engineers to design easily, saving time, material and cost.

REFERENCES

1. SAE world congress papers confirm; *Aluminum technologies offer SUVS safety and fuel economy*, March 5, 2003

2. The Aluminum Association Inc. *Automotive news' show daily*, (2004)

3. The Aluminum Association Inc.; *Automotive aluminum the performance advantage* (2004), Webpage http://www.autoaluminum.org

4. Sheng Mhau Industray Co., Ltd.; *Specialist in steering & suspension system*, (1998) http://www.baw-auto.com.tw/index.html

5. The University of Sheffield; *Weight Reductions Achievable by Thixoforming*, (2004), Webpage: http://www.shef.ac.uk/materials/SSM/commappl.html

6. Alfot Technologies Co., Ltd; Webpage: http://www.manufacturers.com.tw/showroom-5988-3-1-0-3608.php

7. Bethesda, Md.; *Aluminum and its alloys*, (2004)

8. Christopher J Longhurst; *The Suspension Bible*, (1998-2005), Webpage: http://www.carbibles.com/suspension_bible.html

9. Andrew Dimarogonas; *Vibration for Engineers*, second Edition, (1995), Page 57, 61, 649, 654.

10. Francis S. Tse, Ivan E. Morse, Rolland T. Hinkle; *Mechanical vibrations theory and applications*, Second edition, (1978),

11. THOMSON, W.T. Prentice Hall.; *Theory of Vibration and Applications*, Sec. edition, (1988)

12. Williamt.TH, Marie.D.D; *Theory of Vibration with Applications*, 5th edition, (1998), Page 23-33, 49, 50

13. Bouazara Mohamed (PH.D.); *Étude et analyse de la suspension active et semi-active des véhicules*, (1997). Chapitre 3, Page 16-26.

14. William F. Milliken; *Chassis design: Principles and Analysis*, (2002), Page 443.

15. William F. Milliken, Douglas L. Milliken; *Race Car Vehicle Dynamics*, Society of Automotive Engineers, Inc. Warrendale, Pa. (Copyright 2002), Page 207

16. Grabitech Solutions; *Optimization methods*, (2004), Webpage: http://www.grabitech.com/methods.htm

17. Murat F., Simon S., *Études de problèmes d'optimal design*, Lecture Notes in Computer science page 41, 54-62, Springer Verlag, Berlin (1976).

18. Pironneau O., *Optimal shape design for elliptic systems*, Springer-Verlag, New York (1984).

19. Simon J., *Differentiation with respect to the domain in boundary value problems*, Num. Funct. Anal. Optimz., Page 2, 649-687 (1980).

20. Soko lowski J., Zolesio J.P., *Introduction to shape optimization: shape sensitivity analysis,* Springer Series in Computational Mathematics, Vol. 10, Springer, Berlin (1992).

21. Grégoire ALLAIRE, François JOUVE, Anca-Maria Toader; *Une méthode de lignes de niveaux pour l'optimisation de formes;* (Jun. 8, 2005)

22. Grégoire ALLAIRE, François JOUVE, Anca-Maria Toader; *A level-set method for vibration and multiple loads structural optimization;* (2005)

23. Osher S., Sethian J.A., *Front propagating with curvature dependent speed: algorithms based on Hamilton-Jacobi formulations,* J. Comp. Phys., Page 78, 12-49 (1988).

24. Sethian J.*A., Level set Methods and fast marching methods: evolving interfaces in computational geometry, fluid mechanics, computer vision and materials science,* Cambridge University Press (1999).

25. Juan Pablo Trejo; *Simulation D'une suspension automobile,* (2005), Page 41-46

26. J. E. Shigley, C. R. Mischke, McGrawHill; *Mechanical Engineering Design,* 6 edition, (2000)

27. Paul Haney; *Basic Vehicle Dynamics,* (1999), Page 22

28. GILLESPIE, Thomas D.; (1992) *Fundamentals of Vehicle Dynamics,* Warrendale: Society of Automotive Engineers, Inc.

29. Tim Basner; *Rheocasting of Semi-Solid A357 Aluminum,* SAE Technical Paper Series, (2000), Page 3-4

30. MatWeb; *Material property data,* (2005), Webpage: http://www.matweb.com/search/SpecificMaterial.asp?bassnum=MA6016

31. George W. Housner and Thad Vreeland, JR. *The analysis of stress and deformation,* (1966), Page 79-81

32. Abaqus V6.4 PDF Documentation; *Getting Started with ABAQUS, 7.5.1 and 7.8*

33. Abaqus V6.4 PDF Documentation; *ABAQUS/CAE User's Manual*

34. Abaqus V6.4 PDF Documentation; *Analysis User's Manual*

35. Abaqus V6.4 PDF Documentation; *Example problems Manual*

36. T. Lindby and J.L.T. Santos; Shape optimization of three-dimensional shell structures with the shape parametrization of a CAD system, (1999), Page 6.2.